Institut für Technische Chemie, Lehrstuhl II

Selective Hydrogenation of Butyronitrile over Raney-Metals

Adam Chojecki

Vollständiger Abdruck der von der Fakultät für Chemie der Technischen Universität München zur Erlangung des akademischen Grades eines

Doktors der Naturwissenschaften (Dr. rer. nat.)

genehmigten Dissertation.

Vorsitzender: Univ-Prof. Dr. K. Köhler

Prüfer der Dissertation:

1. Univ. Prof. Dr. J. A. Lercher
2. Univ. Prof. Dr. Th. Bach

Die Dissertation wurde am 25.02.04 bei der Technischen Universität München eingereicht und durch die Fakultät für Chemie am 17.03.04 angenommen.

Acknowledgment

The scientific work presented in the thesis is a result of the collaboration among a good few people.

First of all, I do thank Prof. Dr. Johannes A. Lercher for inviting me to the fellowship of Technische Chemie 2 and for his scientific guidance. I am also much obliged to my mentor PD. Thomas E. Müller, PhD for taking care on daily bases of this work and for helping in correcting the thesis. The scientific help of PD. Andreas Jentys, PhD (DFT calculations), Dr. Hervé Jobic (Institut de Recherches sur la Catalyse, France; INS spectroscopy) and Prof. Dr. Stan Veprek (Institut für Chemie Anorganischer Materialien, TUM; XPS spectroscopy) is gratefully acknowledged.

Over those years I have met many people that in one or the other way have supported me, especially the fellows of the TC2 group. I would like to let you know at this place that I really appreciate the help I received from you.

Last but not least Air Products & Chemicals Inc. is gratefully thanked for the financial support; Institut Laue-Langevin is thanked for access to the IN1-BeF spectrometer.

1 General Introduction 2

1.1 Aliphatic Amines 2

1.1.1 Catalytic Routes to Lower Aliphatic Amines 2

1.2 Metals as Catalysts 4

1.2.1 Dispersed Metal Catalysts 4

1.2.2 Chemical Bonding at Metal Surfaces 6

1.2.2.1 Solid State Theory of Transition Metals 6

1.2.3 Surface Catalyzed Step-Wise Hydrogenation of Nitriles 7

1.3 The Scope of the Thesis 9

Acknowledgment 10

References 10

2 Experimental Methods and Setups 14

2.1 Preparation of Catalysts and Chemicals 14

2.1.1 Catalysts 14

2.1.2 Chemicals 14

2.1.2.1 Synthesis of N-butylidene-butylamine 15

2.2 Characterization of the Catalyst Samples 16

2.2.1 Elemental Analysis 16

2.2.2 Surface Area and Porosity 16

2.2.3 Particle Size and Dispersion Measurements 17

2.2.3.1 X-Ray Diffraction Line Broadening Analysis 18

2.2.3.2 Hydrogen Chemisorption 18

2.2.4 Temperature Programmed Desorption 20

2.2.5 Photoelectron Spectroscopy 21

2.2.6 Adsorption at Solid-Liquid Interface 22

2.2.7 Calorimetrically Measured Heat of Adsorption 23

2.3 Catalytic Tests 23

2.3.1 Catalytic Testing Procedure 24

2.4 Characterization of the Catalytic Process with Vibrational Spectroscopy 24

2.4.1 In Situ Attenuated Total Internal Reflectance Infrared Spectroscopy (ATR-IR) 24

2.4.1.1 The Nature of ATR Spectra 25

2.4.1.2 ReactIR 1000 Setup 26

2.4.2 Inelastic Neutron Scattering (INS) 27

2.4.2.1 The INS Theory 27

2.4.2.2 The INS Spectrometer 29

2.5 Calculation Methods ***29***

2.5.1 Thermodynamic Equilibrium 29

2.5.1.1 Thermodynamic Equilibrium Calculated from the Experimental Data. 29

2.5.1.2 Thermodynamic Equilibrium Computed ab initio 30

2.5.2 DFT Search for a Transition State 31

Acknowledgment **32**

References **32**

3 Characterization of Raney-Ni and Raney-Co Catalysts and Their Use in the Selective Hydrogenation of Butyronitrile **35**

3.1 Introduction ***35***

3.2 Experimental ***36***

3.2.1 Catalysts and Chemicals 36

3.2.2 Setups and Experimental Procedures 37

3.3 Results ***40***

3.3.1 Particle Size and Structure of Raney-Co 40

3.3.2 Specific Surface and Accessible Metal Surface Area 40

3.3.3 Temperature Programmed Desorption (TPD) 44

3.3.3.1 TPD of Residual Hydrogen and Water 44

3.3.3.2 Ammonia-TPD 46

3.3.4 X-ray Photoelectron Spectroscopy (XPS) 49

3.3.5 Adsorption of Butyronitrile and n-Butylamine from the Liquid Phase 53

3.3.5.1 Heat of Adsorption of Butyronitrile at 371.9 K 56

3.3.6 Catalytic Tests 57

3.3.6.1 Kinetics of the Hydrogenation of Butyronitrile 61

3.4 Discussion ***61***

3.4.1 The Activity of the Raney-Catalysts in the Hydrogenation of Butyronitrile. 61

3.4.2 The Selectivity to n-Butylamine over Raney-Catalysts in the Hydrogenation of Butyronitrile 62

3.5 Conclusions ***63***

Acknowledgment **64**

References **64**

4 Towards Understanding the Selectivity in the Hydrogenation of Butyronitrile over Raney-Co Catalysts - Formation and Cleavage of N-butylidene-butylamine **70**

4.1 Introduction ***70***

4.2 Experimental ***71***

4.2.1 Calculations of thermodynamic parameters 71

4.2.2 Catalysts and Chemicals 71

4.2.3 Setup 73

4.3 Results ***74***

4.3.1 Formation of N-butylidene-butylamine in the Hydrogenation of Butyronitrile 74

4.3.1.1 Control of the Condensation Reaction 78

4.3.2 Reactions of N-butylidene-butylamine 79

4.3.2.1 Cleavage of N-butylidene-butylamine to n-butylamine 80

4.3.2.2 Hydrogenation and Deuteration of N-butylidene-butylamine 84

4.3.2.3 Imine-Enamine Tautomerism of N-butylidene-butylamine 87

4.4 Discussion ***89***

4.4.1 Formation of N-butylidene-butylamine 90

4.4.2 Cleavage of N-butylidene-butylamine 91

4.5 Conclusions ***91***

Acknowledgment **92**

References **92**

5 Inelastic Neutron Scattering Study of Hydrogen and Butyronitrile Adsorbed on Raney-Co Catalysts **96**

5.1 Introduction ***96***

5.2 Experimental ***97***

5.2.1 Sample preparation 97

5.2.2 Measurement 97

5.2.3 Data treatment 98

5.3 Results and Discussion ***99***

5.4 Conclusions ***108***

Acknowledgment **108**

References **108**

6 Summary **112**

6.1 Summary of the Research ***112***

6.2 Conclusions ***113***

References **116**

Chapter 1

This chapter features a general introduction that highlights the importance of lower aliphatic amines in the industry, presents catalytic routes to lower aliphatic amines and discusses Raney-catalysts and the process of hydrogenation of nitriles to amines in detail. The research problem encountered during the selective hydrogenation of nitriles to primary amines is formulated. Finally, the milestones of the research work presented in the subsequent chapters are highlighted.

1 General Introduction

1.1 Aliphatic Amines

Lower aliphatic amines are of considerable industrial importance. A large number of drugs, plasticizers, agrochemicals (herbicides and pesticides), dyes and other chemicals originate from reactions with such intermediates. For example, n-butylamine is an intermediate for the production of the antidiabetic drug Tolbutamide (Figure 1-1). To illustrate their significance in modern industrial chemistry, manufacturing data for aliphatic amines are given in Figure 1-2 [1].

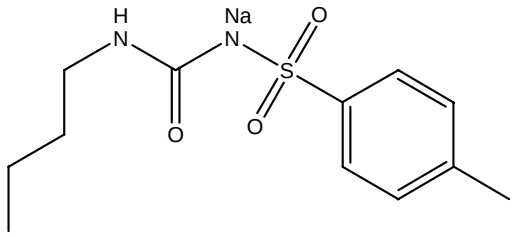

Figure 1-1: The chemical structure of Tolbutamide.

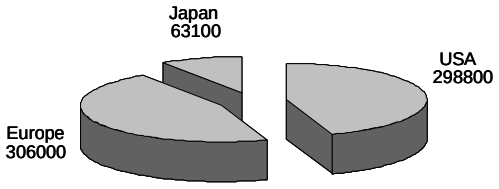

Figure 1-2: Production of lower aliphatic amines in tons per annum (1990) [1].

1.1.1 Catalytic Routes to Lower Aliphatic Amines

On the industrial scale a number of heterogeneous catalytic processes are practiced in the production of lower aliphatic amines using different types of feedstock [1, 2]. The most important technologies include:

1. Amination of alcohols with ammonia and primary and secondary amines using:
    a. solid acid catalysts (e.g., silica-alumina, silica, alumina, titania, zeolites) [3, 4]; or
    b. group VIII transition metal catalysts in the presence of hydrogen [5].

2. Amination of carbonyl compounds (reductive amination) with ammonia or amines (primary and secondary) and hydrogen over group VIII transition metals [6].
3. Catalytic reduction of nitriles with molecular hydrogen over Raney-Ni, Raney-Co, or rhodium, palladium and platinum on various supports (e.g., Al_2O_3, carbon) [7].
4. Amination of iso-butene over zeolites and other solid acids [8].

Process technologies for all methods utilize fixed bed reactors. A scheme depicting the typical industrial flow process for amination of alcohols is presented in Figure 1-3. Liquid phase stirred-tank equipment is operated either continuously or batchwise.

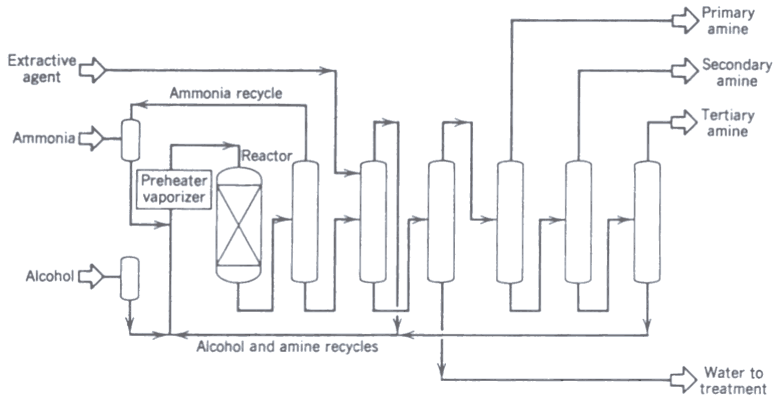

Figure 1-3 Typical amination reactor and separation train [1].

During the reduction of nitriles to primary amines (Method 3) formation of secondary and tertiary amines considered as by-products is encountered. The product distribution in is determined by the extend of coupling reactions between intermediate partially hydrogenated products (in particular imines) and the primary (or secondary) amine. These side reactions are very sensitive to the reaction conditions, increasing in rate with increasing temperature and decreasing with increasing pressure. Also, sterically hindered substrates will be less prone to coupling reactions [9, 10]. The solvent is of considerable importance as both acidic and basic media can effectively suppress coupling reactions [11, 12]. Strongly acidic solutions (e.g., in the presence of HCl, or H_2SO_4) prevent further reaction of the initially formed primary amine by formation of an ammonium salt.

Another effective way of preventing coupling reactions is to carry out the reduction in acylating solvents such as acetic acid or acetic anhydride. A common technique in industry for minimizing the formation of secondary amines is to perform the hydrogenation in the presence of excess ammonia. Latter shifts the thermodynamic equilibrium in favor of the primary amine. Ammonia may function in other ways as well, for a variety of bases, such as tertiary amines, carbonates, and hydroxides, also lead to a decrease in the formation of condensation products. Greenfield suggested that bases may decrease the rate of the hydrogenolysis reaction leading to secondary and tertiary amines [13].

1.2 Metals as Catalysts

1.2.1 Dispersed Metal Catalysts

One of the major functionalities of transition metals in catalysis is their ability to catalyze hydrogenation reactions due to dissociative chemisorption of molecular hydrogen. Finely dispersed metal is desired for practical catalysis because of the high surface area. In its simplest form an unsupported metal powder can be used for these purposes. Typical methods of preparation of such powders (metal 'blacks') [14, 15] include (i) reduction of a metal salt in solution [e.g., 16, 17] (ii) reduction of metal oxides (prepared *via* precipitation as hydroxides carbonatesetc.) in the gas phase with hydrogen [e.g., 18, 19] (iii) thermal decomposition under vacuum of salts of organic acids as well as nitrates, oxalates, carbonyls and organometallic compounds [e.g., 20].

Another class of commercially important metal powders generically called 'skeletal' metal catalysts was invented by Murray Raney [21]. These Raney-catalysts are prepared by melting the active metal (e.g., Co, Ni, Cu) together with aluminum (usually 50+ wt. %). Up to 10 wt. % of promoters (e.g., Fe, Cr, Mo) are added to the melt. The alloy is then crushed and screened according to the particle size. Finally, the parent alloy is activated by selective leaching of aluminium at elevated temperatures using $NaOH_{(aq.)}$. The leaching reaction is given in Figure 1-4.

$$2\ M - Al_{(s)} + 2\ OH^-_{(aq.)} + 6\ H_2O_{(l)} \rightarrow 2\ M_{(s)} + 2\ Al(OH)_4^-{}_{(aq.)} + 3\ H_{2(g)}$$

Figure 1-4: Leaching reaction during preparation of Raney-catalysts.

The resulting powdered skeletal catalyst is subsequently washed and stored under slightly alkaline conditions (pH 9 ~ 10) to avoid precipitation of aluminum hydroxide as bayerite. The procedure leaves microcrystallites of the active metal joined randomly to create sponge-like particles incorporating a large void volume within the intensive pore system so formed. Typical particle diameters for these catalysts range from 20 to 100 μm which is much higher than the crystallite size as measured by X-ray diffraction line broadening (approximately 5 nm [22]). The typical surface area of Raney-Ni (50 – 100 $m^2 \cdot g^{-1}$) is usually larger than that of Raney-Co (26 $m^2 \cdot g^{-1}$) [23].

The activity of transition metal promoted Raney-Ni in the hydrogenation of the butyronitrile has been studied by Mongomery [24] (Figure 1-5). Relationship between the composition of several bimetallic catalysts and the rate of hydrogenation of butyronitrile over several transition-metal promoted Raney-Ni catalysts

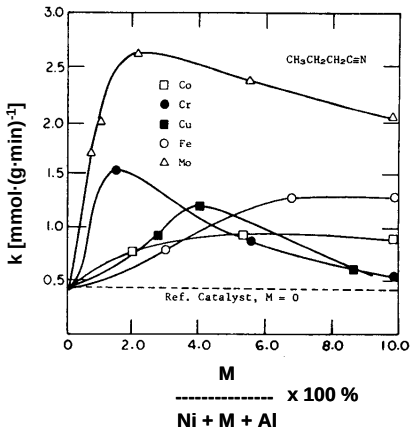

Figure 1-5: Relationship between the composition of several bimetallic catalysts and the rate of hydrogenation of butyronitrile over several transition-metal promoted Raney-Ni catalysts [24].

It should be noted, that the abrupt increase in activity under the influence of alloying modifiers may rather originate from a simple increase in the specific surface area, which is essentially the metal surface area available for catalysis [25 and references therein, 26].

Selectivity of a given catalyst can be influenced by surface modifiers that change the adsorption properties of the Raney catalyst. Consequently one reaction pathway maybe favoured over another [27, 28, 29, 30, 31, 32, 33].

One of the most important drawbacks of Raney-catalysts is their pyrophority in dry form. This problem has been tackled by removing most of the adsorbed hydrogen and mild oxidization applied at controlled circumstances [34 and references therein, 35].

1.2.2 Chemical Bonding at Metal Surfaces

As the catalyst itself participates in chemical reactions with adsorbed molecules, the metal surface is the place for various reactions such as bond formation between the adsorbate and surface atoms, reconstruction of the surface and penetration of erosive adatoms into subsurfaces. It has been long realized that a good catalyst is characterized by a low activation energy and weak binding of the intermediates (the Sabatier principle). However, only over the last two decades a qualitative approach to catalysis by metals could be applied thanks to the progress in computer modeling of the quantum chemical molecule-surface interactions [36, 37, 38, 39].

1.2.2.1 Solid State Theory of Transition Metals [40, 41, 42].

Chemisorption properties of metals are in the first place correlated either with the number of holes in the *d*-band or with the percentage of *d*-character of the metal (Table 1-1).

Metal	Percentage *d* character	Number of holes in *d*-band
Fe	39.7	2.22
Co	39.5	1.70
Ni	40.0	0.60
Cu	36.0	0.00
Pt	44.0	0.60
Pd	46.0	0.55

Table 1-1: Number of holes in the *d*-band and the percentage of *d*-character for some metals of interest [43].

In the quantum-mechanical theories the potential energy is taken as varying periodically through the crystal structure of a metal, owing to the presence of the atomic nuclei. The Schrödinger equation is set up and solved on that basis. A solution for a single atom shows that an electron may occupy an *s*-, *p*-, *d*- or *f*-orbital, thus, the ground electronic

state of the atom is uniquely defined. However, when a number of atoms are assembled to form a crystal, each orbital is compelled by the Pauli principle and needs to be replaced by an energy level within the band. The bands of valence electrons in metals overlap so that electrons may be exchanged between two or more bands (Figure 1-6). Because of their great importance in catalysis, much interest has been devoted to the band structure of the transition metals that have partly filled shells of d-electrons. For a number of reasons it seems that the *s*-band is broad with a low maximum level density while the *d*-band is narrow with a much higher maximum level density (Figure 1-7). Paramagnetism is associated with unoccupied states in the *d*-band, and copper is diamagnetic, as observed. The number of unoccupied *d*-band states is equal to the saturation moment, and metallic nickel therefore has the electronic structure $3d^{9.4}4s^{0.6}$, with 0.6 'holes'.

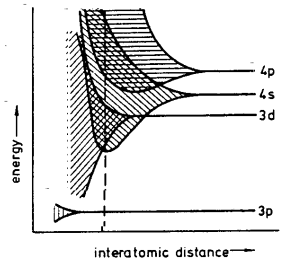

Figure 1-6: The dependence of electron band widths upon the interatomic distance in copper (schematic) [37]

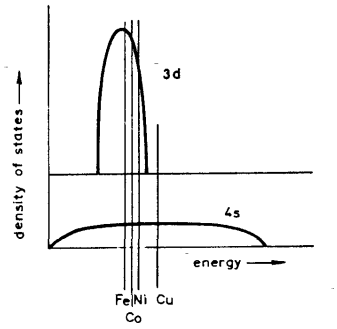

Figure 1-7: Approximate representation of the band structure of iron, cobalt, nickel and copper; vertical lines are representing the Fermi energies [37].

1.2.3 Surface Catalyzed Step-Wise Hydrogenation of Nitriles

For the catalytic hydrogenation of nitriles transition metals are used, however, the highest selectivities to the primary amines have been reported for cobalt, nickel and ruthenium

[44]. Typically, nitriles can bind to metal centers either as terminal σ-bonded (I), or bridging σ,-π-bonded way (II) to the metal centers [45]. In the presence of hydrogen partial hydrogenation can lead to either nitrogen bonded μ-N=C(H)-R (III) or nitrogen-carbon bonded μ-N(H)=C-R (IV) [46]. Further stepwise addition of hydrogen may lead to a number of intermediates: nitrene μ^2-N–CH_2-R (V), imine (VI) or aminoalkylcarbene species (VII). Further hydrogenation yields the surface-adsorbed products VIII and IX, respectively, and finally after addition of the fourth hydrogen atom the primary amine (X) is formed (Figure 1-8). Note, that the majority of surface-adsorbed species is susceptible to a nucleophilic attack because of the presence of an unsaturated carbon atom (marked as Rxn).

The main side reaction in the hydrogenation of nitriles, condensation, may occur between the partially hydrogenated intermediates (e.g., addition of VII to VI or with the 1° (2°) amine). Only nitrene species (V and VIII) are not susceptible to a nucleophilic attack because the carbon atom is saturated. It has been pointed out that the more selective route in the step-wise hydrogenation of nitriles probably leads *via* surface-adsorbed nitrene species rather than aminoalkylcarbene species [47].

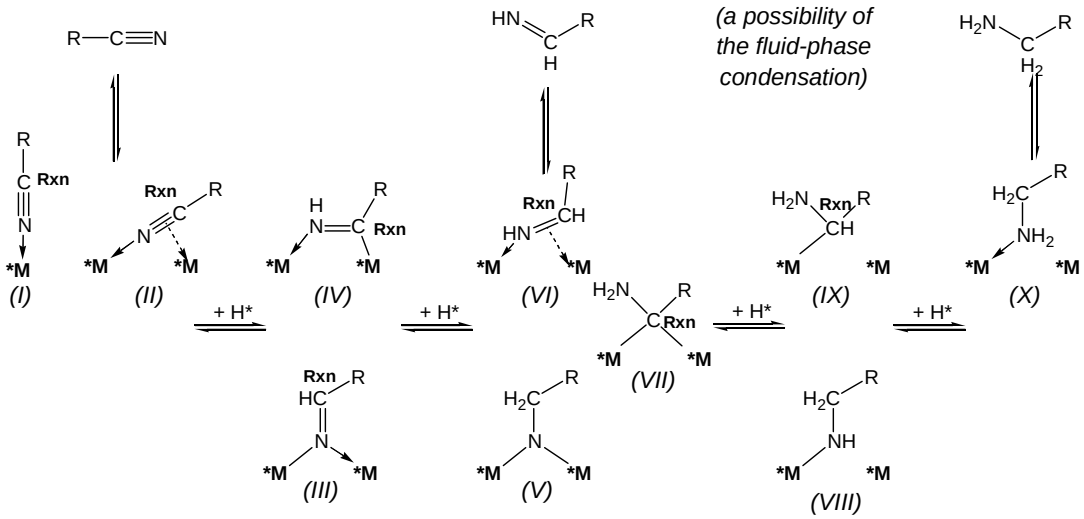

Figure 1-8: Surface catalyzed step-wise hydrogenation of nitriles.

Huang and Sachtler observed that the hydrogenation of acetonitrile is a concerted reaction with a H-donor molecule where the alkyl groups in the nitrile, or in the reaction products, can act as H donors. The lower selectivity observed for some metals has been

related to their low propensity for the formation of metal-nitrogen multiple bonds [48, 49, 50, 51, 52].

1.3 The Scope of the Thesis

The research work presented in this thesis has been initiated by an industry project in collaboration with Air Products and Chemicals, Inc. The aim was to explore the role of LiOH as promoter for Raney-catalysts. It was known that the co-catalyst LiOH leads to an increased selectivity in the hydrogenation of nitriles to primary amines [53, 54].

In Chapter 2 the characterization and experimental methods used in this thesis are reviewed.

In Chapter 3 the hydrogenation of butyronitrile was explored as a model reaction for the catalytic reduction of nitriles over Raney-Co and Raney-Ni. The aim was to understand the differences in the catalytic performance between the two metals. Furthermore, the increase in selectivity towards primary amines which is observed after modifying Raney-Co with LiOH was explored and discussed on the basis of a detailed characterization of the catalysts. Changes in the mechanism that may lead to the higher selectivity were examined.

In Chapter 4 the possible mechanism of side-reactions in the hydrogenation of butyronitrile over parent and LiOH-modified Raney-Co was investigated. The questions that were addressed concern the pathways which lead to the formation of the reaction intermediate N-butylidene-butylamine and the factors, which lead to the significantly lower amount of this intermediate over LiOH-modified Raney-Co. Further, reactions of N-butylidene-butylamine with special interest in a possibility of cleaving the imine bond to yield n-butylamine were explored.

In Chapter 5 an Inelastic Neutron Scattering study (INS) of co-adsorbed butyronitrile and hydrogen on parent and LiOH-modified Raney-Co is presented. The study was aimed at detecting partially hydrogenated cobalt-adsorbed species and in identifying surface bound intermediates in the hydrogenation of butyronitrile to n-butylamine.

In Chapter 6 the main results and conclusions of this thesis are summarized.

Acknowledgment

Air Products & Chemicals Inc. is gratefully thanked for the launch of the project and the generous financial support.

References

1 M. G. Turcotte, T. A. Johnson in: J. I. Kroschwitz (Ed.), Kirk-Othmer Encyclopedia of Chemical Technology Vol. 2 (4th Ed.), John Wiley & Sons, NY, 1992, p.369 - 386

2 G. Heilen in: W. Gerhartz (Ed.), Ullmann's Encyclopedia of Industrial Chemistry Vol. A2, VCH, Weinheim, 1985, p. 1 – 10

3 D.M. Roundhill, Chem. Rev. 92 (1992) 1

4 Y. Takita, Y. Nishida, T. Seiyama, Bull. Soc. Chem. Jpn. 49 (1976) 3699

5 A. Baker, J. Kijenski, Catal. Rev. Sci. Eng. 27(4) (1985) 653

6 T. Mallat, A. Baiker in: G. Ertl, H. Knözinger, J. Weitkamp (Eds.) Handbook of Heterogeneous Catalysis Vol. 5, Wiley-VCH, Weinheim, 1997, p. 2334 – 2348

7 P. R. Rylander, Hydrogenation Methods, Academic Press, London, 1988 (2nd Ed.), p. 94 - 103

8 T. E. Müller, M. Beller, Chem. Rev. 98 (1998) 675

9 M. Hudlicky, Reductions in Organic Chemistry - ACS Monograph Vol. 188, American Chemical Society, Washington DC, 1996, p. 239 - 241

10 A. G. M. Barrett in: B. M. Trost (Ed.-in-Chief), Comprehensive Organic Synthesis Vol. 8 – Reduction, Pergamon Press, Oxford, 1991, p. 251 – 257

11 P. N. Rylander, Hydrogenation Methods, Academic Press, London, 1988 (2nd Ed.), p. 94 – 103

12 P. N. Rylander, Catalytic Hydrogenation over Platinum Metals, Academic Press, NY and London, 1967, p. 203 – 226

13 H. Greenfield, Ind. Eng. Chem. Prod. Rev. Dev. 6 (1967) 142

14 J. R. Anderson, Structure of Metallic Catalysts, Academic Press, London, 1975, p. 218 – 236

15 G. C. Bond, Catalysis by Metals, Academic Press, London, 1962, p. 33 – 36

16 H. Wang, Z. Yu, H. Chen, J. Yang, J. Deng, Appl. Cat. A 129 (1995) L143

17 H. Li, X. Chen, M. Wang, Y. Xu, Appl. Cat. A 225 (2002) 117

18 K. Schachter, P. Tetenyi, Acta Chim. Hung. 46 (1965) 229

19 D. W. McKee, J. Catal. 8 (1967) 240

20 J. van Wonterghem, S. Mørup, S. W. Charles, S. Villadeen Wells, J. Phys. Lett. 55 (1985) 410

21 M. Raney, US Patent 1 563 587 (1925)

22 J. P. Orchard, A. D. Tomsett, M. S. Wainwright and D. J. Young, J. Catal. 84 (1983) 189

23 M. S. Wainwright in: G. Ertl, H. Knözinger, J. Weitkamp (Eds.), Preparation of Solid Catalysts, Wiley-VCH, Weinheim, 1999, p. 28 – 43

24 S. R. Montgomery in: W.R. Moser (Ed.) Catalysis of Organic Reactions - Chemical Industries Series Vol. 5, Marcel Dekker, 1981, p. 383 – 409

25 A.B. Fasman in: F. Herkes (Ed.) Catalysis of Organic Reactions - Chemical Industries Series Vol. 75, Marcel Dekker, 1998, p. 151 – 168

26 Y. Kiros , M. Majari and T.A. Nissinen, J. Alloys Compd. 360 (2003) 279

27 K. Hotta and T. Kubomatsu, Bull. Chem. Soc. Jpn. 46 (1973) 3566

28 G. V. Smith, M. Musoiu, J. Catal. 60 (1979) 184

29 B. Liu, L. Lu, B. Wang, T. Cai, K. Iwatani, Appl. Cat. A 171 (1998) 117

30 B. Liu, L. Lu, T. Cai, K. Iwatani, Appl. Cat. A 180 (1999) 105

31 P. Kukula and L. Cervený, Appl. Catal., A 223 (2002) 43

32 P. Kukula and L. Cervený, J. Mol. Catal. A: Chem. 185 (2002) 195

33 P. Tundo, A. Perosa and S. Zinovyev, J. Mol. Catal. A: Chem. 204-205 (2003) 747

34 S. D. Mikhailenko, T. A. Khodareva, E. V. Leongardt, A. I. Lyashenko, A. B. Fasman, J. Catal. 141 (1993) 688

35 A. Bota, G. Goerigk, T. Drucker, H.-G. Haubold, and J. Petro, J. Catal. 205 (2002), 354

36 S. Yoshida, S. Sakaki and H. Kobayashi, Electronic Processes in Catalysis – A Quantum Chemical Approach to Catalysis, Wiley-VCH, Weinheim, 1994, p. 213 – 240

37 J. K. Nørskov, P. Stoltze, Catal. Lett. 9 (1991) 173

38 G. D. Yadav, M. R. Kharkara, Appl. Cat. A 126 (1995) 115

39 J. K. Nørskov, T. Bligaard, A. Logadottir, S. Bahn, L. B. Hansen, M. Bollinger, H. Bengaard, B. Hammer, Z. Sljivancanin, M. Mavrikakis, Y. Xu, S. Dahl, C. J. H. Jacobsen, J. Catal. 209 (2002) 275

40 G. V. Raynor, Rep. Prog. Phys. 15 (1952) 173

41 G. C. Bond, Catalysis by Metals, Academic Press, London, 1962, p. 17 – 28

42 J. R. Anderson, Structure of Metallic Catalysts, Academic Press, London, 1975, p. 1 – 28

43 K. J. Laidler, Chemical Kinetics, McGraw-Hill, London, 1965 (2nd Ed.), p. 309

44 J. Volf and J. Pasek, in: L. Cerveny (Ed.), Stud. Surf. Sci. Catal. 27, Elsevier, Amsterdam, 1986, p.105

45 C. M. Friend, E. L. Muetterties and J. L. Gland, J. Phys. Chem. 85 (1981) 3256

46 F. J. G. Alonso, M. G. Sanz and V. Riera, Organometallics 11 (1992) 801

47 B. Coq, D. Tichit and S. Ribet, J. Catal. 189 (2000) 117 and references therein

48 Y. Huang and W. M. H. Sachtler, J.Phys. Chem. B 102 (1998) 102

49 Y. Huang and W. M. H. Sachtler, J. Catal. 184 (1999) 247

50 Y. Huang and W. M. H. Sachtler, J. Catal. 190 (2000) 69

51 Y. Huang and W. M. H. Sachtler, Appl. Catal., A 182 (1999) 365

52 Y. Huang and W. M. H. Sachtler, Appl. Catal., A 191 (2000) 35

53 T. A. Johnson, US Patent No. 5 869 653 (1999), to Air Products and Chemicals, Inc.

54 T. A. Johnson and D. P. Freyberger in: M. E. Ford (Ed.), Catalysis of Organic Reactions - Chemical Industries Series Vol. 82, Marcel Dekker, 2000, p. 201 – 227

Chapter 2

This chapter introduces the reader to the experimental methods and presents the experimental setups that were used during the research work.

2 Experimental Methods and Setups

2.1 Preparation of Catalysts and Chemicals

2.1.1 Catalysts

Active Raney-catalysts were obtained as aqueous suspension from the GRACE Davison Chemical Division of W.R. Grace & Co. [1]. The chemical composition of the parent samples, the grain size distribution and the pH of the storing solutions are summarized in Table 2-1.

	Raney-Co grade # 2700 lot # 7865	Raney-Co grade # 2724 lot # 7733	Raney-Ni grade # 2800 lot # 7716
Chemical composition [wt. %]			
Al	1.85	3.5	6.77
Co	97.51	91.26	0
Cr	0	2.15	0
Fe	0.3	0.32	0.4
Ni	0.34	2.79	92.83
pH of the storing solution			
	10.2	10.6	11.0
Raney-catalyst grain size [µm]			
< 10th %	7.33	5.91	8.7
< 50th %	30.08	28.52	45.61
< 90th %	81.79	75.03	151.99

Table 2-1: Release data for Raney-Catalysts as provided by GRACE Davision.

Prior to the experiments described in Chapters 3, 4 and 5 the catalyst samples were washed, if necessary, doped with LiOH and dried (details are provided in the corresponding chapters).

2.1.2 Chemicals

All chemicals except N-butylidene-butylamine were supplied by commercial providers and used as received (Table 2-2); N-butylidene-butylamine was synthesized according to reference [2].

Compound [mol·g^{-1}], [g·cm^{-3}]	Purity [%]	Company
butyronitrile M = 69.11, d = 0.794	≥ 99	Fluka
hydrogen	99.999	Messer-Griesheim GmbH
deuterium	99.8	Deutero GmbH
argon	99.999	Messer-Griesheim GmbH
nitrogen	99.999	Messer-Griesheim GmbH
ammonia	99.98	Messer-Griesheim GmbH
n-butylamine M = 73.14, d = 0.740	≥ 99	Aldrich Chemie
di-n-butylamine M = 129.25, d = 0.760	> 99	Aldrich Chemie
tri-n-butylamine M =185.36, d = 0.778	> 99	Aldrich Chemie
n-butyraldehyde M = 72.11, d = 0.800	≥ 99	Fluka
n-pentane M = 72.15, d = 0.626	≥ 99	Alfa
n-octane M = 114.23, d = 0.703	99.5	Aldrich
n-undecane M = 156.31, d =0.740	99.5	Aldrich
lithium hydroxide M = 23.95	98 (2 % Li_2CO_3)	Merck
potassium hydroxide M = 56.11	86	Fluka

Table 2-2: Chemicals used in this study.

2.1.2.1 Synthesis of N-butylidene-butylamine

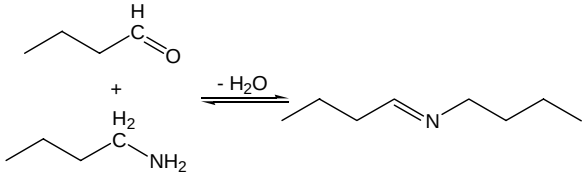

Figure 2-1: Synthesis of N-butylidene-butylamine.

n-Butyraldehyde (0.3 mol, 21.6 g, 24.0 cm^3) was stirred in a 100-cm^3 flask equipped with a thermometer and an addition funnel and cooled in an ice/water bath. n-Butylamine (0.3 mol, 21.9 g, 29.7 cm^3) was added dropwise over a period of 1.5 h at such a rate that the temperature of the reaction mixture remained below 285 K. After the addition was completed, KOH pellets (10 g) were added and the solution was stirred at 287 K for 12 h. The solution was then decanted into a 100-cm^3 flask containing 10 g of KOH and

allowed to stand for 6 h in the freezer (271 K). Finally, the mixture was transferred into another 100-cm^3 flask and distilled through a 15-cm Vigreux column over a few KOH pellets to give 5.99 g of N-butylidene-butylamine as a colorless liquid collected at 315 – 316 K (16 - 17 mbar) (16 % yield, purity ≥ 99 % according to the NMR spectrum). The product was kept in the refrigerator (271 K) and used within of days.

2.2 Characterization of the Catalyst Samples

2.2.1 Elemental Analysis

Atomic absorption spectroscopy (AAS) is a technique for determining the concentration of an element (usually metals and some metalloids) within a sample. AAS uses the absorption of light to measure the concentration of gas-phase atoms. Ions or atoms in a sample must undergo desolvation and vaporization in a high-temperature source such as a flame or graphite furnace. Flame AA can only analyze solutions, while graphite furnace AA can accept solutions, slurries, or solid samples. The amount of the LiOH deposited on the surface of Raney-Co was measured by atomic adsorption spectroscopy on a UNICAM 939 AA-Spectrometer. The concentration measurements were determined from a working curve after calibrating the instrument with standards of known concentration.

2.2.2 Surface Area and Porosity

The specific surface area (a_s) of a solid material is obtained by measuring the molecular cross-sectional area occupied by adsorbate molecules in a complete monolayer [3]. The monolayer capacity ($n_m{}^a$) is defined as the amount of adsorbate required to form a complete monolayer on the surface. Brunauer, Emmett and Teller derived an isothermal equation describing the dynamic equilibrium of the multilayer adsorption [4]. Equation 2-1 represents a linear form of that equation, where c is a constant. The intercept and the tangent of α readily permit the calculation of $n_m{}^a$.

$$\frac{p/p_0}{n^a\left(1-p/p_0\right)} = \frac{1}{n_m^a \cdot c} + \frac{c-1}{n_m^a \cdot c} \cdot \frac{p}{p_0} \qquad \text{Equation 2-1}$$

Calculation methods for the pore volume use the Kelvin equation (Equation 2-2), where r_k, σ, v_l are the Kelvin radius, surface tension of the liquid condensate and its molar volume, respectively [5].

$$r_k = \frac{2 \cdot \sigma \cdot v_l}{RT \ln(p / p_0)} \qquad \text{Equation 2-2}$$

A study of the BET surface area and the pore volume for Raney-metals was carried out on a Sorptomatic 1990 instrument (ThermoFinnigan [6]). Nitrogen was used as adsorbate with a molecular cross-section area of 0.162 nm^2. A typical adsorption/desorption isotherm recorded at 77.4 K over Raney-Co sample is presented in Figure 2-2. The range of partial pressure where the BET theory is applicable is usually limited to $0.05 < p/p_0 < 0.3$. Therefore, the linear approximation of the BET equation was performed within this region; the typical R-squared value of the linear fit was > 0.999. Pore specific volume was calculated with the Dollimore and Heal method [7].

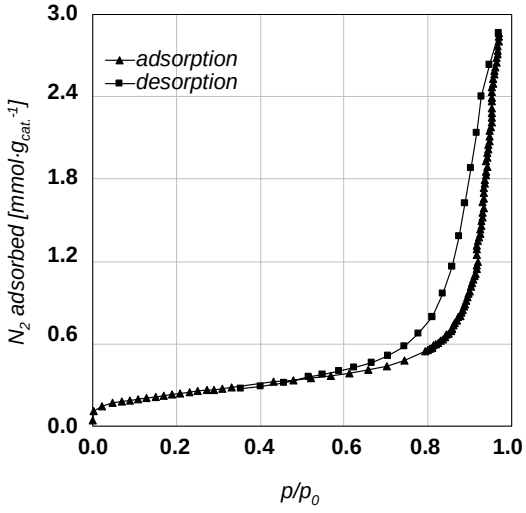

Figure 2-2: An adsorption/desorption isotherm over Raney-Co at T = 77.4 K using N_2 as probe molecule.

2.2.3 Particle Size and Dispersion Measurements

Small solid objects with a size > 10^{-6} m are usually called grains. If the size is in the range 10^{-5} – 10^{-9} m, then the term particles is used. Objects smaller than $2 \cdot 10^{-9}$ m are frequently referred to as aggregates (metals) or clusters (metals, oxides). The term crystallite describes a small single crystal; particles can be formed by one or more

crystallites. The crystallite size of the Raney-cobalt was determined from the line broadening in X-ray diffraction

2.2.3.1 X-Ray Diffraction Line Broadening Analysis (LBA) [8]

Considering an X-ray reflection on N lattice planes of spacing $d_{hkl,}$ Scherrer showed that the thickness of a crystallite $L_{hkl} = N \cdot d_{hkl}$ in the direction perpendicular to the diffracting planes (*hkl*) can be obtained from the breadth β of the diffraction profile using the relationship expressed in Equation 2-3:

$$L_{hkl} = \frac{k \cdot \lambda}{\beta \cdot \cos\theta_0} \qquad \text{Equation 2-3}$$

where, k is a constant (shape factor), λ is the wavelength of the X-radiation employed, and θ_0 is the angular position of the peak maximum. The size of the crystallites is thus inversely proportional to the breadth of the diffraction line.

Due to pyrophoric nature of the Raney-catalysts it was necessary to coat the powdered catalyst with wax prior to examination. A sample of Raney-Co # 2700 (ca. 0.2 g) was washed with ethanol (3 x 5 cm^3) and decanted. The wet catalyst sample was then mixed with molten wax (T ~ 373 K) and ethanol was allowed to evaporate. Finally, the suspension was cooled down on a silicon wafer. The measurement was carried out on a Semens D-5000 powder diffractometer. An estimate of the crystallite size was obtained from X-ray LBA using the software package Diffract v.3.0. The true peak breadth was found from the Warren formula (Equation 2-4) using cobalt foil (99.95 wt. % metal basis, Alfa Aesar) as reference.

$$\beta^2 = \beta^2_{observed} - \beta^2_{reference} \qquad \text{Equation 2-4}$$

2.2.3.2 Hydrogen Chemisorption [9]

Formation of chemisorbed monolayer is the most frequently used method for characterization of metallic catalysts. Generally, hydrogen adsorbs dissociatively on metals according to Equation 2-5:

$$H_2 + 2\ M_{(s)} \rightarrow 2\ M_{(s)}\text{-}H$$

Equation 2-5: Hydrogen chemisorption on metal surfaces.

From the volume of chemisorbed hydrogen required the formation of a monolayer v_m (cm^3, STP) on a sample with mass m (g) containing metal M ($g \cdot mol^{-1}$) with loading *wt.* (%), the metal dispersion D as a fraction of surface atoms is directly obtained from Equation 2-6:

$$D = v_m \cdot \frac{2}{22414} \cdot \frac{M}{m} \cdot \frac{100}{wt.} \qquad \text{Equation 2-6}$$

The hydrogen uptake was measured by a static volumetric method and conducted in a Sorptomatic 1990 instrument (ThermoFinnigan [10]). The Raney-catalyst (ca. 0.4 g) was activated at T = 383 K for 1 h in high vacuum (10^{-6} Torr). The sample was then equilibrated at 298 K and successive doses of hydrogen were admitted. The amount of adsorbed hydrogen was determined by measuring the pressure after a time delay (2 – 180 min) which was needed for reaching the adsorption equilibrium. To evaluate the volume of the chemisorbed monolayer v_m and the adsorption constant (b) a Langmuir isotherm was fitted assuming dissociatie adsorption of hydrogen (in linear form given by Equation 2-7). The linear fit included the data points that were recorded at the beginning of each isotherm and were equilibrated for at least 60 min; the R-squared value of the fit was 0.97 and 0.99 for Raney-Ni and Raney-Co catalysts, respectively. Figure 2-3 shows the results of the fitting procedure.

$$\frac{1}{v} = \frac{1}{v_m \cdot b^{0.5}} \cdot \frac{1}{p^{0.5}} + \frac{1}{v_m} \qquad \text{Equation 2-7}$$

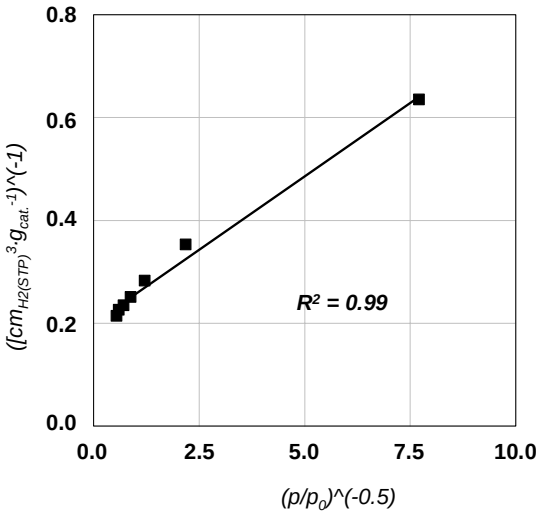

Figure 2-3: H_2-chemisorption on Raney-Co; data treatment.

The rate of rise of the Langmuir adsorption isotherm (b) in the region of low equilibrium pressures is determined by the heat of adsorption (q) and the temperature (T) [11].

2.2.4 Temperature Programmed Desorption

Temperature Programmed Desorption (TPD) is a technique in which a chemical process in monitored while the temperature is increased linearly in time [12, 13]. Following a pretreatment procedure, a probe molecule is first adsorbed on the surface. After removing the excess of the adsorbate (i.e., physisorbed molecules) the catalyst is heated and the amount and composition of the desorbing effluent is detected as a function of temperature. The surface coverage in the adsorbate (θ) can be obtained on a qualitative basis from the peak area). The peak position gives some information on the strength of the interaction between adsorbate and different adsorption sites.

The TPD experiments were performed in a custom built apparatus (Figure 2-4) consisting of a quartz sample tube (*1*) heated uniformly by an electrical oven (*2*). The sample tube is connected to a vacuum system separated from the pump by a liquid nitrogen trap (*3*). The sample was placed in the quartz tube under inert gas and activated *in situ* (details are provided in the corresponding chapters). A fraction of the desorbing molecules were passed to a mass spectrometer *via* a leak valve (*4*). The resulting MS-signals were normalized to the sample mass and the data series analyzed using m/e = 2 for hydrogen, m/e = 15 for ammonia, m/e = 18 for water, and m/e = 28 for nitrogen.

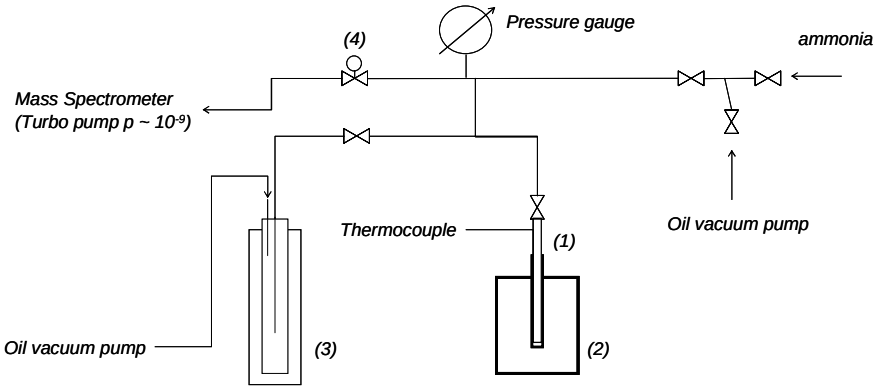

Figure 2-4: The TPD Setup.

2.2.5 Photoelectron Spectroscopy

With photoelectron spectroscopy, electrons are emitted by photoemmision, i.e., ionization with photons. When X-rays are used as excitation source the information about the core electrons of the sample is obtained. The kinetic energy of an emitted electron reflects the immediate surroundings of the parent atom. The binding energy (BE) of the electron in the parent atom is defined as equal to the difference between the initial photon energy ($h\nu$, where ν is the frequency of the monochromatic radiation used) and the maximum kinetic energy (KE) possessed by the electron when it is ejected (Equation 8) [14].

$$BE = h\nu - KE \qquad \text{Equation 2-8}$$

In X-ray photoelectron spectroscopy (XPS), X-ray radiation (commonly Mg Kα (1254 eV, 0.98 nm) or Al Kα (1487 eV, 0.83 nm)) are used to eject inner electrons in the core orbitals of atoms in the sample. The method is non-destructive and probes the material surface. Sampling depth is typically 20 – 100 Å, however, it varies in dependence on electron KE and material. Chemical shifts give information about oxidation states and chemical environment. One of the drawbacks is that surface charging (for example that of insulators) shifts BE scale. A simple method to remove the charging effect is the use of the C 1s signal due to carbon contamination [15].

Leybold LH 10 surface analytic system was used for the measurement of the Raney-catalyst surface composition by means of X-ray photoelectron spectroscopy (XPS). The samples were deposited on an adhesive, conducting tape and transferred to the instrument under protective atmosphere (Ar). Over each sample a survey spectra were collected. The detail spectra were excited with the Al Kα source and recorded in ΔE = constant mode. Repetitive scans of selected spectral regions and signal averaging were used in order to obtain a sufficient signal-to-noise ratio. To compensate for the charging the C 1s signal at 285 eV due to carbon contamination was used as a reference. The spectra resolution was 0.5 eV.

2.2.6 Adsorption at Solid-Liquid Interface

A rigorous thermodynamic treatment of the adsorption process from solution is somewhat complex because solute and solvent are both adsorbed at the liquid-solid interface [16]. However, if the solute is preferentially adsorbed and covers virtually all surface sites at low concentration, then frequently an empirical isotherm of Langmuir type is found (Equation 2-9) [17].

$$\frac{n^a}{n_L} = \frac{b \cdot c_a}{(1 + b \cdot c_a)}$$ Equation 2-9

where n^a is the amount of solute adsorbed at concentration c_a, n_L the amount adsorbed at the plateau, b an empirical constant To study adsorption in liquid phase, the chromatographic method was employed (the breakthrough method) using a custom built setup (Figure 2-5).

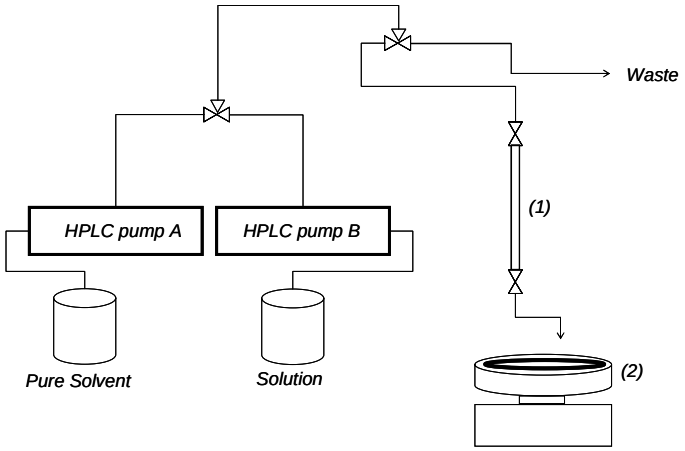

Figure 2-5: The solid-liquid interphase adsorption setup.

The setup includes a bed of catalyst (*1*) through which solutions (either pure solvent, or a solution of the adsorbate) were pumped at a constant rate. The effluent was sampled (*2*) and the composition evaluated by GC-chromatography. The flow was continued until a steady state for the adsorbate concentration was reached at the exit of the reactor. The concentration of adsorbate on the catalyst surface was calculated from the area between the breakthrough curves of adsorbate and a reference.

2.2.7 Calorimetrically Measured Heat of Adsorption

Calorimetry is used to determine the heat released or absorbed in a chemical reaction. To measure the heat of adsorption of butyronitrile over different catalyst sample a C80 II Calvet Calorimeter was used (Setaram Scientific and Industrial Equipment [18]).Calorimetric experiments were carried out in a C80 II Calvet Calorimeter (Setaram Scientific and Industrial Equipment). For a typical calorimetric experiment catalyst sample (0.5 g) was sealed under vacuum in a glass ampoule. The ampoule was placed in a metal vessel and covered with butyronitrile (2.5 g). The vessel was closed and placed inside the calorimeter together with a reference vessel of the same mass, and heated up to 371.85 K (ramp 1 $K \cdot min^{-1}$). The vessel was equilibrated at this temperature over 5 h. At the end of the equilibration period the ampoule was broken and the heat flow was recorded over next hours (2 - 3 h) until all the heat transfer effects ceased. An average of 2 - 3 results over each catalyst was taken as a measure of the heat of adsorption of butyronitrile. The estimated error of the measurement was about 1 $J \cdot g_{catalyst}^{-1}$.

2.3 Catalytic Tests

A schematic diagram of the setup used in the catalytic tests is presented in Figure 2-6.

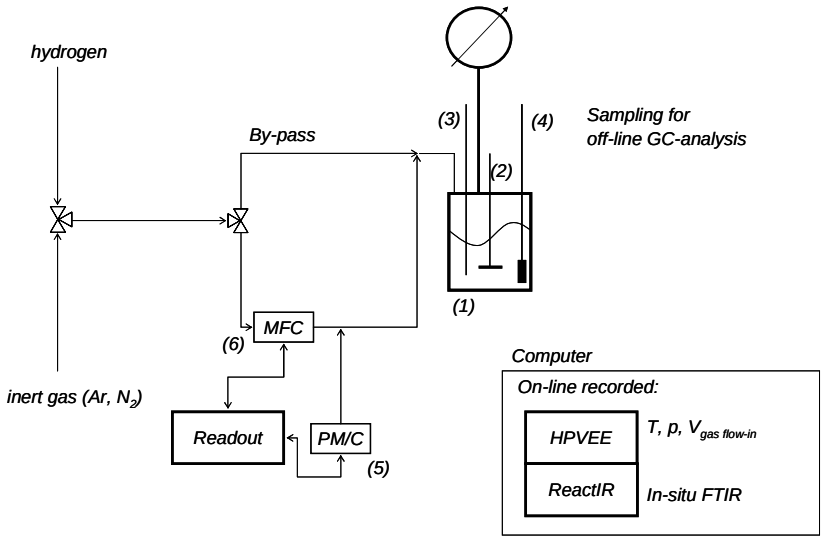

Figure 2-6: Experimental setup for catalytic testing.

The setup includes a high-pressure 160-cm^3 batch reactor (Parr) (1) equipped with a mechanical stirrer (2), a thermocouple (3), and a sampling loop (0.59-cm^3) (4) ended with a metal filter. A pressure meter/controller (5) (Bronkhorst High-Tech B.V P-502C-FZC-

39-V) and a mass flow controller (6) (Bronkhorst High-Tech B.V. F-201C-FAC-33-V) allowed to maintain a constant pressure during the experiments. The temperature, pressure and hydrogen consumption were recorded on-line using a program written in Hewlett-Packard Visual Engineering Environment (HP VEE 5.0). In conjunction with the setup the composition of the reaction mixture was analyzed by *in situ* IR spectroscopy using a diamond ATR crystal (ReactIR).

2.3.1 Catalytic Testing Procedure

The autoclave was charged at ambient conditions with catalyst suspended in the reaction mixture. Then, the autoclave was pressurized several times with inert gas (up to 7.5 bar) to expel air. If necessary, ammonia was then added from a loop with defined volume. The reaction mixture was heated and allowed to equilibrate at the desired temperature. The experiment was started by pressurizing the reactor with hydrogen: the reactor was filled within several seconds to the desired hydrogen pressure *via* a by-pass. Subsequently the hydrogen flow was switched to stream *via* the mass flow controller. The sampling procedure for off-line GC-analysis was as follows: through a three-way valve a sample was taken to the sample loop and released into a single use syringe. Then the loop was cleaned with pentane (3 - 5 cm^3) and flushed with dry air. The samples were sealed inside 1.5-cm^3 vials. GC-analysis was performed on a HP Gas Chromatograph 5890 equipped with Automatic Sampler and Injector HP 7673A using a 30-m RESTEK Rtx - 5 Amine column. The GC temperature program was as follows: dwell 4 min at 313 K; ramp 15 $K \cdot min^{-1}$ up to 473 K, dwell 5.33 min at 473 K. The retention times for n-butylamine, butyronitrile, N-butylidene-butylamine, di-n-butylamine and tri-n-butylamine were 5.9, 6.9, 11.75, 12.2, 15.4 minutes, respectively.

2.4 Characterization of the Catalytic Process with Vibrational Spectroscopy

Vibrational spectroscopy was used to provide both qualitative and quantitative information on molecular species present during catalysis.

2.4.1 *In Situ* Attenuated Total Internal Reflectance Infrared Spectroscopy (ATR-IR)

Vibrations in a molecule can be excited by the absorption of photons of electromagnetic radiation with wavelengths in the range: 500 to 1.1 μm (infrared region). A great

advantage of IR spectroscopy is that the technique can be used to study a catalytic process *in situ.* In particular, ATR-IR technique was employed to follow the concentration of reactants in the liquid phase at high hydrogen pressure and temperature.

2.4.1.1 The Nature of ATR Spectra [19, 20]

Total internal reflection can occur on the interface of an IR-transparent crystal and a sample. There are certain geometric requirements for this and importantly the refractive index of the crystal must exceed that of the sample. Specifically, if the IR beam comes in at incident angle α_i , the condition for the total internal reflection is:

$$\sin(\alpha_i) > \frac{n_{sample}}{n_{crystal}} \qquad \text{Equation 2-10}$$

The IR-radiation is actually not perfectly confined inside of the crystal and penetrates a very short distance into the sample (depth typically in the order of the wavelength of the radiation, see Figure 2-7). As a result, the internally reflected light carries information about the infrared absorption of the sample. The sampling depth changes in two fundamental ways: it decreases as the refractive index of the crystal increases and decreases as the incidence angle is increased.

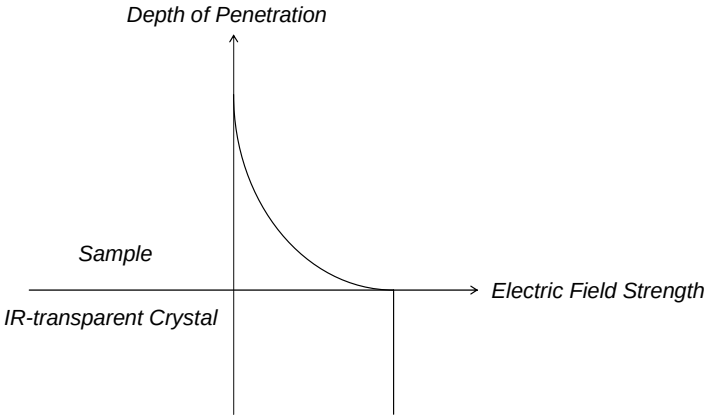

Figure 2-7: The ATR Experiment.

In most ATR probes multiple reflections are used to enhance the resolution, e.g., in the horizontal arrangement as presented in Figure 2-8.

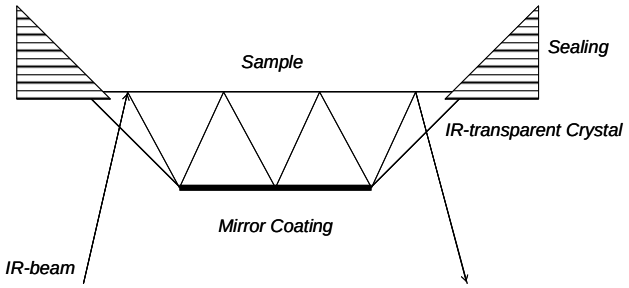

Figure 2-8: Arrangement of an ATR-probe for Multiple Internal Reflections.

In situ IR analysis of the reaction mixture provided time resolved (TR) IR-spectra. Quantification of the transient concentration of butyronitrile, mono- and di-n-butylamines and N-butylidene-butylamine was based on integration of the IR peaks using two (or one) baseline points. Butyronitrile, mono- and di-n-butylamines and N-butylidene-butylamine were identified by characteristic IR-regions (Table 2-3). A linear correlation between the IR-band intensity and the transient concentration of each compound in the reaction mixture was assumed. The IR-profiles were referenced to the corresponding concentration profiles obtained by GC chromatography. Experimental details for the experiment are included in Appendix 1.

compound	IR-position [cm^{-1}]	description
butyronitrile	1348 - 1337	fingerprint region; some specific vibration of the whole molecule
n-butylamine	broad band 850 - 750	$-NH_2$ wagging and twisting vibrations
di-n-butylamine	1133	asymmetric CH_2-NH-CH_2 stretching vibration
N-butylidene-butylamine	1671	C=N stretching vibration

Table 2-3: Characteristic bands for butyronitrile, mono and di-n-butylamine and N-butylidene-butylamine.

2.4.1.2 ReactIR 1000 setup

A Fourier Transform Infrared (FTIR) ReactIR 1000 Reaction Analysis System (Mettler Toledo GmbH [21]) was used to follow the concentration of reactants in the liquid phase. The setup includes an optical module, electronic module, sample interface module (SIM) and a computer workstation. A 0.625'' DiComp probe (diamond, gold seal) with an optical range 4400 - 2150 and 1950 - 650 cm^{-1} was used. The probe operates in the

temperature range 193 – 523 K and pressure up to 100 bar. The software ReactIR v. 2.21 was used to analyze the infrared spectra collected.

2.4.2 Inelastic Neutron Scattering (INS)

Alternatively to absorption, an inelastic scattering can be used as a method for measuring the vibrational spectrum. Here, the energy of incident and scattered quantum particles are compared. The INS spectroscopy has no selection rules and is highly sensitive with respect to hydrogen-involved motions.

2.4.2.1 The INS Theory [22]

James Chadwick was awarded the Nobel Price in Physics in 1935 for the discovery of the neutron [23]. The most important feature of a neutron is that while passing through matter, it loses energy in collisions with the atomic nuclei but not with the electrons as its charge is zero. Neutrons possess a mass and a nuclear spin of ½. The collision of a neutron with an atomic nucleus, although much more frequent than with an electron, is a rare event, for the forces between a neutron and a nucleus are very small except at distances of the order of 10^{-14} m. Thus, neutrons are highly penetrating and can be used as nondestructive probes. Neutrons are quantum particles and their wavelengths (according to the de Broglie relation) and energy at thermal equilibrium with the surrounding match the typical interatomic spacing and excitation, respectively, in condensed matter. This is in contrast to other probes which typically have either the appropriate wavelength range (X-rays) or energy range (photons) but not both.

In the scattering process neutrons will impart momentum to the scatter and their spin can be flipped. The most general neutron scattering process is described by the energy (Equation 2-13) and momentum transfer (Equation 2-14):

$$\hbar\omega = E_0 - E \qquad \text{Equation 2-11}$$

$$\hbar\vec{Q} = \hbar(\vec{k}_0 - \vec{k}) \qquad \text{Equation 2-12}$$

where E_0 is the incident neutron energy. The incident neutron wavelength is related to its wavevector by $k_0 = 2\pi/\lambda$. Elastic scattering corresponds to $k = k_0$, so that only momentum is transferred. The neutron – nuclear interaction is essentially a point

interaction, though, it is fairly complex and there is no simple way of knowing *a priori* which nuclei have larger neutron scattering length. The interaction potential can be represented by a δ function (Equation 2-15).

$$V(\mathbf{r}) = \frac{2 \cdot \pi \cdot \hbar^2}{m} \cdot b \cdot \delta(\mathbf{r}) \qquad \text{Equation 2-13}$$

where *b* is the nuclear scattering length (a complex number). The total scattering cross-section can be separated into a coherent and an incoherent part (Equations 2-16). In addition, the nucleus may absorb neutrons (absorption cross-section). All those values are usually determined by experiment and are tabulated [24] (Table 2-4).

$$\sigma_{coh} = 4\pi \langle b \rangle^2 \quad \sigma_{inc} = 4\pi \left(\langle b^2 \rangle - \langle b \rangle^2 \right) \qquad \text{Equation 2-14}$$

Element	$\sigma_{coherent}$	$\sigma_{incoherent}$	σ_{abs}
^{1}H	1.7583	80.27	0.3326
^{2}H	5.592	2.05	0.000519
^{3}H	2.89	0.14	0
Be	7.63	0.0018	0.0076
^{12}C	5.559	0.0	0.00353
^{14}N	11.03	0.5	1.91
Al	1.495	0.0082	0.231
Co	0.779	4.8	37.18

Table 2-4: Coherent, incoherent and absorption cross-sections, in barns (1 barn = 10^{-28} m^2) for the elements of interest [21].

INS can be used as a surface sensitive technique due to the high scattering contrast. For example, hydrogen containing adsorbates on metal surfaces can be studied due to the low absorption cross-section of most elements whereas the incoherent scattering length for ^{1}H is high.

2.4.2.2 The INS Spectrometer

The INS experiments were carried out at Institut Laue Langevin (ILL) (Grenoble/France). Neutrons were provided by the high-flux reactor which operates at a thermal power of 58 MW using a single fuel-element with an operating cycle of 50 days [25, 26]. The INS spectra were recorded on the IN1-BeF three-axis spectrometer. The main components are shown in Figure 2-9 [27]. The monochromatization of the incident beam is achieved in three energy ranges by Bragg scattering from the (200), (220) and (331) planes of a copper monochromator. During the energy scans, the spectra are normalized to an incident neutron flux monitor which has efficiency proportional to the wavelength. The scattered neutrons are passed through a beryllium filter which transmits only those neutrons that have a mean energy of approximately 30 cm^{-1} and analyzed in a ^{3}H-detector.

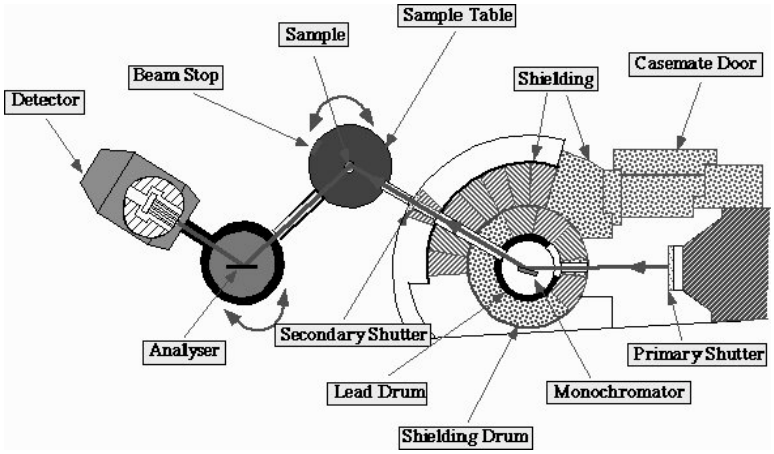

Figure 2-9: IN1 Hot Neutron Three-Axis Spectrometer at ILL (Grenoble/France) [23]

2.5 Calculation Methods

2.5.1 Thermodynamic equilibrium

2.5.1.1 Thermodynamic Equilibrium Calculated from the Experimental Data.

Thermochemical calculations were based on enthalpy H, entropy S, heat capacity Cp or Gibbs energy G values for each chemical species. Thses values can all be derived from experimental observations and are stored in data bases. A simulation of the thermodynamic equilibrium for a mixture of hydrogen, butyronitrile, n-butylamine, di-n-butylamine, tri-n-butylamine and ammonia was performed in the range 1 to 100 bar

pressure and 298 to 423 K temperature using HSC Chemistry 5.1 software (Outokumpu Research Oy [28]). For the calculations a two-phase system comprising gas (H_2, NH_3) and liquid (all other species) was assumed. As starting point for the calculations an excess of hydrogen relative to butyronitrile was used (99:1 mole ratio) and zero mole amount of all other species. Ideal solutions with activity coefficient = 1 and a constant heat capacity C_p for butyronitrile and butylamines were assumed. It should also be noted, that at some temperatures and pressures the equilibrium was inaccurate due to a phase change of the reactants (e.g., at high pressure and low temperature only liquid ammonia exists). The selectivity to n-butylamine was calculated as the molar ratio of n-butylamine to the sum of all other products (i.e., ammonia, and primary, secondary and tertiary n-butylamines).

Compound	Phase	Enthalpy [kJ·mol^{-1}]	Entropy [J·mol^{-1}·K^{-1}]	[(a)]Heat Capacity Coefficients	Temperature range [K]
hydrogen H_2	gas	0	130.679	A =16.92 B = 61.459 C = 0.59 D = -79.559	T_1 = 298.15 T_2 = 400.00
ammonia NH_3	gas	-45.94	192.778	A =25.794 B = 31.623 C = 0.351 D = 0	T_1 = 298.15 T_2 = 800.00
butyronitrile C_4H_7N	liquid	-7.272	221.702	A = 149.909 B = 0 C = 0 D = 0	T_1 = 298.15 T_2 = 298.16
n-butylamine $C_4H_{11}N$	liquid	-129.541	252.149	A = 190.33 B = 0 C = 0 D = 0	T_1 = 298.15 T_2 = 298.16
di-n-butylamine $C_8H_{19}N$	liquid	-208.242	392.97	A = 314.85 B = 0 C = 0 D = 0	T_1 = 298.15 T_2 = 298.16
tri-n-butylamine $C_{12}H_{27}N$	liquid	-277.608	502.699	A =409.329 B = 0 C = 0 D = 0	T_1 = 298.15 T_2 = 298.16

[(a)] *Heat Capacity Formula (The Kelly equation) :* $C_p = A + B\cdot10^{-3}\cdot T + C\cdot10^{5}\cdot T^{-2} + D\cdot10^{-6}\cdot T^{2}$ *[J·mol^{-1}·K^{-1}]*

Table 2-5: Thermodynamic data for the calculation of the equilibrium composition of a mixture hydrogen, ammonia, butyronitrile, and 1°, 2° and 3° n-butylamines.

2.5.1.2 Thermodynamic Equilibrium Computed *ab initio*.

Using density-functional theory (DFT) the total ionic and electronic energy of a molecule (E_{Total}) can be calculated at 0 K. At the ground state (optimal geometric structure) a vibrational frequency run for 3N-6(5) normal mode frequencies can provide electronic, vibrational, translational and rotational contributions for the internal energy (U) and entropy of the molecule i.e., $\Delta U = \Delta E_{total} + \Delta E_{vib} + \Delta E_{trans} + \Delta E_{rot}$ and $\Delta S = \Delta S_{vib} + \Delta S_{trans}$

$+\Delta S_{rot}$, (at T = 0 K, $S^0 = 0$), respectively. To determine ΔG^T of a reaction from first principles calculations one uses the relation: G = H - T·S and a thermodynamic cycle. In the cycle ΔH^T and ΔS^T can be calculated knowing the reaction enthalpy and entropy at T_0 and the heat capacities of the product and reactants between T_0 and T.

In order to calculate thermodynamic properties of a molecule different Dmol[3] software from Cerius[2] suite was used. Each run 'Optimization & Frequency' included (*i*.) minimization of the energy for a molecule followed by (*ii*.) computation of the IR/Raman frequencies of the system at the optimized geometry. Generalized gradient approximation (gga) DFT method with Perdew-Wang 1991 (p91) Hamiltonian and double numeric functions together with polarization functions atomic basis functions (DNP) in expansion of molecular orbitals was used in the runs [29]. Finally, the equilibrium constant as a function of temperature was calculated.

2.5.2 DFT Search for a Transition State

Feasibility and rate of a certain chemical reaction crucially depends on the transition state energy and structure. A transition state (TS) is defined as the geometry at the energy peak of a chemical reaction from reactant to product molecules. Halgren and Lipscomb [30] introduced the linear synchronous transit (LST) and quadratic synchronous transit (QST) methods for searching for the transition states. The LST method performs a linear geometric interpolation between the reactant and product structures and a series of single point energy calculations are performed to find the maximum energy along this path. The energy of the system at this geometry gives an upper limit to the transition state energy. For refining the LST transition state structure a single energy minimization is performed in a direction perpendicular to the original LST path to yield a new intermediate structure. A quadratic interpolation is then performed between the reactant, product and this intermediate structure to define a QST path. Single point energy calculations are then performed to obtain the maximum energy on the QST path. This procedure gives a refined estimate for the transition state geometry and provides a good approximation of the transition state energy.

A search for the TS of the tautomerization reaction from ethylideneamine to vinylamine was done with Dmol[3]. Both reactants were optimized at the ground state (0 K) with DFT

gga(p91) functional using double numeric (DN) atomic basis functions. Next, a run for QST Transiton State search was performed. Finally, TS was optimized [31].

Acknowledgment

Xavier Hecht and Andreas Marx are thanked for the help during constructing of the catalytic test setup and HPVEE programming. Martin Neukamm and Jan Prochazka (Institut für Chemie Anorganischer Materialien, TUM) are thanked for the AAS and XRD measurements, respectively. Alexander Guzman, Dr. Olaf Jaurich (Mettler Toledo) and Carsten Minkley (Porotec) are thanked for the introduction to the TPD, ReactIR and the Sorptomatic 1990 instruments, respectively. Dr. Maritza Veprek-Heijman (Institut für Chemie Anorganischer Materialien, TUM) is thanked for the XPS measurement and help with the data interpretation. Dr. Alexander Ivanov (Institut Laue-Langevin, France) is thanked for supervising of the IN1-BeF spectrometer during the INS experiments.

References

1 http://www.gracedavison.com/

2 R.A. Benkeser and D.C. Snyder, J. Organomet. Chem. 225 (1982) 107

3 K.S.W. Sing and J. Rouquerol in: G. Ertl, H. Knözinger, J. Weitkamp (Eds.) Handbook of Heterogeneous Catalysis Vol.2, VCH-Wiley, Weinheim, 1997, p. 429

4 S. Brunauer, P.H. Emmett and E. Teller, J. Am. Chem. Soc. 60 (1938) 309

5 K.S.W. Sing and J. Rouquerol in: G. Ertl, H. Knözinger, J. Weitkamp (Eds.) Handbook of Heterogeneous Catalysis Vol.2, VCH-Wiley, Weinheim, 1997, p. 430

6 http://www.porotec.de/ and http://www.thermo.com/

7 D. Dollimore and G.R. Heal, J. Appl. Chem.14 (1964) 109

8 G. Bergeret and P. Gallezot in: G. Ertl, H. Knözinger, J. Weitkamp (Eds.) Handbook of Heterogeneous Catalysis Vol.2, VCH-Wiley, Weinheim, 1997, p. 446 – 450

9 G. Bergeret and P. Gallezot in: G. Ertl, H. Knözinger, J. Weitkamp (Eds.) Handbook of Heterogeneous Catalysis Vol.2, VCH-Wiley, Weinheim, 1997, p. 442 – 446

10 http://www.porotec.de/ and http://www.thermo.com/

11 G. Wedler, Chemisorption: An Experimental Approach, Butterworths, London, 1976, 22 – 32

12 J.W. Niemantsverdriet, Spectroscopy in Catalysis – An Introduction, VCH-Wiley, Weinheim, 1993, p. 11 – 35

13 J.L. Falconer and J.A. Schwarz, Catal. Rev. Sci. Eng. 25(2) (1983) 141

14 I.M. Campbell, Catalysis at Surfaces, Chapman and Hall Ltd., London and New York, 1988, p. 115 - 116

15 G. Moretti, in: G. Ertl, H. Knözinger, J. Weitkamp (Eds.) Handbook of Heterogeneous Catalysis Vol.2, VCH-Wiley, Weinheim, 1997, p. 632 – 641

16 A. Dabrowski and M. Jaroniec, Adv. Colloid Interface Sci. 31 (1990) 155

17 K.S.W. Sing and J. Rouquerol in: G. Ertl, H. Knözinger, J. Weitkamp (Eds.) Handbook of Heterogeneous Catalysis Vol.2, VCH-Wiley, Weinheim, 1997, p. 435

18 http://www.setaram.fr

19 A. Shchegolikhin and O. Lazareva, Int. J. Vib. Spect. [www.ijvs.com] 1(4) (1997) 38 - 47

20 D. Coombs, Int. J. Vib. Spect. [www.ijvs.com] 2(2) (1998) 3 – 4

21 http://www.asirxn.com/

22 J. Eckert, Spectrochim. Acta 48 (1992) 271

23 J. Chadwick, Nobel Lecture entitled: 'The neutron and its properties' (1935)

24 http://www.ncnr.nist.gov/resources/n-lengths/list.html from Neutron News 3(3) (1992) 29

25 Commissariat a l'Energie Atomique, Bulletin d'Informations Scientifiques et Techniques (BIST), 165 (December 1971) and 166 (January 1971)

26 P. Ageron , Nucl. Instr. and Meth. A 284 (1989) 197199

27 The Yellow Book: Guide to Neutron Research Facilities at the ILL, Institut Max von Laue-Paul Langevin, Grenoble-France, December 1997

28 http://www.outokumpu.com/

29 Accelrys Training Manual: Calculating free energies of chemical reactions, Catalysis Consortium, Cambridge UK, February 2002

30 T.A. Halgren and W.N. Lipscomb, Chem. Phys. Lett. 49 (1977) 225

31 Accelrys Training Manual: Optimization and TS search using DMol^3

Chapter 3

The performance of Raney-Ni, Raney-Co, Ni-Cr promoted Raney-Co and LiOH-modified Raney-Co as catalysts in the hydrogenation of butyronitrile to n-butylamine in a three-phase reactor was studied. Each catalyst was characterized thoroughly to explain differences in the activity and the selectivity.

The rate of the hydrogenation reaction depends on the fraction of the catalyst BET area that is free from inactive multi-oxide deposits and is able to adsorb the reactants. The adsorption of the reactants depends on the catalyst metal and surface applied modifiers (i.e., LiOH). The selectivity of the reaction depends on the rate of a bi-molecular side-reaction forming N-butylidene-butylamine. The most important factor that controls the rate of the side-reaction is the surface concentration in partially hydrogenated species. Later could be lowered by doping cobalt catalysts with LiOH due to adsorption phenomena and an increased ratio of reactive hydrogen to unsaturated surface-adsorbed species.

3 Characterization of Raney-Ni and Raney-Co Catalysts and Their Use in the Selective Hydrogenation of Butyronitrile

3.1 Introduction

The reduction of nitriles with hydrogen to primary amines is a large-scale commercial process [1]. One of the most important applications is the synthesis of the nylon-6,6 monomer 1,6-diaminohexane from 1,4-dicyanobutane [2, 3]. The hydrogenation of the C≡N group proceeds through reactive intermediates such as imines [4, 5]. As a consequence condensation reactions can occur and mixtures of ammonia and primary, secondary and tertiary amines are frequently obtained. The factors that influence the selectivity of the heterogeneous catalysts are manifold and originate from catalyst composition (i.e., choice of the catalytically active metal and support, presence of promoters) and reaction conditions [6]. The highest selectivities in the conversion of nitriles to primary amines have been reported for Co, Ni and Ru catalysts [7]. In contrast, nitriles can be hydrogenated to secondary and tertiary amines using Rh, Pd and Pt catalysts [8]. In the industrial process elevated hydrogen pressures (up to 600 bar), and ammonia as solvent are employed in order to ensure a high selectivity to primary amines. Skeletal metal catalysts (mainly Raney-Ni and Raney-Co) provide the lowest cost per unit mass of active catalyst and are widely used [9]. The selectivity of Raney-Ni and Raney-Co in the synthesis of primary amines can be enhanced by addition of small amounts of alkali metal hydroxides [10, 11, 12]. Raney-Ni is one of the most frequently studied unsupported catalysts and the base effect on selectivity has been investigated in respect to the catalytic performance [13, 14]. In contrast, only few reports on Raney-Co have been published [e.g., 15, 16, 17, 18]. In this work, the hydrogenation of butyronitrile was used as a model reaction for the catalytic reduction of nitriles over Raney-catalysts (Figure 3-1). The aim was to understand the differences in the catalytic performance of Raney-Ni and Raney-Co.

In general, Raney-Co provides a higher selectivity to amines compared to Raney-Ni. Potential factors are evaluated on the basis of a detailed characterization of the catalysts. Furthermore, the increase in the selectivity to n-butylamine which is observed after

modifying Raney-Co with LiOH was explored. It is shown, that a high selectivity to n-butylamine can be achieved without using ammonia as solvent.

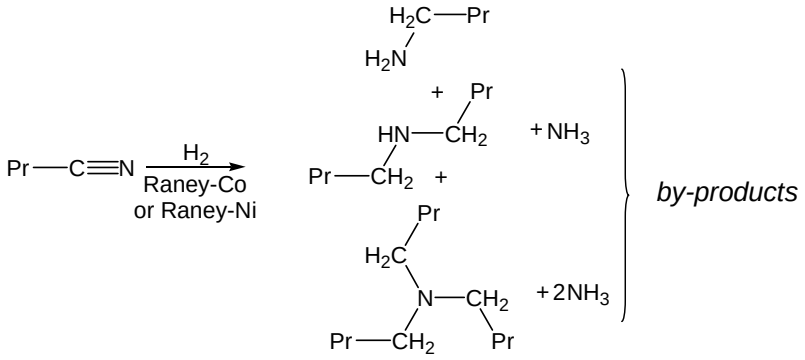

Figure 3-1: The hydrogenation of butyronitrile can yield a mixture of primary, secondary and tertiary n-butylamines and ammonia.

3.2 Experimental

3.2.1 Catalysts and Chemicals

Active Raney-Ni, Raney-Co and NiCr-promoted Raney-Co were obtained as aqueous suspension from the GRACE Davison Chemical Division of W.R. Grace & Co. The promoted Raney-Co catalyst contained about 2.8 and 2.2 wt. % of Ni and Cr, respectively. The concentration of added transition metals in the unpromoted Raney-Co and Raney-Ni was below 0.5 wt. %. Each sample contained some unleached aluminum (6.77, 1.85 and 3.50 wt. %, respectively). The mean grain size of Raney-Ni, Raney-Co and Raney-Co (NiCr) was 45.61, 30.08 and 28.52 μm, respectively. The catalysts were washed with de-ionized water until pH 7 was reached, dried in a flow of Ar (4 h at 328 K, and 1 h at 378 K) and subsequently handled under inert atmospheres. For doping with LiOH, a washed sample of Raney-Co (143 g) was suspended in an aqueous solution of LiOH (3.254 g in 100 cm^3 de-ionized water), water was removed in partial vacuum (< 4 mbar) and dried (10 h at 323 K). The concentration of Li^+ in the dry sample was 0.5 wt. % as measured with AAS (UNICAM 939 AA-Spectrometer). All chemicals used in this study were obtained from commercial suppliers and used as provided. These were as follows: butyronitrile, (≥ 99 % GC-assay, Fluka), 1°, 2° and 3° n-butylamines (> 99 % gc-assay, Aldrich), solvents: n-octane and n-undecane (≥ 99 GC-assay, Aldrich) and gases: H_2, Ar, NH_3 (99.999, 99.999 and 99.98 vol. %, respectively).

3.2.2 Setups and Experimental Procedures

Powder X-ray diffraction using Siemens D-5000 powder diffractometer was done on a wax-coated sample of Raney-Co.

The BET and H_2-chemisorption measurements were carried out in a fully computerized Sorptomatic 1990 instrument (ThermoFinnigan). The catalyst samples (ca. 1 and 0.4 g, respectively) were outgassed in high vacuum using turbomolecular pump for 1 h at the desired temperature of activation (298 – 633 K). The BET measurements were carried out at T = 77 K using N_2 as probe molecule. The H_2-chemisorption isotherms were recorded at T = 298 K, allowing to equilibrate between 2 and 180 min for each equilibration point.

Temperature programmed desorption measurements were carried out in a custom built vacuum setup (Figure 2-4). For TPD of residual adsorbates (i.e., hydrogen and water), the catalysts sample (ca. 50 mg) was outgassed for 8 h at 378(5) K. Then the temperature was raised with an increment of 10 $K \cdot min^{-1}$ up to 973 K. The mass spectrometer (MS) signal for $m/z^+ = 2$ and 18 was used to monitor hydrogen and water, respectively. The relative number of desorbing molecules was estimated from the area under the corresponding MS trace. To determine the location of the desorption maxima each MS trace was fitted with Gaussian curves. For NH_3-TPD experiments, samples (ca. 100 mg) were outgassed and heated at 5 $K \cdot min^{-1}$ up to 473 K. After maintaining this temperature for 5 min the sample was cooled to 423(5) K at which temperature it was left in dynamic vacuum for ca. 12 h. Subsequently, the sample was equilibrated with ammonia (T = 423 K, $p_{NH3} = 1 \pm 0.3$ mbar, 1 h) and outgassed for another 3 h. Finally, the sample was heated (10 $K \cdot min^{-1}$) and desorption of ammonia was followed with MS using $m/z^+ = 15$.

For X-ray photoelectron spectroscopy (XPS) a Leybold LH 10 surface analytic system was used. The samples were deposited on an adhesive, conducting tape and transferred to the instrument under Argon. For each sample a survey spectrum was collected. The detailed spectra were excited with an Al Kα (1486.6 eV, 0.83 nm) source and recorded in ΔE = constant mode. Repetitive scans of selected spectral regions and signal averaging were used in order to obtain a sufficient signal-to-noise ratio. To compensate for charging the C 1s signal at 285 eV due to carbon contamination was used as a reference [19]. The spectral resolution was 0.5 eV.

Adsorption study at liquid-solid interphase was carried out in a custom built setup (Figure 2-5). For the adsorption isotherms (at T = 293 K) a chromatographic column of the catalyst (ca. 2.5 g) was equilibrated with pure solvent. A solution of the adsorbate and octane (both 12.5 $mmol \cdot dm^{-3}$) in pentane was passed at constant rate (2.2-2.3 $cm^{3} \cdot min^{-1}$) over the column. The effluent was sampled every 0.2 min and the composition evaluated by gas chromatography. The concentration of the adsorbate was then increased step-wise to 25, 50, 75 or 100 $mmol \cdot dm^{-3}$ and the flow continued until a steady state for the adsorbate concentration was reached at the exit of the reactor. To follow the characteristics of the setup, the concentration of a weakly adsorbing marker (octane) was increased in parallel to the adsorbate. In order to estimate the competitive sorption of two adsorbates, an equimolar solution of n-butylamine and butyronitrile was passed over the catalyst column. The reversibility of the adsorption of n-butylamine and butyronitrile on parent and LiOH-modified catalyst surface was also tested. First, a solution of the adsorbate (either n-butylamine or butyronitrile) was pumped through the catalyst column. Once the breakthrough of the reference and the adsorbate was observed and a steady state was reached at the outlet of the column, the pure solvent was passed over the column. The concentration of adsorbate on the catalyst surface in the adsorption experiment was calculated from the area between the breakthrough curves of adsorbate and reference.

Calorimetric experiments were carried out in a C80 II Calvet Calorimeter (Setaram Scientific and Industrial Equipment). The catalyst (0.5 g) was sealed under vacuum in a glass ampoule. The ampoule was placed in the sample holder and covered with butyronitrile (2.5 g). The vessel was closed and placed inside the calorimeter together with a reference vessel of the same mass, and heated to 371.85 K (1 $K \cdot min^{-1}$). The vessel was equilibrated at this temperature over 5 h. The ampoule was broken and the heat flow was recorded over 2 - 3 h until all heat transfer effects had ceased. The average of 2 - 3 measurements is stated as the heat of adsorption of butyronitrile. The estimated error of the measurement was about 1 $J \cdot g_{catalyst}^{-1}$.

The hydrogenation of butyronitrile was carried out in a high-pressure 160-cm^3 semi-batch reactor at constant hydrogen pressure. The reactor was equipped with a mechanical stirrer, a thermocouple, and a sampling loop (Figure 2-6). A test on mass transfer limitations showed that the reaction rate for the hydrogenation of butyronitrile over

Raney-Co at 393 K did not depend on the stirring speed in the range 1000 – 1850 rpm. Because of the lower rate of reaction at lower temperatures used in this study no mass transfer limitations were projected. The reactor was charged with a suspension of the catalyst (0.200 g) in octane. The mixture was outgassed and butyronitrile added under a flow of argon. The mixture was stirred at 1500 rpm and equilibrated at the desired reaction temperature for 45 - 60 min. Introduction of hydrogen was defined as the start of the hydrogenation. During the experiment a number of samples were taken for off-line GC-analysis. The GC-samples were analyzed with HP Gas Chromatograph 5890 equipped with a crosslinked 5% diphenyl-95% dimethyl-polysiloxane column 30 m, Restek GmbH, Rtx-5 Amine. n-Undecane was used as an internal standard. The hydrogenation of butyronitrile in dependence on the starting concentration of butyronitrile (0.25, 0.50 and 0.75 $mol \cdot dm^{-3}$), the hydrogen pressure (15, 30 and 45 bar) and the reaction temperature (353, 373 and 383 K) was tested.

3.3 Results

3.3.1 Particle Size and Structure of Raney-Co

X-ray diffraction patterns for Raney-Co and metallic cobalt foil are shown in Figure 3-2.

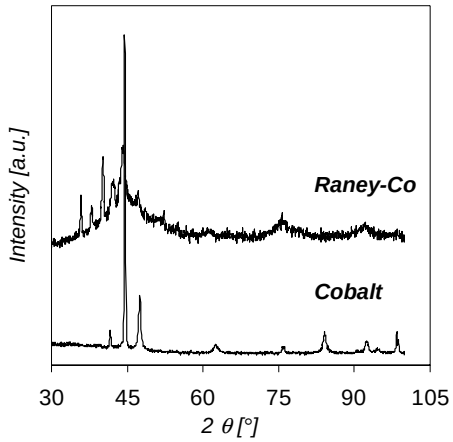

Figure 3-2: X-ray diffraction pattern for Raney-Co and cobalt foil.

The crystallite size of the hexagonal closed packed Raney-Co was between 12 and 15 nm (the signal intensity was too poor to allow for an exact calculation of crystallite size using the Warren-Averbach analysis). Some peaks in the diffractogram could not be identified or attributed to face center cubic cobalt. The comparison of the mean grain size of Raney-Co (30 μm) to the crystallite size indicates that a large spongy particle of Raney-Co consists of a number of strongly associated primary crystallites.

3.3.2 Specific Surface and Accessible Metal Surface Area

In principle, the specific surface area for a skeletal metal catalyst corresponds to the number of exposed metal atoms, because the material contains (apart from its main metallic constituent) only small amounts of aluminum and alumina, which were not removed during preparation (Table 2-1). In order to check the validity of that assumption the specific surface area measured according to the BET method is compared with the concentration of chemisorbed hydrogen. The nitrogen and hydrogen adsorption results for the four catalysts are presented in Table 3-3 and in Figure 3-4 and Table 3-1, respectively.

$T_{activation}$ [K]	Raney-Co	Raney-Co/LiOH	Ni-Cr promoted Raney-Co	Raney-Ni
298	[(a)]19.16 [(b)](0.094)	14.78	67.50	55.38
383	19.27	14.84 (0.095)	66.75 (0.133)	57.65 (0.130)
483	24.60	-	61.71	52.18
533	24.07	-	-	-
583	23.70	-	-	47.93
633	19.46	-	-	45.72

(a) in [$m^2 \cdot g^{-1}$]

(b) the numbers in brackets indicate the pore volume [$cm^3 \cdot g^{-1}$]

Table 3-1: BET area measured after outgassing the catalyst samples (ca. 1 g) at $T_{activation}$ for 1 h.

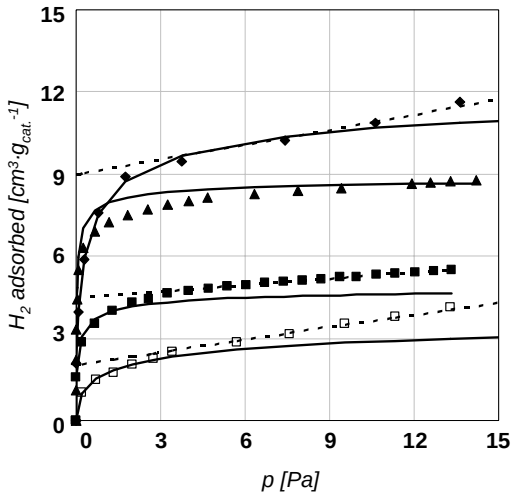

Figure 3-3: Hydrogen adsorption isotherms at 298 K, after outgassing ca. 0.4 g catalyst samples at 383 K for 1 h. (♦) Raney-Co (NiCr), (▲) Raney-Ni, (■) Raney-Co and (□) Raney-Co(LiOH). At higher pressures the Langmuir isotherm fit was inadequate for Raney-Co catalysts. Thus, two different types of adsorption sites were assumed representing strong (i.e., Langmuir isotherm - solid lines - at low pressure) and weak (Henry's isotherm - broken lines - at high pressure) hydrogen adsorption on the surface.

catalyst	(a) v_m [$cm^3_{H2} \cdot g_{cat}^{-1}$]	b [kPa^{-1}]	n_{H2} [mmol]	$n_{catalyst\ metal}$ [mmol]	(b) Dispersion [%]
Raney-Ni 92.83 [wt. %] Ni	8.9(2)	26 - 50	0.40197	15.8161	5.08
Raney-Co 97.51 [wt. %] Co	5.0	12.2	0.22583	16.5459	2.73
Raney-Co (NiCr) 91.26 [wt. %] Co	12.6	2.8	0.56908	15.4853	7.35
Raney-Co (LiOH) 80.69 [wt. %] Co	4.2	0.5	0.18970	13.6915	2.77

(a) STP

(b) Assuming that (i) stoichiometry was 1 H-atom per 1 surface-metal atom and (ii) only nickel (for Raney-Ni) or cobalt atoms (for the other catalysts) are probed by H_2-chemisorption.

Table 3-2: The chemisorbed monolayer (v_m) and the adsorption constant (b) estimated from the dissociative Langmuir isotherm fitting into data presented in Figure 3-3.

The BET surface areas increased in the sequence Raney-Co (19.3 $m^2 \cdot g^{-1}$), < Raney-Ni (57.7 $m^2 \cdot g^{-1}$)< Ni-Cr promoted Raney-Co (66.8 $m^2 \cdot g^{-1}$). The LiOH doped Raney-Co had a lower surface area (14.8 $m^2 \cdot g_{cat}^{-1}$). The pore volumes varied in a similar sequence between 0.094 $cm^3 \cdot g^{-1}$ and 0.133 $cm^3 \cdot g^{-1}$. Note that after LiOH modification of Raney-Co the pore volume did not change. The BET surface area for Raney-Ni and Co depended significantly on the temperature treatment. For Raney-Ni the maximum BET area was measured after activation at 383 K (57.7 $m^2 \cdot g_{cat}^{-1}$) whereas 483 K was required for Raney-Co (24.6 $m^2 \cdot g_{cat}^{-1}$). Probably, at lower temperatures outgassing for 1 h was insufficient to remove all hydrogen and water from the catalyst. This implies stronger adsorption on Raney-Co compared to Raney-Ni. The presence of the Ni-Cr promoters stabilized high BET area. Note that the mean grain diameter for Ni-Cr promoted Raney-Co was smaller than for the unpromoted sample (30 and 28 μm, respectively). A similar influence of the alloying promoters on the mean grain size of Raney-Ni has been observed [20]. At higher temperatures, the specific surface area of Raney-Ni and Raney-Co catalysts decreased, because of particle sintering.

Assuming that only Ni and Co atoms exist on the Raney-Ni and Raney-Co catalyst surface and one hydrogen atom adsorbs per metal atom H_2-chemisorption was fitted using the Langmuir equation model [21]. The amount of hydrogen adsorbed at saturation coverage was 402.0, 225.8, 569.1 and 189.7 $\mu mol_{H2} \cdot g_{cat}^{-1}$ for Raney-Ni, Raney-Co, Ni-Cr-promoted Raney-Co and LiOH-modified Raney-Co, respectively. Thus, the fraction of

accessible metal atoms was calculated to be 5.1, 2.7, 7.4 and 2.8 %, respectively. The adsorption constant (*b*) was approximately twice as high for Raney-Ni compared to Raney-Co. The Ni-Cr promotion and LiOH-doping of Raney-Co lead to a decreased adsorption constant (4 and 24 times, respectively) compared to Raney-Co. Thus, it is concluded that hydrogen adsorbs weaker on cobalt than on nickel. The promoters further reduced the strength of hydrogen chemisorption. The total amount of hydrogen adsorbed on the catalysts correlated directly with the variations in the BET surface area.

In order to compare the BET area with the data from hydrogen chemisorption, the morphology of nickel and cobalt particles was approximated with the Bravais-Friedel Donnay-Harker method that uses unit cell and crystal symmetry information, ranking possible crystal faces by their interplanar spacing [22]. The crystal structure of nickel is cubic closed packed with dominant crystal morphology of the (111) and (200) planes (77.60 and 22.40 % of the facet area, respectively). The crystal structure of cobalt is hexagonal closed packed with dominant crystal morphology of (100), (101) and (002) planes (40.79, 39.65 and 19.65 % of the facet area, respectively). Based on these approximations the number of Ni and Co surface atoms was calculated to 29.84 and 32.04 $\mu mol \cdot m^{-2}$, respectively. Thus, Raney-Ni (BET area = 57.7 $m^2 \cdot g_{cat}^{-1}$), Raney-Co (BET area = 19.27 $m^2 \cdot g_{cat}^{-1}$), Ni-Cr promoted Raney-Co (BET area = 66.8 $m^2 \cdot g_{cat}^{-1}$) and LiOH-doped Raney-Co (BET area = 14.84 $m^2 \cdot g_{cat}^{-1}$) would exhibit the ideal dispersion of 10.89, 3.75, 13.82 and 3.47 %, respectively. It compares with the measured dispersion of 5.08, 2.73, 7.35 and 2.77 %, respectively. Therefore, neither catalyst surface was fully accessible for hydrogen chemisorption after activation at 383 K. Note that, the fraction of surface consisting of accessible metals is 0.47, 0.73, 0.53 and 0.80 of the theoretically accessible surface sites for Raney-Ni, Raney-Co, Ni-Cr-promoted Raney-Co and LiOH-modified Raney-Co, respectively.

This shows that a significant fraction of the Raney-catalyst surface is inaccessible for hydrogen and can be considered as inactive for hydrogenation. During the preparation of sponge catalysts binary- and multicomponent oxides and hydroxides are formed and deposited on the surface [23, 24]. According to Hochard-Poncet *et al.*, NaOH applied to

Raney-Ni removes uncreative Al_2O_3 *via* agglomeration and, thus, cleans the metal surface [25]. Similar effects of LiOH on Raney-Co are conceivable in the present case.

3.3.3 Temperature Programmed Desorption (TPD)

3.3.3.1 TPD of Residual Hydrogen and Water

After the preparation, water and hydrogen may be bound on the surface of the Raney-catalyst. The concentration of these residual molecules left on the catalyst surface after outgassing was determined by temperature programmed desorption [26]. The results are presented in Figure 3-4 and Figure 3-5 for hydrogen and water, respectively.

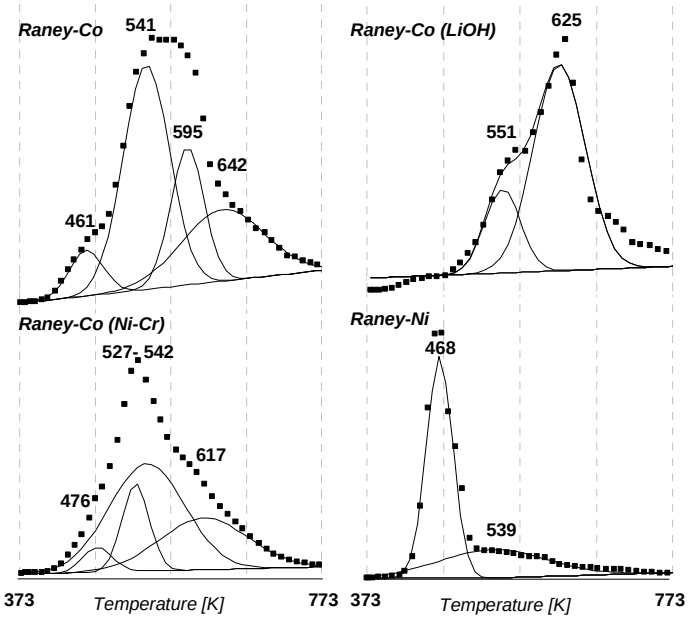

Figure 3-4: TPD traces of residual hydrogen from the studied catalysts samples (Raney-Co, LiOH-modified Raney-Co, Ni-Cr promoted Raney-Co and Raney-Ni). The experimental data (m/z = 2 (■)) were normalized to the sample mass and fitted with Gaussian curves (solid lines).

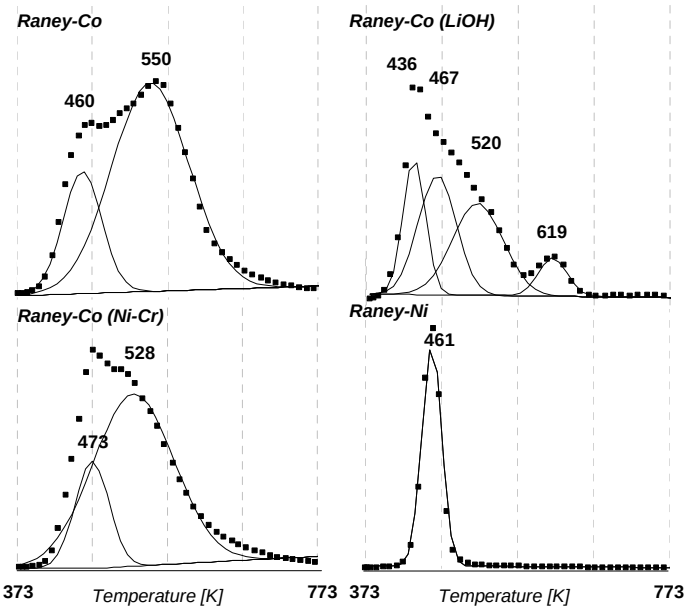

Figure 3-5: TPD traces of residual water from the studied catalysts samples (Raney-Co, LiOH-modified Raney-Co, Ni-Cr promoted Raney-Co and Raney-Ni). The experimental data (m/z = 2 (■)) were normalized to the sample mass and fitted with Gaussian curves (solid lines).

From both unpromoted and Ni-Cr-promoted Raney-Co hydrogen and water desorbed over a broad temperature range (400 – 730 K), while, Raney-Ni exhibited a relatively narrow temperature range of desorption (400 – 530 K). In comparison to unpromoted Raney-Co, significantly more hydrogen desorbed from Ni-Cr-promoted Raney-Co (7 times) and Raney-Ni (10 times). Similarly, more water desorbed from Ni-Cr promoted Raney-Co compared to the unpromoted Raney-Co (7 times). In contrast, about the same amount of water desorbed from Raney-Co and Raney-Ni. Thus, the concentration of adsorbed molecules varied sympathetically with the specific surface area of the materials investigated.

For Raney-Co the rates of desorption of hydrogen and water showed two significant maxima indicating the presence of at least two adsorption sites in the material. The maxima were observed at roughly the same temperature for unpromoted and promoted Raney-Co. Desorption maxima for water occurred at a lower temperature relative to those for hydrogen. Desorption traces of hydrogen and water from LiOH-modified Raney-Co showed two main desorption peaks for hydrogen (peak temperatures at 551 and 625 K). The highest rates of desorbing water were detected within 436 - 520 K. The small high-temperature peak (619 K) for water correlates very well with the peak of hydrogen

desorption (625 K) from that sample. The amount of desorbing hydrogen and water was much lower than for the parent Raney-Co sample (25 and 5 %, respectively).

The broad temperature range for desorbing hydrogen and water from Raney-Co samples is attributed to a broad distribution of adsorption sites. Even if Raney-cobalt surface consists mainly made of low-index planes, the surface will contain a large fraction of defects, steps and kinks. Martin *et al.* demonstrated, by measuring the saturation magnetization of Raney-type Ni in an electromagnetic field, that the evolved hydrogen during TPD cannot be the result of the reaction of water with metallic Al [27]. In contrast, Raney-Ni exhibited relatively narrow distribution of adsorption sites, which is speculated to be related to a fairly uniform surface structure with a lower concentration of defects. The amount of desorbing hydrogen related to the BET surface suggests a lower concentration for Raney-Co and Raney-Co (NiCr) (5 and 10 a.u.·m^{-2}_{cat}, respectively) than for Raney-Ni (17 a.u.·m^{-2}_{cat}). Note, that the hydrogen desorbing at high temperatures could be inert for the hydrogenation reaction carried out at temperatures close to 373 K.

During desorption of hydrogen and water from the LiOH-modified Raney-Co sample chemical reactions might occur on the surface. The first hydrogen desorption maximum probably indicates desorption of residual hydrogen from the metal surface as observed for the other two Raney-Co samples. It is overlapped by a more intense hydrogen peak (at 625 K) that is probably the result from the secondary reaction between Al and LiOH. The desorption trace of water differs from desorption trace for the parent Raney-Co. While the low temperature maximum occurs at roughly the same temperature (up to 467 K vs. maximum at 460 K, respectively), the second desorption maximum (520 K) has a much lower intensity. This indicates that the LiOH deposit occupies the second adsorption site for H_2O. Further, LiOH decomposes at roughly 623 K in vacuum, leading to a low intensity desorption feature in the H_2O desorption trace. Some water is consumed in the surface leaching reaction with Al (the desorption maximum in the hydrogen trace at 625 K).

3.3.3.2 Ammonia-TPD

The acid-base properties of Raney-Co and Raney-Ni originating from residual alumina are of important due to the possible acid-catalyzed side reactions during the

hydrogenation of nitriles [28]. Thus, ammonia-TPD was carried out. The rate of ammonia desorption with increasing temperature is presented in Figure 3-6.

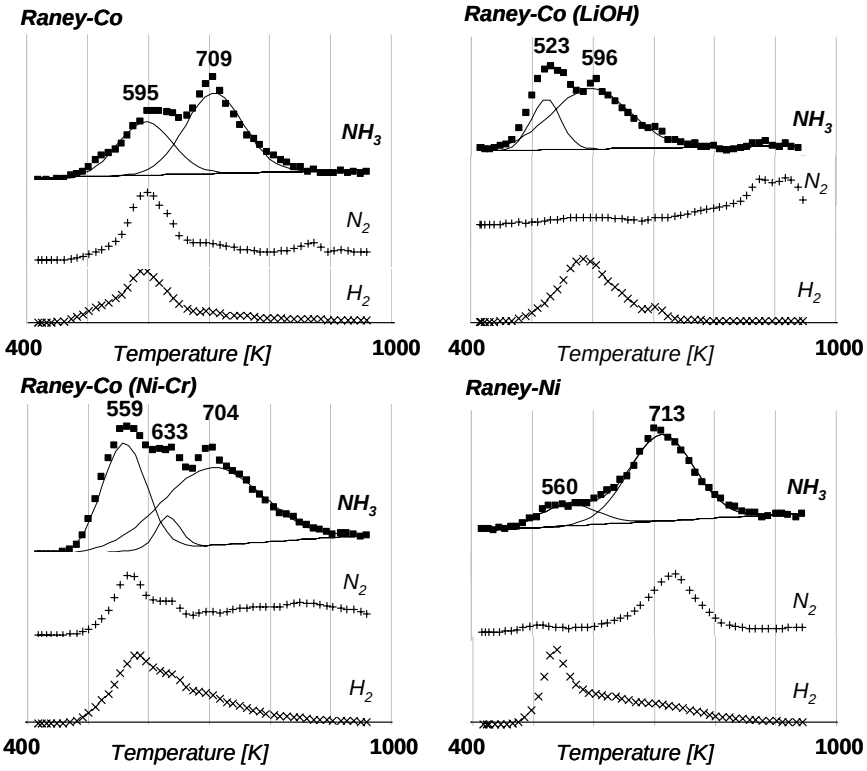

Figure 3-6: TPD of NH_3 (■), H_2 (×) and N_2 (+) desorbing from Raney-Co, Raney-Co (LiOH), Raney-Co (NiCr) and Raney-Ni after adsorption of NH_3 at 423 K.

For the sample of Raney-Co, Ni-Cr promoted Raney-Co and Raney-Ni the desorption curves of ammonia showed two maxima. For Raney-Co the maxima in the rate of NH_3 desorption were at 595 and 709 K. For Ni-Cr promoted Raney-Co peak temperatures were observed at 559 with a shoulder at 633 and 704 K. For Raney-Ni the maxima in the rate of NH_3 desorption were at 560 and 713 K. It is particularly noteworthy that, apart from ammonia, also N_2 and H_2 desorbed. For unpromoted and Ni-Cr promoted Raney-Co the maxima of N_2 and H_2 desorption occurred in parallel between 590 and 575 K, respectively, and correlated roughly with the first desorption peak of NH_3. In contrast to the cobalt catalysts, N_2 and H_2 desorption were not correlated for Raney-Ni. The maximum in hydrogen desorption was associated with the low-temperature desorption peak of ammonia at 560 K, whereas the maximum in desorbing nitrogen was correlated with the high-temperature peak in NH_3 desorption at 713 K.

For the LiOH-modified Raney-Co the NH_3 desorption trace showed two maxima at 523 and 596 K. The H_2 desorption rate showed one desorption peak at 573 K, while hardly any nitrogen desorbed from the sample.

The maxima in desorption rates suggest different (reactive) adsorption states of ammonia on the studied samples. The low temperature NH_3-desorption peak (595 and 559 K for Raney-Co and Raney-Ni, respectively) is assigned to ammonia desorbing from the metal surface. At the temperature of adsorption (423 K) the ammonia molecules are dehydrogenated to give surface hydrogen atoms and nitrene species (NH_n, n = 2, 1) [29]. During desorption, the surface species can either recombine to ammonia or form molecular hydrogen and nitrogen. The ammonia trace for Raney-Co promoted with Ni-Cr showed a peak at the same temperature as the nickel catalyst (559 K) with a shoulder at 633 K. Both could indicate that the promoting transition metals (Ni and Cr) are also present on the surface. For all samples the second maximum occurred at roughly 710 K. This is attributed to desorption of ammonia from Al^{3+} Lewis acid sites. The presence of Al^{3+} on the surface of Raney-Ni, which had been washed thoroughly with distilled water, has been reported [30]. Due to their high stability the Lewis adducts ($H_3N{:}\rightarrow Al^{3+}$) decompose only at high temperatures [31].

In comparison to the parent catalyst, the desorption of ammonia from LiOH-modified Raney-Co showed an extra peak at 523 K, together with the peak that has been proposed to indicate NH_3 desorption from metallic cobalt (at 596 K). It is noteworthy that the latter peak was accompanied only by H_2-desorption (no N_2). It is speculated that ammonia is only partially dehydrogenated in the presence of LiOH. A fraction of ammonia molecules could even be coordinated to the metal atoms without any dissociative chemisorption. Of course, molecular-state ammonia would be desorbed easier (i.e., at lower temperature) in line with the peak at 523 K. No desorption from the alumina sites was found (~ 710 [K]). A surface reaction of lithium hydroxide ($LiOH{\cdot}H_2O$) with bayerite (the form of aluminum hydroxide found in Raney-catalysts) will produce lithium dialuminate ($LiAl_2(OH)_7{\cdot}2H_2O$) [32]. Note that the removal of structural water from $LiAl_2(OH)_7{\cdot}2H_2O$ occurs below 473 K [33]. Thus, LiOH quenches the sites which are associated with the alumina Lewis acidity.

The significant differences in the desorption of molecular nitrogen between cobalt and nickel can be explained by considering the different temperatures of formation and decomposition of cobalt and nickel nitrides [34, 35]. Baiker *et al.* described that the interaction of nickel with ammonia at elevated temperatures leads to the formation of nickel nitride Ni_3N and hydrogen [36]. Nickel nitride is formed at temperatures above 395 K and is stable in inert atmospheres up to ~ 683 K. Further increase in temperature leads to decomposition of Ni_3N to metallic nickel and nitrogen. In agreement with this description ammonia, which is dissociated on the Ni-surface at the temperature of adsorption (423 K), can react with the bulk nickel to form nickel nitride. As the catalyst is heated to more than 563 K in vacuum all adsorbed species desorb except the nitrogen that reacted with nickel. At higher temperatures Ni_3N decomposes resulting in the maximum rate of nitrogen evolution at ~ 733 K. Dissociative adsorption of ammonia onto Raney-Co can also be accompanied by formation of cobalt nitride. However, in contrast to nickel, Co_3N is less stable and decomposes when heated to 549 K [37]. Therefore, hardly any cobalt nitride is formed.

3.3.4 X-ray Photoelectron Spectroscopy (XPS)

The occurrence and the nature of different phases at the catalyst surface was evaluated from the position of XPS emission lines. In Figure 3-7 XPS spectra of Raney-Co, Raney-Co(LiOH), Raney-Co(NiCr) and Raney-Ni are presented.

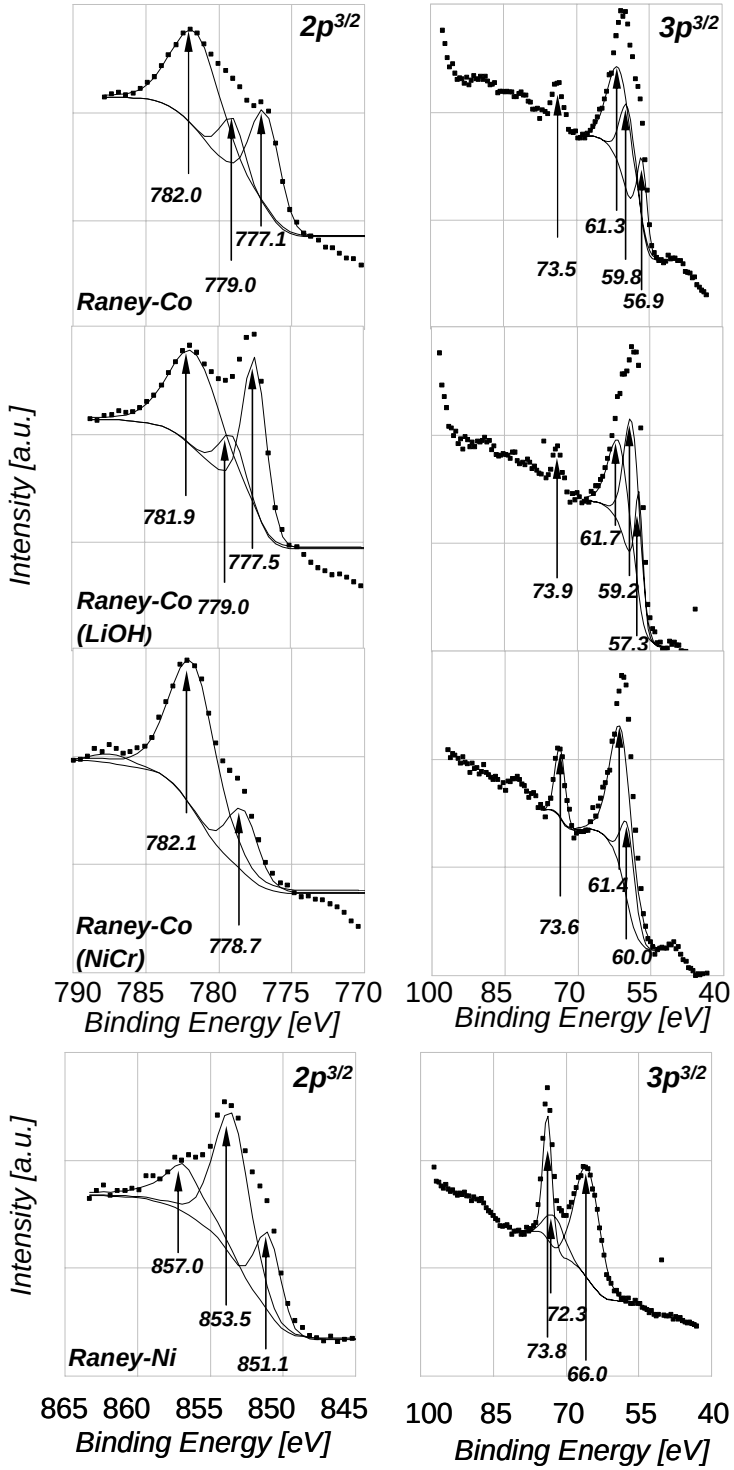

Figure 3-7: XPS spectra of Raney-Co, Raney-Co(LiOH), Raney-Co(NiCr) and Raney-Ni. The binding energy scale was corrected for charging. Data were fitted (solid lines) to approximate the occurrence of different species on the catalyst surface. Note that the fitting procedure was moderately satisfactory when the background was problematic. As a result the error in the peak position increased.

The XPS spectra of cobalt samples in the high binding energy region between 790 and 770 eV (Co $2p^{3/2}$ region) exhibited at least two maxima at 782.0(5) and 779.0(5) eV. Additionally, the spectra of Raney-Co and Raney-Co(LiOH) showed a peak at 777.5(5) eV, which was absent in the spectrum of Raney-Co(NiCr). Note that the intensity of the peak at 777.5(5) eV increased relative to the other peaks in the spectrum after LiOH-modification of Raney-Co. Similarly, for Raney-Ni three peaks at 857.0(5), 853.5(5) and 851.1(5) eV were observed in the Ni $2p^{3/2}$ region (i.e., 865 – 845 eV).

In the region between 100 and 40 eV spectra all three cobalt samples featured a peak at 73.5(5) eV. Additionally, a broad peak between 70 and 55 eV was observed with a contribution from peaks at roughly 61(1) and 60(1) eV. It was further speculated that the spectra of Raney-Co and Raney-Co(LiOH) might include one further peak at 57(1) eV. The spectrum of Raney-Ni, apart from the peak at 73.8(5) eV, revealed a small peak at 72.3(5) eV and an intense peak at 66.0(5) eV.

The XPS spectra of the cobalt catalysts (Co $2p^{3/2}$) showed the highest binding energy at 782.0(5) eV that was probably related to oxidized cobalt in a strongly ionic ligand field. Probably Co-O-Al species give rise to this peak. The small peak at 770.0(5) eV also observed for in each cobalt sample likely indicates the presence of Co_2O_3 (779.2 eV [38]), although CoOOH could also be present (779.2 [39]). The photoelectron contribution at 777.5(5) eV shows that metallic cobalt Co^0 is present at the outermost surface (777.8 [40]). Note that the latter (i) was not detected for Raney-Co(NiCr) and (ii) its relative contribution increased after LiOH modification of the surface. In the XPS spectrum of Raney-Ni (Ni $2p^{3/2}$) two peaks at 857.0(5) and 853.5(5) eV correspond to oxidized nickel (Ni^{2+}). This is probably $NiAl_2O_4$ (857.1 eV [41]) and NiO (853.5 eV [42]), respectively. In literature, Ni_2O_3 [43], $Ni(OH)_2$ and $NiAl_2O_4$ [44] have been claimed to be present at the surface of Raney-type Ni catalysts. However, the peak at 853.5(5) eV could also be attributed to an alloy Al_3Ni (853.6 eV [45]). Note that Al_3Ni is one of the components of the parent alloy used in the preparation of Raney-Ni. Metallic nickel (Ni^0) was observed at 851.1(5) eV, although the peak position was lower than reported in the literature (852.1 eV [46]).

In the low binding energy region of the XPS spectra the peak at 73.5(5) and at 73.8(5) eV for the cobalt and nickel samples, respectively, is readily attributed to oxidized aluminum (Al $2p^{3/2}$ emission line). That could be α- and γ-Al_2O_3 (73.8 [47] and 73.5 [48] eV, respectively), or $Al(OH)_3$ (73.6 eV [49]). Note that this was the only state of aluminum in the cobalt samples. In contrast, a contribution of Al^0 peak to the XPS spectrum of Raney-Ni is observed at 72.3(5) eV (72.3 eV [50]). It has been reported that Raney-Ni contains some surface aluminum [51]. When compared to the $2p^{3/2}$ regions the XPS spectrum in the Co and Ni $3p^{3/2}$ region bears information about the catalyst composition deeper in the bulk. In the Co $3p^{3/2}$ region both oxidized and metallic cobalt is found (i.e., 61(1) and 60(1) eV, respectively), although accurate separation of the cobalt species was limited. The contribution of the Co^0 peak increases after LiOH modification of Raney-Co; Raney-Co(NiCr) is the most oxidized among the cobalt samples. This is in line with the observations from the Co $2p^{3/2}$ region of the XPS spectra. Further, the XPS spectra of Raney-Co include a contribution from a peak at 57(1) eV which indicates Fe 3p line (e.g., FeOOH 56.3 eV [52]). Therefore, the presence of Li 1s contribution in the XPS spectrum of in LiOH-modified Raney-Co (e.g., Li_2O 55.6 eV [53]) is difficult to evaluate as XPS is much more sensitive for iron than for lithium. In contrast no iron is observed in Raney-Co(NiCr). The XPS spectrum of Raney-Ni in the Ni $3p^{3/2}$ region shows mainly metallic Ni^0 (66.0(5) compared to 66.3 eV [54]).

An estimation of the elemental surface composition was attempted (Table 3-3). The carbon contamination is not included in the calculation and it is assumed to be a homogeneous top layer. Consequently, the oxygen concentration exceeds the oxide concentration on the surface as some contribution from the carbon contamination is included (i.e., carbon monoxide).

	Raney-Co	Raney-Co(LiOH)[(a)]			Raney-Co(NiCr)	Raney-Ni
		assuming 100 % Fe	equal contribution of Li and Fe	assuming 100 % Fe		
O 1s	**71.1**	68.1	**46.6**	35.5	**76.8**	**74.9**
Co 3p	**19.0**	21.2	**14.5**	11.1	**17.9**	**0**
Ni 3p	**0**	0	**0**	0	**0**	**11.4**
Al 2p	**4.1**	3.0	**2.1**	1.6	**5.3**	**13.7**
Fe 3p	**5.7**	7.7	**2.6**	0	**0**	**0**
Li 1s	**0**	0	**34.1**	51.9	**0**	**0**

(a) The difficulty to separate Fe 3p and Li 1s lines led to ambiguous estimation of iron and lithium in the Raney-Co(LiOH) sample

Table 3-3: An estimation of the elemental surface composition of Raney-Co, Raney-Co(LiOH), Raney-Co(NiCr) and Raney-Ni [%]. The relative amount of each element was concluded from the corresponding peak area justified by the elemental sensitivity factor.

Raney-Co had little aluminum on the surface (4.1 %), altough its amount was higher for Raney-Co(NiCr) and Raney-Ni (5.3 and 13.7 %, respectively). The amount of the catalytically active metal on the surface was in the reverse order (19.0, 17.9 and 11.4 %, respectively). The elemental ratio of catalytic metal to aluminum was 4.6, 3.4 and 0.8, respectively. LiOH applied to the surface of Raney-Co increased the elemental ratio cobalt to aluminum (5.6).

The amount of aluminum on the surface follows the trend expected from the bulk composition (Raney-Co, Raney-Co(NiCr) and Raney-Ni had 1.85, 3.5 and 6.77 wt. % Al in the bulk, respectively). However, the elemental ratio of Co (Ni) to Al determined by XPS is much different as the surface has been enriched in Al. LiOH applied to the surface of Raney-Co has probably reacted with alumina.

3.3.5 Adsorption of Butyronitrile and n-Butylamine from the Liquid Phase

The adsorption of butyronitrile and n-butylamine was studied to characterize (competitive) sorption properties relevant during the hydrogenation of butyronitrile over parent and LiOH-modified Raney-Co. In particular, the concentration of butyronitrile and n-butylamine adsorbing on the catalyst was evaluated from breakthrough curves. Typical

results for the adsorption of n-butylamine on Raney-Co are shown in Figure 3-8 a. Upon stepwise increase of the concentration in the feed the additional amount of n-butylamine that adsorbed on the catalyst sample decreased. The corresponding isotherms (at 293 K) for adsorption of butyronitrile and n-butylamine on parent and LiOH-modified Raney-Co are shown in Figure 3-8 b.

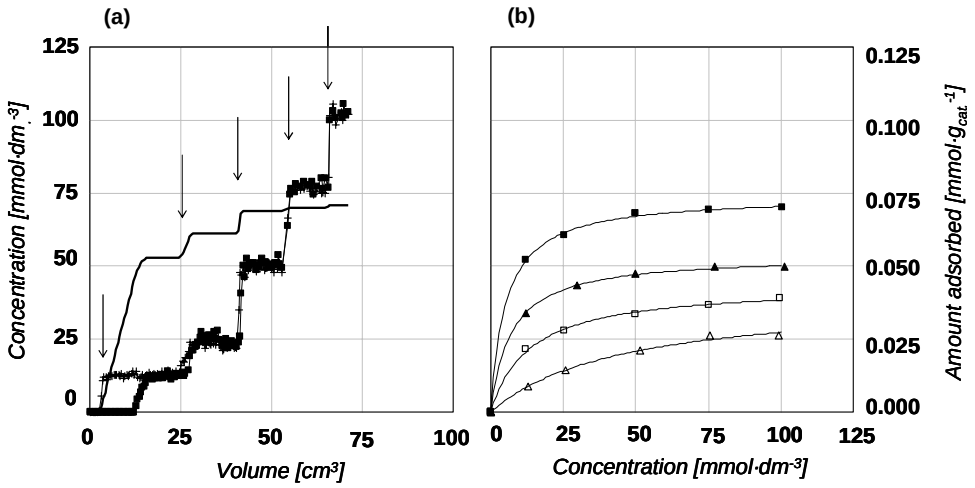

Figure 3-8:

(a) Concentration of n-butylamine (■) and octane (+) at the exit of a column of Raney-Co during a typical adsorption experiment. Solid line represent integrated amount of adsorbed n-butylamine on the catalyst surface (right Y-axis). The arrows (↓) indicate a stepwise increase in concentration of the feed.

(b) Adsorption isotherms at 293 K for adsorption of n-butylamine (■) and butyronitrile (▲) on parent (full symbols) and LiOH-doped Raney-Co (open symbols). Solid lines represent a Langmuir equation fit.

The adsorption isotherms were fitted with a Langmuir-type equation (Equation 2-9) [55]. The amount adsorbed at the plateau (n_L) and the empirical constant (b) are summarized in Table 3-4.

Catalyst	Adsorbate			
	n-butylamine		butyronitrile	
	n_L [mmol·g_{cat}^{-1}]	b [(mmol·dm^{-3})$^{-1}$]	n_L [mmol·g_{cat}^{-1}]	b [(mmol·dm^{-3})$^{-1}$]
parent Raney-Co	$7.39 \cdot 10^{-2}$	$19.5 \cdot 10^{-2}$	$5.37 \cdot 10^{-2}$	$14.2 \cdot 10^{-2}$
LiOH-modified Raney-Co	$4.25 \cdot 10^{-2}$	$8.15 \cdot 10^{-2}$	$4.06 \cdot 10^{-2}$	$2.1 \cdot 10^{-2}$

Table 3-4: The results of fitting the liquid-phase adsorption isotherms with a Langmuir-type equation.

The amount of n-butylamine, which was adsorbed on the parent catalyst, was 1.4 times higher than that of butyronitrile ($7.39 \cdot 10^{-2}$ and $5.37 \cdot 10^{-2}$ $mmol \cdot g_{cat.}^{-1}$, respectively). The empirical constant (*b*) related to the heat of adsorption was also higher for n-butylamine than for butyronitrile ($19.5 \cdot 10^{-2}$ and $14.2 \cdot 10^{-2}$ $(mmol \cdot dm^3)^{-1}$, respectively). Thus, n-butylamine adsorbs in a larger quantity and stronger on parent catalyst than butyronitrile. Upon LiOH-modification of Raney-Co only $4.25 \cdot 10^{-2}$ $mmol \cdot g_{cat.}^{-1}$ of n-butylamine could be adsorbed on the catalyst surface (approximately 60 % of the saturation amount on the parent catalyst); the *b*-constant decreased to $8.15 \cdot 10^{-2}$ $(mmol \cdot dm^{-3})^{-1}$. Similar observations were noted for butyronitrile: $4.25 \cdot 10^{-2}$ $mmol \cdot g_{cat.}^{-1}$ and $2.1 \cdot 10^{-2}$ $(mmol \cdot dm^{-3})^{-1}$. The amount of butyronitrile ($0.29 \cdot 10^{-2}$ $[mmol \cdot m_{cat.}^{-2}]$) was estimated for the parent and the LiOH-modified catalyst. Over LiOH-doped catalyst the adsorption constants were $8.15 \cdot 10^{-2}$ and $1.97 \cdot 10^{-2}$ $(mmol \cdot dm^{-3})^{-1}$ for n-butylamine and butyronitrile, respectively. Thus, the LiOH-modified catalyst adsorbs less n-butylamine, but approximately the same amount of butyronitrile while the adsorption of ether adsorbate becomes weaker. It is noteworthy that the adsorption of n-butylamine is stronger relative to butyronitrile and this is further increased upon LiOH-modification of Raney-Co.

The competitive adsorption of n-butylamine and butyronitrile on the parent and LiOH-modified Raney-Co showed that after the breakthrough of the reference, butyronitrile appeared first in the eluent. The concentration of butyronitrile quickly rose above the starting concentration, passed through a maximum and reached steady state at the same time as the breakthrough of n-butylamine was observed. At steady state, the surface coverage of the parent catalyst was higher for n-butylamine than for butyronitrile.

The reversibility of the adsorption of n-butylamine and butyronitrile on parent and LiOH-modified catalyst surface was tested. Once the breakthrough of the reference followed by the adsorbate was observed and a steady state was reached at the outlet of the column, pure solvent was passed over the column. The concentration of the tracer started to decrease fast whereas the concentration of the adsorbate decreased slowly in the effluent. A comparison of the areas confined between the breakthrough curves for adsorption and desorption showed that a number of molecules of both adsorbates partially remained on

the surface of the parent catalyst. On LiOH-modified catalyst the amount of nbutylamine and butyronitrile which could be adsorbed was lower compared to the parent sample. However, it was possible to leach both adsorbates quantitatively as the process became fully reversible over LiOH-modified Raney-Co.

3.3.5.1 Heat of Adsorption of Butyronitrile at 371.9 K

In order to measure the heat of adsorption of butyronitrile over Raney-Co, Raney-Co(LiOH), Raney-Co(NiCr) or Raney-Ni, a calorimetric study was performed at 371.9 K (Table 3-5).

catalyst	Enthalpy [a] [$J \cdot g_{cat}^{-1}$]	BET area [$m^2 \cdot g_{cat}^{-1}$]	Metal surface area [b] [$m^2 \cdot g_{cat}^{-1}$]	Enthalpy [$kJ \cdot mol_{metal}^{-1}$]
Raney-Co	-15.7	19.3	14.1	-34.8
Raney-Co (LiOH)	-16.8	14.8	11.9	-44.1
Raney-Co (NiCr)	-39.4	66.8	35.4	-34.7
Raney-Ni	-40.3	57.7	24.8	-54.5

(a) Measured at 371.9 K

(b) As measured by hydrogen chemisorption.

Table 3-5: Heat of adsorption of butyronitrile over different catalyst samples at 371.9 K. Note that the error of the measured value was up to 5 $kJ \cdot mol^{-1}$.

The heat of adsorption of butyronitrile normalized to the number of exposed metal atoms was the same for of Raney-Co and Raney-Co(NiCr) ($\Delta H^{371.9} = -35\ kJ \cdot mol^{-1}$) indicating similar adsorption properties. A slightly stronger activation of butyronitrile was observed for Raney-Co(LiOH) ($\Delta H^{371.9} = -44\ kJ \cdot mol^{-1}$). Butyronitrile was more strongly adsorbed on the Raney-Ni surface as the heat of adsorption was about -55 $kJ \cdot mol^{-1}$.

It can be concluded that alloying promoters (Ni, Cr) have little influence on the sorption properties of Raney-Co. On the other hand, modification of the Raney-Co surface with LiOH induces a stronger interaction of butyronitrile with the cobalt surface. Raney-Ni is able to adsorb butyronitrile more strongly than any of the cobalt samples. Thus the activation of butyronitrile is higher on Ni than on Co.

3.3.6 Catalytic Tests

The activity and selectivity of Raney-Ni, Raney-Co, Ni-Cr promoted Raney-Co and LiOH-modified Raney-Co in the hydrogenation of butyronitrile was tested. A concentration profile recorded during the hydrogenation of butyronitrile at 373 K over Raney-Ni is presented in Figure 3-9.

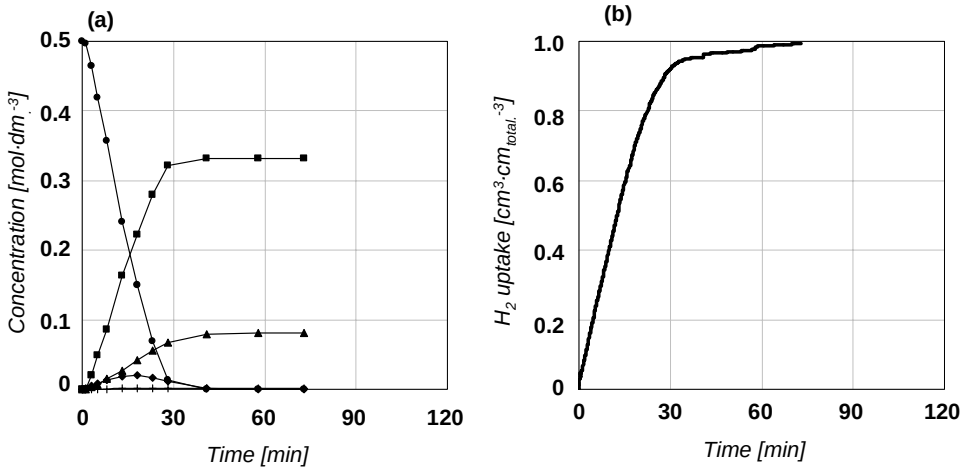

Figure 3-9: (a) Concentration profile during hydrogenation of butyronitrile over Raney-Ni at T = 100 °C, $p(H_2)$ = 30 bar, c_0(butyronitrile) = 0.50 mol·dm^{-3}. GC-data for (•) butyronitrile, (■) n-butylamine, (▲) di-n-butylamine, (♦) N-butylidene-butylamine, (+) tri-n-butylamine. (b) Integral hydrogen uptake during the reaction. The uptake was normalized to the total H_2-uptake.

A short induction time (< 2 min) was observed, after which the hydrogenation of butyronitrile over Raney-Ni proceeded at a high rate. The butyronitrile concentration decreased almost linearly with time; in parallel, hydrogen was consumed. At high conversion (> 80 % conversion) the rate of reaction slowed down. The main product of the hydrogenation of butyronitrile was n-butylamine. However, significant amounts of di-n-butylamine and traces of tri-n-butylamine were formed as by-product. The final selectivity to n-butylamine was ~ 66.0 %. N-butylidene-butylamine was observed as a reaction intermediate. Its concentration started to decrease once more than 70 % of butyronitrile had been converted. At the end of the experiment no N-butylidene-butylamine was found. The maximum concentration of N-butylidene-butylamine during the experiment was 4 times smaller than the final concentration of di-n-butylamine. From a plot yield vs. conversion n-butylamine and N-butylidene-butylamine appear to be primary reaction products; di-n-butylamine and tri-n-butylamine were secondary reaction products.

The formation of N-butylidene-butylamine, di-n-butylamine and tri-n-butylamine indicated that several side reactions occurred. A mechanism for the formation of secondary and tertiary amines has been proposed by von Braun [56] (Figure 3-9). According to the model the hydrogenation of butyronitrile would proceed through reactive butylidenimine which is susceptible to a nucleophilic attack by n-butylamine or di-n-butylamine. Subsequent elimination of ammonia would yield N-butylidene-butylamine or but-1-enyl-dibutylamine as condensation products, respectively. Subsequently these are hydrogenated to di-n-butylamine and tri-n-butylamine, respectively.

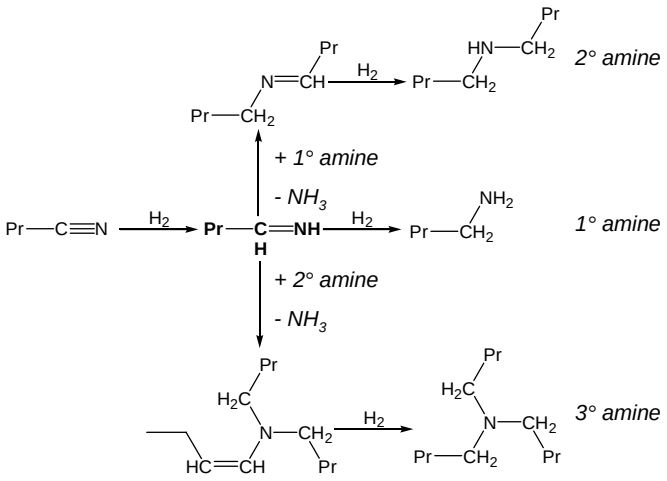

Figure 3-10: The von Braun's mechanism of formation of 2° and 3° n-butylamines during the hydrogenation of butyronitrile.

The postulated intermediate, butylidenimine, was not detected in the reaction mixture, whereas both n-butylamine and N-butylidene-butylamine were apparent primary reaction products. The transient concentration of butylidenimine would be very low if its hydrogenation to n-butylamine proceeds much faster than the rate of its formation. The latter rate consist of two steps where either could be rate determining. This is the first or the second hydrogen addition to the nitrile group in butyronitrile. Consequently, very little of butylidenimine would be desorbed from the catalyst surface before further hydrogenation or condensation. In agreement with the model N-butylidene-butylamine is observed as the formal condensation product of butylidenimine and n-butylamine. The condensation reaction could occur on the catalyst surface and/or in the liquid phase. The liquid-phase concentration of N-butylidene-butylamine increased steadily. At the same

time, however, some of it is directly hydrogenated to di-n-butylamine on the catalyst surface (approximately 60 %). At longer reaction times all N-butylidene-butylamine is converted to di-n-butylamine. The model also predicts the formation of but-1-enyl-dibutylamine as the precursor for tri-n-butylamine. The amount of desorbed but-1-enyl-dibutylamine is estimated to be 10 % of the final concentration of tri-n-butylamine. Huang and Sachtler [57] have detected but-1-enyl-dibutylamine in the liquid-phase during the hydrogenation of butyronitrile over PdNi/NaY although in a very low concentration. Compared to the Pd-catalyst, the Raney-Ni catalyst used in this study is more selective to n-butylamine. Thus, the concentration of but-1-enyl-dibutylamine if present at all is significantly lower and below the detection limit.

The concentration profile for the hydrogenation of butyronitrile over Raney-Co at 373 K is presented in Figure 3-10.

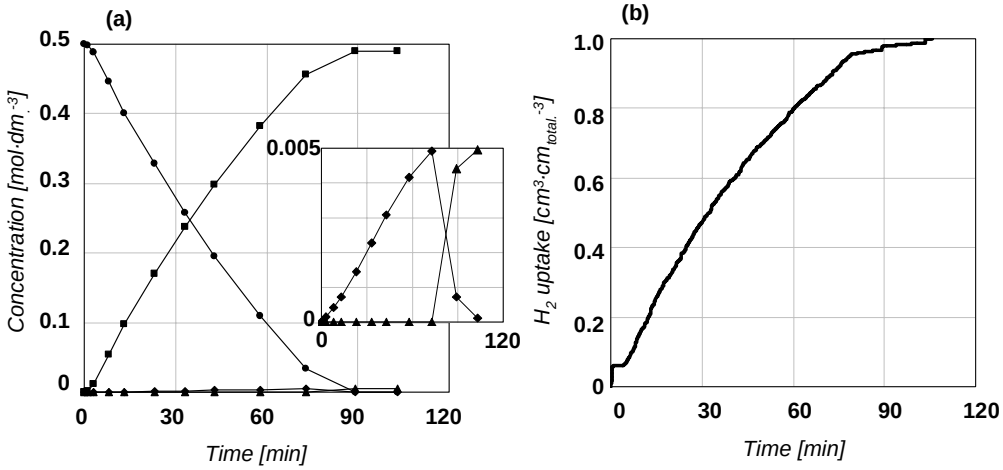

Figure 3-11: (a) Concentration profile during hydrogenation of butyronitrile over Raney-Co at T = 373 K ($p(H_2)$ = 30 bar, c_0(butyronitrile) = 0.50 mol·dm^{-3}). GC-data for (●) butyronitrile, (■) n-butylamine, (▲) di-n-butylamine, (♦). The inset shows concentration vs. time for N-butylidene-butylamine and di-n-butylamine only. (b) Hydrogen uptake was normalized to the total H_2-uptake.

The hydrogenation commenced at a high rate after a short induction period (< 3 min). The selectivity to n-butylamine was very high (~ 98 %) and this was the primary reaction product. N-butylidene-butylamine was detected instantly in small concentrations, and it also appeared to be a primary reaction product. The formation of di-n-butylamine was observed once more than 90 % of butyronitrile had been hydrogenated. It is noteworthy that the final concentration of di-n-butylamine was correlated to the maximum concentration of N-butylidene-butylamine. Thus, all the di-n-butylamine formed is a

sequential product of the hydrogenation of N-butylidene-butylamine re-adsorbed from the liquid phase. Tri-n-butylamine was not found.

Over Ni-Cr promoted Raney-Co and over LiOH-modified Raney-Co the evolution of the by-products was similar: the final concentration of di-n-butylamine was always correlated to the maximum transient concentration of N-butylidene-butylamine. The maximum transient concentration of N-butylidene-butylamine was approximately 40 and 20 %, respectively, of that over the unpromoted Raney-Co. N-butylidene-butylamine was hydrogenated only at the end of each experiment. The selectivity to n-butylamine was ~ 99 and ~ 99.5 %, respectively. Note that LiOH was not leached to the liquid phase during the reaction. The slope of a linear approximation within 20 – 80 % conversion of butyronitrile (GC-data) was used as a measure of the reaction rate over each catalyst. The rate was related to the total BET area and the active surface area measured with H_2-chemisorption (Table 3-4).

Catalyst	BET area $[m^2 \cdot g_{cat}^{-1}]$	TOF[(b)] $[mol_{butyronitrile} \cdot mol_{surface\ metal}^{-1} \cdot s^{-1}]$
Raney-Co	19.27 (73)[(a)]	0.072
Raney-Co (LiOH)	14.84 (80)	0.102
Raney-Co (NiCr)	66.80 (53)	0.217
Raney-Ni	57.70 (47)	0.121

(a) Fraction of the BET area available for H_2-chemisorption in %.

(b) Rate normalized to surface metal atoms measured with hydrogen chemisorption.

Table 3-6: Rates of the hydrogenation of butyronitrile related to the accessible metal atoms.

The rate of hydrogenation related to the surface metal atoms available was higher over Raney-Ni than over Raney-Co. However, Ni-Cr promoted Raney-Co exhibited drastically improved activity. Surprisingly, also LiOH modification of Raney-Co caused some activity enhancement.

3.3.6.1 Kinetics of the Hydrogenation of Butyronitrile

Based on a linear approximation of the rate of conversion of butyronitrile of the kinetic data were evaluated. Over Raney-Ni the reaction order in both butyronitrile and hydrogen was positive at low concentrations (0.8), but decreased to zero at higher concentrations of butyronitrile and hydrogen pressure. This is in agreement with the Langmuir-Hinshelwood kinetic model reported for the hydrogenation of nitriles [58, 59]. Over parent and LiOH-modified Raney-Co the reaction order in butyronitrile was close to zero. The reaction order in hydrogen was approximately 0.5 for the parent catalyst and close to zero for the LiOH-modified. The Arrhenius plot indicated an increase in the apparent activation energy from Raney-Ni (56 $kJ \cdot mol^{-1}$) to Raney-Co (62 $kJ \cdot mol^{-1}$) to the LiOH-modified Raney-Co (65 $kJ \cdot mol^{-1}$).

3.4 Discussion

3.4.1 The Activity of the Raney-Catalysts in the Hydrogenation of Butyronitrile.

The metal surface active for hydrogenation is only a fraction of the total surface area of the Raney-catalysts studied. The XPS data indicate that the Raney-Ni sample with 6.8 wt. % Al in the bulk is covered with alumina to a larger extend than Ni-Cr promoted Raney-Co with 3.5 wt. % Al and Raney-Co with 1.9 wt. % Al. For all three samples a high temperature peak at 710 K in NH_3-TPD was observed and associated with ammonia desorbing from Lewis acid sites (most likely Al^{3+}). The nature of the oxide deposit and its morphology are influenced by the LiOH additives. Firstly, LiOH quenches the sites which are associated with the alumina Lewis acidity and lithium dialuminate $LiAl_2(OH)_7 \cdot 2H_2O$ is probably formed [60]. Secondly, the fraction of the clean metal surface area increases relative to the BET area as indicated by XPS and H_2-chemisorption data. Probably clustering of the oxide deposit takes place.

Assuming a simple Langmuir-Hinshelwood model with the first hydrogen transfer as the rate determining step, the rate can be expressed as $r = k \cdot \theta_H \cdot \theta_{butyronitrile}$. Hydrogen is activated by dissociative chemisorption. In respect to hydrogenation atomic hydrogen is already the best reactant. As week as possible chemical bonding to the catalyst surface is preferable. It has been reported that weakly (‘on-top’) bonded hydrogen is the reactive

species in the gas phase hydrogenation of acetonitrile over Raney-Ni in [61]. In contrast, activation of the C≡N group is well-founded in a strong adsorption of butyronitrile on metal surface. The adsorption mode of butyronitrile on the surface probably changes from binding through the nitrogen atom only with the C≡N bond vector largely normal to the surface plane (on cobalt; low activation, low rate) into aslant mode where the C≡N π-system also interacts with the surface (on nickel, high activation, high rate) [62] (Figure 3-12). Modification of Raney-Co with LiOH gives the catalyst with an intermediate heat of adsorption. In line, the rate of the reaction is higher than that over the parent cobalt catalyst but lower than that over Raney-Ni.

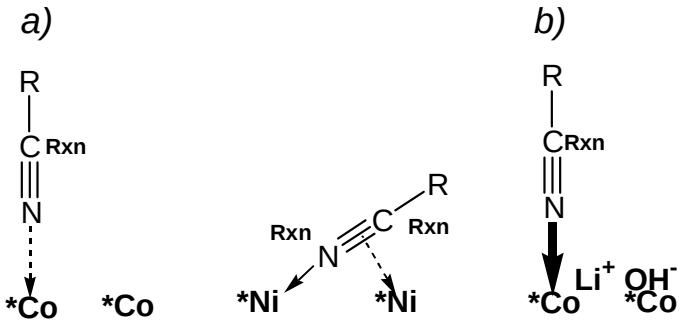

Figure 3-12: a) Different ways in which nitriles can be bound to cobalt and nickel. *Co and *Ni denotes surface-exposed cobalt and nickel atoms, respectively. Rnx indicates reaction centers in the activated nitrile molecule. b) Increased strength of adsorption *via* nitrogen bonding to the cobalt surface on Raney-Co(LiOH).

However, no speculation can be presented on how the promotion of Raney-Co with Ni and Cr could significantly increase the rate while the adsorption process of butyronitrile remains comparable to the unpromoted Raney-Co.

3.4.2 The Selectivity to n-Butylamine over Raney-Catalysts in the Hydrogenation of Butyronitrile

During the hydrogenation of butyronitrile to n-butylamine over Raney-Ni and Raney-Co the formation of a side-product, N-butylidene-butylamine, has been observed. The side-product stems from a bi-molecular condensation reaction. The reaction may take place on the catalyst surface or in the liquid phase after desorption of butylidenimine (see von Braun's mechanism). The surface-based condensation reaction seems more likely and would be similar to the metal catalyzed disproportionation of amines through condensation of partially dehydrogenated amine residues [63]. Thus, surface bound

carbene and nitrene species should be included in the mechanism [64]. In the very initial step of the formation of the new C-N bond, a species with a free electron pair on nitrogen will nucleophilic attack a reactive carbon atom. For example, the carbon atom of a strongly activated nitrile group or the carbon atom present in a partially hydrogenated derivative of the nitrile. This step of the condensation process is likely acid-catalyzed [65, 66]. Note that nitrene species where the carbon atom is fully hydrogenated (μ-N-CH_2-R) are protected from nucleophilic addition [67].

Based on the presented picture one can attempt to explain the higher selectivity over cobalt relative to nickel and the beneficial effect of doping with LiOH. A direct control over the rate of surface condensation reactions can be realized by decreasing the surface coverage in the reacting molecules. These species will exist in a low steady-state surface concentration if a high ratio of active hydrogen to butyronitrile is maintained. However, atomic hydrogen should be reactive hence weakly adsorbed on the catalyst surface. Note that our TPD data indicate a higher density of strongly adsorbing hydrogen sites on Raney-Ni than on Raney-Co. On the other hand, stronger adsorption of butyronitrile on nickel than on cobalt could also have implications for the selectivity. Firstly, if more butyronitrile is adsorbed the concentration in the partially hydrogenated species is higher. Thus, LiOH-modification is beneficial because it reduces the sorption capacity for butyronitrile (as well as butylamine) and consequently diminishes the concentration of surface substrates for bi-molecular condensation reactions. Secondly, upon strong activation of the nitrile group the molecule is more susceptible to undesired reaction pathways (Figure 3-12 a, reaction center simultaneously on carbon and nitrogen). Doping of Raney-Co with LiOH brings about a slight increase in the heat of adsorption and enhances the selectivity. It is speculated that this modification actually increases the strength of the nitrogen binding to the cobalt surface) and the step-wise hydrogenation process proceeds *via* nitrene species.

3.5 Conclusions

Properties of Raney-catalysts depend on the amount of aluminum, which precipitates as alumina and mixed oxides on the catalyst surface. The nature and morphology of the deposit can by modified by doping with LiOH. Most likely islands of lithium dialuminate

and lithium hydroxide are formed on the catalyst surface exposing a higher fraction of clean metal surface. The selectivity to primary amine depends on the rate of a bi-molecular reaction forming N-butylidene-butylamine. The concentration of the reactive species on the surface decreases after LiOH doping the selectivity increases. In particular, LiOH modification of Raney-Co leads to enhanced selectivity by (i) reducing the catalyst sorption capacity for butyronitrile and amines, (ii) increasing the probability of the step-wise hydrogenation *via* nitrene species and (iii) poisoning of Al^{3+} Lewis acid sites that catalyze the condensation reaction.

Acknowledgments

Air Products & Chemicals Inc. is gratefully thanked for the generous financial support. Dr. Maritza Veprek-Heijman and Prof. Dr. Stan Veprek (Institut für Chemie Anorganischer Materialien, TUM) are thanked for the XPS measurement, help with the data interpretation and many discussions. Dr. Jeno Bodis is gratefully acknowledged for many stimulating discussions.

References

1 M. G. Turcotte, T. A. Johnson in: J. I. Kroschwitz (Ed.), Kirk-Othmer Encyclopedia of Chemical Technology Vol. 2 (4th Ed.), John Wiley & Sons, NY, 1992, p.369 - 386

2 M. Serra, P. Salagre, Y. Cesteros, F. Medina, and J. E. Sueiras, J. Catal. 209 (2002) 202

3 S. Alini, A. Bottino, G. Capannelli, R. Carbone, A. Comite and G. Vitulli, J. Mol. Catal. A: Chem. 206 (2003) 363

4 A. G. M. Barrett in: B. M. Trost (Ed.-in-Chief), Comprehensive Organic Synthesis Vol. 8 – Reduction, Pergamon Press, Oxford, 1991, p. 251 – 257

5 J. Barrault and Y. Pouilloux, Catal. Today 37 (1997) 137

6 P. Baumeister, M. Studer and F. Roessler in: G. Ertl, H. Knözinger, J. Weitkamp (Eds.), Handbook of Heterogenious Catalysis Vol. 5, Wiley-VCH, Weinheim, 1997, p. 2186 – 2195

7 F. Medina, P. Salagre and J.E. Sueiras, J. Mol. Catal. 81 (1993) 363

8 P. N. Rylander, Catalytic Hydrogenation over Platinum Metals, Academic Press, NY and London, 1967, p. 203 – 226

9 M. S. Wainwright in: G. Ertl, H. Knözinger, J. Weitkamp (Eds.), Preparation of Solid Catalysts, Wiley-VCH, Weinheim, 1999, p. 28 – 43

10 G. Cordier, P. Fouilloux, N. Laurain and J.F. Spindler, US Patent No. 5,777,166 (1998), to Rhone-Poulene Chimie

11 T. A. Johnson, US Patent No. 5 869 653 (1999), to Air Products and Chemicals, Inc

12 A. F. Elsasser, US Patent No. 5,874,625 (1999), to Henkel Corporation

13 F. Hochard-Poncet, P. Delichere, B. Moraweck, J. Jobic and A. Renouprez, J. Chem. Soc. Faraday Trans. 91 (1995) 2891

14 S. N. Thomas-Pryor, T. A. Manz, Z. Liu, T. A. Koch, S. K. Sengupta and W.N. Delgass, Catalysis of Organic Reactions - Chemical Industries Series Vol. 75, Marcel Dekker, 1998, p. 195

15 W. Reeve and J. Christian, J. Am. Chem. Soc. 78 (1956) 860

16 A. J. Chadwell Jr. and H. A. Smith, J. Phys. Chem. – US 60 (1956) 1339

17 J. P. Orchard, A. D. Tomsett, M. S. Wainwright and D. J. Young, J. Catal. 84 (1983) 189

18 S. Nishimura,M. Kawashuma, S. Inoue, S. Takeoka, M. Shimizu and Y. Takagai, Appl. Catal. 76 (1991) 19

19 G. Moretti, in: G. Ertl, H. Knözinger, J. Weitkamp (Eds.) Handbook of Heterogeneous Catalysis Vol.2, VCH-Wiley, Weinheim, 1997, p. 632 – 641

20 S. R. Montgomery in: W.R. Moser (Ed.) Catalysis of Organic Reactions - Chemical Industries Series Vol. 5, Marcel Dekker, 1981, p. 383 – 409

21 The fit included the data points that were recorded at the beginning of the isotherm and the equilibration time was at least 60 min; the R-squared value of the fit was 0.97 and 0.99 for Raney-Ni and Raney-Co catalysts, respectively.

22 J. D. Donnay and G. Harker, Am. Mineral. 22 (1937) 446; particles morphology was computed in Cerius^2 Modeling and Simulation Environment using Crystal Builder and Surface Builder modules.

23 J. R. Anderson, Structure of Metallic Catalysts, AP, London, 1975, p. 228

24 A. B. Fasman in: F. Herkes (Ed.) Catalysis of Organic Reactions - Chemical Industries Series Vol. 75, Marcel Dekker, 1998, p. 151 – 168

25 F. Hochard-Poncet, P. Delichere, B. Moraweck, H. Jobic and A. J. Renouprez, J. Chem. Soc. Faraday Trans. 91 (1995) 2891 and references therein

26 J. L. Falconer and J. A. Schwarz, Catal. Rev. – Sci. Eng., 25 (1983) 141

27 G. A. Martin and P- Fouilloux, J. Catal. 38 (1975) 231

28 M. J. F. M. Verhaak, A. J. van Dillen and J. W. Geus, Catal.Lett. 26 (1994) 37

29 A. Borgna, R. Frety, M. Primet and M. Guenin, Appl. Catal., 76 (1991) 233 and references therein

30 S. N. Thomas-Pryor, T. A. Manz, Z. Liu, T. A. Koch, S. K. Sengupta and W.N. Delgass, Catalysis of Organic Reactions - Chemical Industries Series Vol. 75, Marcel Dekker, 1998, p. 195

31 Y. Okamoto, J. Cryst. Growth 191 (1998) 405

32 J. P. Thiel, C. K. Chiang, and K. R. Poeppelmeier, Chem. Mater. 5 (1993) 297

33 M. Nayak, T. R. N. Kutty, V. Jayaraman and G. Periaswamy, J. Mater. Chem. 7 (1997) 2131

34 M. J. F. M. Verhaak, A. J. van Dillen and J. W. Geus, Appl. Catal., A 105 (1993) 251

35 Gmelin, System-Nr. 58: Kobalt, Teil A, Erg'bd. P. 511 (1961)

36 A. Baiker and M. Maciejewski, J. Chem. Soc. Faraday Trans.1 80 (1984) 2331

37 Gmelin, System-Nr. 58: Kobalt, Teil A, Erg'bd. P. 511 (1961)

38 C. D. Wagner, W. M. Riggs, L. E. Davis, J. F. Moulder in: G. E. Muilenberg (Ed.): Handbook of X-ray photoelectron spectroscopy, Perking-Elmer Corporation (Physical Electronics Division), 1979 (1st Edition)

39 C. D. Wagner, W. M. Riggs, L. E. Davis, J. F. Moulder in: G. E. Muilenberg (Ed.): Handbook of X-ray photoelectron spectroscopy, Perking-Elmer Corporation (Physical Electronics Division), 1979 (1st Edition)

40 C. D. Wagner, W. M. Riggs, L. E. Davis, J. F. Moulder in: G. E. Muilenberg (Ed.): Handbook of X-ray photoelectron spectroscopy, Perking-Elmer Corporation (Physical Electronics Division), 1979 (1st Ed.)

41 C. D. Wagner, W. M. Riggs, L. E. Davis, J. F. Moulder in: G. E. Muilenberg (Ed.): Handbook of X-ray photoelectron spectroscopy, Perking-Elmer Corporation (Physical Electronics Division), 1979 (1st Ed.)

42 C. D. Wagner, W. M. Riggs, L. E. Davis, J. F. Moulder in: G. E. Muilenberg (Ed.): Handbook of X-ray photoelectron spectroscopy, Perking-Elmer Corporation (Physical Electronics Division), 1979 (1st Ed.)

43 T. Yoshino, T. Abe and I. Nakabayashi, J. Catal. 118 (1989) 436

44 F. Hochard-Poncet, P. Delichere, B. Moraweck, J. Jobic and A. Renouprez, J. Chem. Soc. Faraday Trans. 91 (1995) 2891

45 D. Briggs and M. P. Seah (Eds.) Pratical surface analysis, Vol. 1, John WILLEY & SONS, 1993 (2nd Ed.)

46 C. D. Wagner, W. M. Riggs, L. E. Davis, J. F. Moulder in: G. E. Muilenberg (Ed.): Handbook of X-ray photoelectron spectroscopy, Perking-Elmer Corporation (Physical Electronics Division), 1979 (1st Ed.)

47 T. L. Barr, J. Vac. Sci. Technol A, 9, (1991) 1793

48 C. D. Wagner, W. M. Riggs, L. E. Davis, J. F. Moulder in: G. E. Muilenberg (Ed.): Handbook of X-ray photoelectron spectroscopy, Perking-Elmer Corporation (Physical Electronics Division), 1979 (1st Ed.)

49 T. L. Barr, J. Vac. Sci. Technol A, 9 (1991) 1793

50 C. D. Wagner, W. M. Riggs, L. E. Davis, J. F. Moulder in: G. E. Muilenberg (Ed.): Handbook of X-ray photoelectron spectroscopy, Perking-Elmer Corporation (Physical Electronics Division), 1979 (1st Ed.)

51 S. N. Thomas-Pryor, T. A. Manz, Z. Liu, T. A. Koch, S. K. Sengupta and W.N. Delgass, Catalysis of Organic Reactions - Chemical Industries Series Vol. 75, Marcel Dekker, 1998, p. 195

52 D. Brion, Appl. Surf. Sci., 5 (1980) 133

53 J. P. Contour, A. Salesse, M. Froment, M. Garreau, J. Thevenin and D. Warin, J. Microsc. Spectrosc. Electron.. 4 (1979) 483

54 N.S. McIntyre, M. G. Cook, Anal. Chem, 47 (1975) 2208

55 K.S. W. Sing and J. Rouquerol in: G. Ertl, H. Knözinger, J. Weitkamp (Eds.) Handbook of Heterogeneous Catalysis Vol.2, VCH-Wiley, Weinheim, 1997, p. 435

56 J. von Braun, G. Blessing and F. Zobel, Ber. 56B (1923) 1988

57 Y. Huang and W. M. H. Sachtler, Appl. Catal., A 182 (1999) 365

58 Mathieu C., Dietrich E., Delmas H., Jenck J., Chem. Eng. Sci. 47(9-11) (1992) 2289

59 C. Joly-Vuillemin, D. Gavroy, G. Cordier, C. De Bellefon and H. Delmas, Chem. Eng. Sci. 49 (1994) 4839

60 J. P. Thiel, C. K. Chiang, and K. R. Poeppelmeier, Chem. Mater. 5 (1993) 297

61 F. Hochard, H. Jobic, J. Massardier and A. Renouprez, J. Mol. Catal. A 95 (1995) 165

62 F. J. G. Alonso, M. G. Sanz and V. Riera, Organometallics 11 (1992) 801

63 A. Ozaki, Isotopic Studies of Heterogeneous Catalysis, Kodansha Ltd., Tokyo, Academic Press, London, 1977, p.140 - 141

64 B. Coq, D. Tichit and S. Ribet, J. Catal. 189 (2000) 117

65 P. Sykes, A Guidebook to Mechanism in Organic Chemistry, London & Singapore, Longman, 1986 (6^{th} Ed.)

66 M. J. F. M. Verhaak, A.J. van Dillen, J.W. Geus, Catal. Lett. 26 (1994) 37

67 B. Coq, D. Tichit and S. Ribet, J. Catal. 189 (2000) 117

Chapter 4

The catalytic performance of Raney-Co and LiOH-modified Raney-Co was tested in a three-phase high-pressure batch reactor where reactions were followed in-situ by ATR-IR spectroscopy. Catalyst activity and selectivitywere compared for a set of model reaction, in particular, (i) hydrogenation of butyronitrile, (ii) disproportionate of n-butylamine, (iii) hydrogenation of N-butylidene-butylamine in the presence of ammonia and (iv) hydrogenation /deuteration of N-butylidene-butylamine.

N-butylidene-butylamine has been identified as the key species in respect to the selectivity during the catalytic reduction of butyronitrile to n-butylamine over Raney-Co. After hydrogenation di-n-butylamine, the final by-product, is formed. N-butylidene-butylamine is formed on the catalyst surface, where unsaturated species react with one another. In the presence of LiOH this reaction is significantly retarded. It has been proposed, that improved hydrogenation-dehydrogenation properties of the modified catalyst drastically lower the transient concentration in reactive species on the catalyst surface. Additionally, the nucleophilic condensation among products of partial hydrogenation of butyronitrile is probably inhibited in the presence of a stronger nucleophile (OH-).

4 Towards Understanding the Selectivity in the Hydrogenation of Butyronitrile over Raney-Co Catalysts - Formation and Cleavage of N-butylidene-butylamine

4.1 Introduction

Industrially, primary amines are frequently synthesized by hydrogenation of the corresponding nitriles with molecular hydrogen [1]. However, the process is not selective and the formation of secondary and tertiary amines is observed [2]. A simulation of the thermodynamic equilibrium composition of a mixture of hydrogen, butyronitrile, 1°, 2° and 3° n-butylamines (Figure 4-1), shows that the selectivity to n-butylamine would be very low with a tendency to decrease at higher temperatures and low pressure [3].

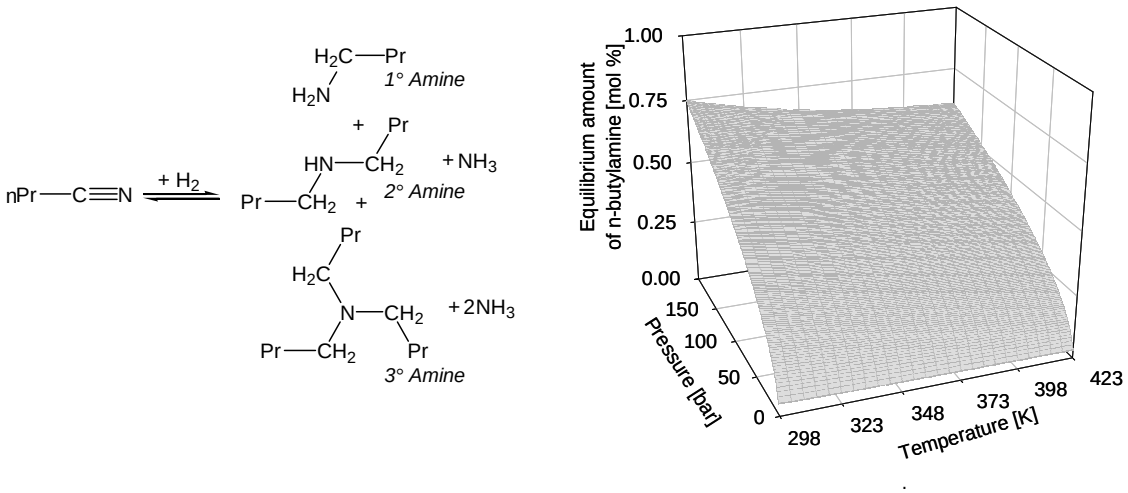

Figure 4-1: Simulation of thermodynamic equilibrium amount of n-butylamine formed in the reaction of hydrogen and butyronitrile in dependence on temperature and pressure. Possible products are 1°, 2° and 3° n-butylamines and ammonia. As starting composition butyronitrile (1 mol) and hydrogen (99 mol) were used.

With respect to the selectivity in primary amine (*i*) the choice of the catalytically active metal plays a key role [4] and (*ii*) an increasing fraction of secondary and tertiary amines is found in the reaction mixture, if the products are not separated from the catalyst once the hydrogenation is completed [5]. The selectivity can be kinetically controlled. Thus, for a high yield in 1° amine, the rate of the hydrogenation of unsaturated CN groups should be higher than that of the condensation reactions leading to 2° and 3° amines.

In the hydrogenation of butyronitrile over Raney-Co N-butylidene-butylamine had been observed as a reaction intermediate, which was hydrogenated to di-n-butylamine at the end of the reaction. In the presence of LiOH on the catalyst surface, the selectivity was

improved whereas the fraction of N-butylidene-butylamine was significantly reduced [6]. This catalytic system is important for a model study because N-butylidene-butylamine can be identified as the key species in respect to the selectivity (Figure 4-2).

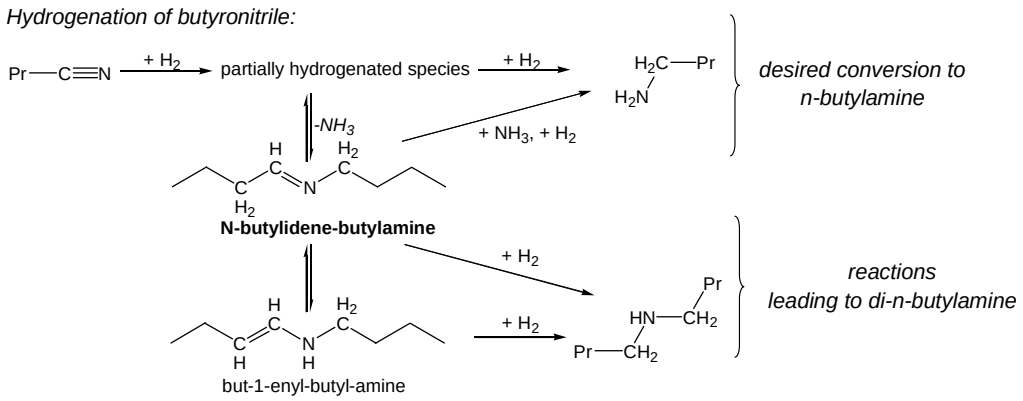

Figure 4-2: The studied network of reaction involving N-butylidene-butylamine.

The present study focuses on exploring the mechanism of formation of N-butylidene-butylamine over parent and LiOH-modified Raney-Co. The most important questions that were addressed concern the nature of the species reacting to N-butylidene-butylamine and the factors, which lead to the high selectivity over LiOH-modified Raney-Co. With N-butylidene-butylamine it was explored, if it is possible to cleave the imine bond to yield n-butylamine.

4.2 Experimental

4.2.1 Calculations of thermodynamic parameters

A simulation of the thermodynamic equilibrium for a mixture of hydrogen, butyronitrile, n-butylamine, di-n-butylamine, tri-n-butylamine and ammonia was performed in the range 1 to 200 bar pressure and 298 to 423 K temperature using HSC Chemistry 5.1 software (Outokumpu Research Oy). Density Functional Theory (DFT) Electronic Structure Program Dmol^3 version 4.2.1 [7] from Cerius^2 suite (Accelrys) was used to perform *ab initio* calculations.

4.2.2 Catalysts and Chemicals

Active Raney-Co^{TM} catalyst grade # 2700 lot # 2865 was obtained as aqueous suspension from the GRACE Davison Chemical Division of W.R. Grace & Co. The catalyst

chemical composition (wt. %) according to the company's release data sheets was as follows: Al (1.85), Co (97.51), Fe (0.3), Ni (0.34). The catalyst was weighted under water, washed by decantation and dried at ambient conditions under vacuum (BET area = 19.16 $m^2 \cdot g_{cat}^{-1}$). For doping with LiOH, a washed sample of Raney-Co was suspended in a solution of LiOH in water. Next, the catalysts was dried in a partial vacuum and subsequently handled under inert atmospheres or under reaction mixture. The amount of the LiOH deposited was ca. 0.4 wt.% as measured with AAS (UNICAM 939 AA-Spectrometer). The BET area was approximately 14.78 $m^2 \cdot g_{cat}^{-1}$ [8]. All chemicals but N-butylidene-butylamine were supplied by commercial providers and used as received (Table 2-2). These were as follows: butyronitrile, (≥ 99 % gc-assay, Fluka), 1°, 2° and 3° n-butylamines (> 99 % gc-assay, Aldrich), hydrocarbons octane and undecane (≥ 99 gc-assay, Aldrich) and gases: H_2, Ar, NH_3 (99.999, 99.999 and 99.98 vol. %, respectively, Messer-Griesheim GmbH) and D_2 (99.8 vol. %, Deutero GmbH). N-butylidene-butylamine (CAS No. 4853-56-9) was synthesized from n-butyraldehyde and n-butylamine and purified (> 99 % ^{1}H NMR-assay) according to ref. [9]. The analysis results of the synthesized N-butylidene-butylamine sample were as follows:

Elemental analysis for C, H and N was 76.52, 13.98 and 10.79 wt. %, respectively. This compares to the theoretical values of 75.52, 13.47 and 11.01 wt. %, respectively.

^{1}H NMR analysis (in $CDCl_3$ δ 7.24): δ 0.94 - 0.86 (two superimposed methyl groups, 6 H), δ 1.33 - 1.24 (m, 2 H), δ 1.58 -1.47 (two superimposed methylene groups, m, 4 H), δ 2.21 - 2.16 (m, 2 H), δ 3.3 (t, 2 H), δ 7.95 (t, 1H)

IR (ReactIR 1000): $\nu_{C=N}$ = 1670-1672 cm^{-1}

Positive identification of the reaction intermediate observed during hydrogenation of butyronitrile over parent Raney-Co as N-butylidene-butylamine was obtained by comparing the GC-MS spectra of the intermediate with the synthesized sample of N-butylidene-butylamine. The MS spectra were obtained with Mass Selective Detector HP-5971A after separation on Rtx - 5 Amine RESTEK column (Gas Chromatograph HP-5890 II).

4.2.3 Setup

Experiments were carried out in a mechanically stirred 160 cm^3 Parr reactor in conjunction with a ReactIR 1000 setup for *in situ* IR-analysis. The autoclave was charged at ambient conditions with catalyst suspended in the reaction mixture. The autoclave was pressurized several times with argon (up to 4.5 bar) to expel oxygen. If necessary, ammonia was then added from a loop. The reaction mixture was allowed to equilibrate at the reaction temperature and only then the hydrogen line was opened (defined as start of the reaction). Pressure, hydrogen flow and temperature were recorded on-line. In addition to the real-time IR analysis of the reaction mixture, a number of samples were withdrawn through a sampling loop for off-line gas chromatography analysis (GC). Identification of butyronitrile, mono- and di-n-butylamines and N-butylidene-butylamine was based on characteristic IR-regions for each compound (1348-1337; ~ 800; ~ 1133 and ~ 1671 cm^{-1}, respectively). The IR-data were referenced to the GC analyses (HP Gas Chromatograph 5890 equipped with a crosslinked 5% diphenyl-95% dimethyl-polysiloxane column 30 m, Restek GmbH, Rtx-5 Amine).

4.3 Results

4.3.1 Formation of N-butylidene-butylamine in the Hydrogenation of Butyronitrile

The hydrogenation of butyronitrile over parent Raney-Co was followed by *in situ* infrared spectroscopy (Figure 4-3). In Figure 4-4 concentration profiles for butyronitrile, mono- and di-n-butylamine and N-butylidene-butylamine derived from the integration of the IR-bands in the selected wavenumber regions are presented.

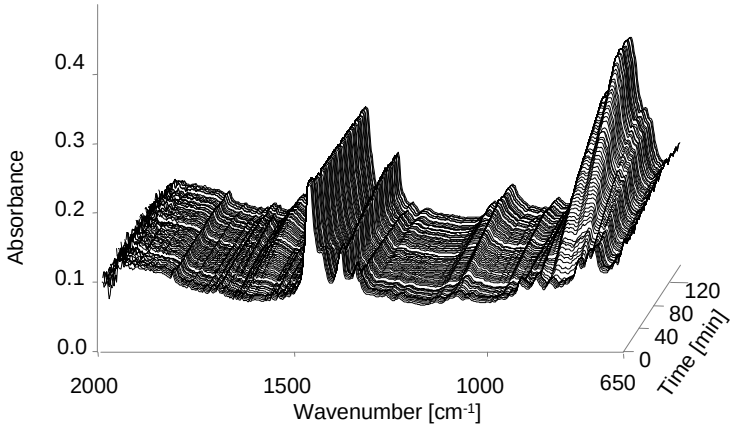

Figure 4-3: Time-resolved *in-situ* IR spectra of the reaction mixture during the hydrogenation of butyronitrile over 1.500 g catalyst sample of parent Raney-Co after 14 h pre-reaction equilibration at 373 K with the reaction mixture. Reaction conditions: T = 373 K, p_{H2} = 41 bar, c_0(butyronitrile) = 5.0 mol·dm^{-3} in octane.

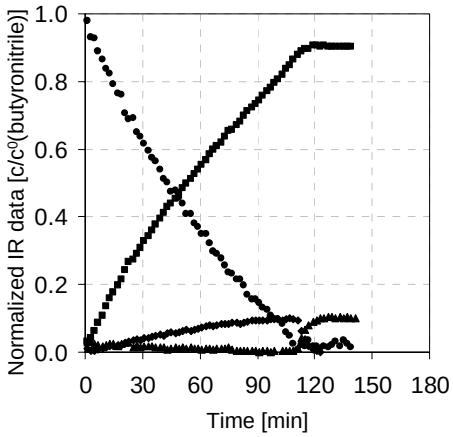

Figure 4-4: Hydrogenation of butyronitrile over 1.500 g catalyst sample of parent Raney-Co at T = 373 K, p_{H2} = 41 bar, c_0(butyronitrile) = 5.0 mol·dm^{-3} in octane. Concentration profiles for (●) butyronitrile, (■) n-butylamine, (♦) N-butylidene-butylamine and (▲) di-n-butylamine.

A mixture of butyronitrile in octane was pre-equilibrated for 14 h under inert atmosphere (N_2) in the presence of Raney-Co. Only minute changes in the intensity of the IR bands

corresponding to n-butylamine (934 – 662 cm^{-1}) and butyronitrile (1348 – 1337 cm^{-1}) were observed. Thus, it was concluded that reaction did not occur. Then, the hydrogenation was started by adding hydrogen (p = 41 bar). The intensity of the IR-bands increased in the region 934 – 662 cm^{-1} indicating n-butylamine formation, while at the same time the intensity decreased in the region 1348 – 1337 cm^{-1} indicating the consumption of butyronitrile. After more than 116 minutes further changes were not observed in the spectra and the hydrogenation of butyronitrile was finished.

Closer inspection of the IR spectrum between 1679 and 1659 cm^{-1} revealed a characteristic band due to the imine group (ca. 1671 cm^{-1} [10]), which was identified as N-butylidene-butylamine. Its presence was confirmed by gas chromatography (GC) and by comparison with the IR spectra of the pure substance. A gradual increase in intensity was observed reaching a maximum after 106 minutes. Then, an abrupt decrease in the intensity was observed (108 – 120 min). This correlated with a rapid increase in a band between 1152 – 1123 cm^{-1} attributed to di-n-butylamine. At longer reaction times (more than 120 minutes) the IR spectra showed a constant, but low absorption in the imine region. The hydrogenation of butyronitrile was also carried out after the equilibration time over Raney-Co had been extended to 40 h. The concentration profiles for butyronitrile, n-butylamine, N-butylidene-butylamine and di-n-butylamine were similar to those obtained from the previous experiment over parent Raney-Co. However, a much longer reaction time was required to complete hydrogenation (270 min). The initial reaction rate decreased from $173.3 \cdot 10^{-6}$ to $70.5 \cdot 10^{-6}$ $mmol_{butyronitrile} \cdot m_{cat.}^{-2} \cdot s^{-1}$. This suggests that Raney-Co deactivates upon prolonged heating in the presence of butyronitrile, while the final selectivity to n-butylamine remains (ca. 90 and 88 wt. %, respectively).

The reactions, which occur on the metal surface during the hydrogenation of nitriles have not been directly observed so far. However, it is generally postulated, that the reaction proceeds step-wise *via* formation of imines [11]. In the liquid phase the only intermediate observed is N-butylidene-butylamine which must have formed by a condensation reaction. Assuming the formation of butylidenimine ($CH_3CH_2CH_2CH{=}NH$) it could readily react with n-butylamine to N-butylidene-butylamine after desorption into the

liquid phase. Alternatively, the condensation reaction could occur on the catalyst surface, followed by desorption of N-butylidene-butylamine into the liquid phase. The rapid disappearance of the band at 1671 cm^{-1} at longer reaction times can be explained by the hydrogenation of N-butylidene-butylamine to di-n-butylamine. This reaction proceeds only at high conversions of butyronitrile. The reaction is inhibited by the presence of butyronitrile when present in significant amounts. Thus we conclude that butyronitrile adsorbs much stronger on Raney-Co than N-butylidene-butylamine.

The significantly reduced activity of Raney-Co after prolonged contact time with butyronitrile at 373 K is explained by the formation of carbonaceous deposits [12]. Additionally, nitrogen rich polyaromatic molecules may cover the metal surface [13].

Concentration profiles for butyronitrile and n-butylamine were also recorded *in situ* during the hydrogenation of butyronitrile over LiOH-modified Raney-Co (Figure 4-5).

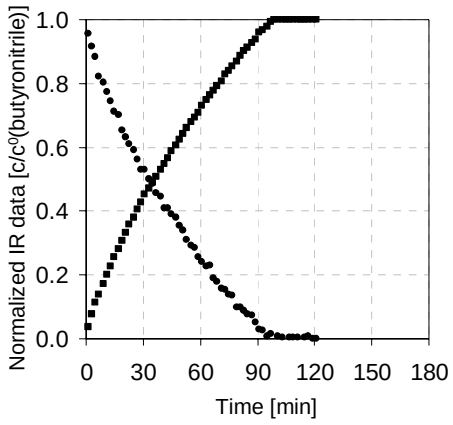

Figure 4-5: Hydrogenation of butyronitrile over 1.500 g catalyst sample of LiOH-modified Raney-Co at T = 373 K, p_{H2} = 41 bar, c_0(butyronitrile) = 5.0 mol·dm^{-3} in octane. Concentration profiles for (•) butyronitrile and (■) n-butylamine.

During the pre-equilibration time (15 h at 373 K) only insignificant changes were noted. About one minute after hydrogen was admitted to the system the band (934 – 662 cm^{-1}) of n-butylamine increased, while the band of butyronitrile (1348 – 1337 cm^{-1}) decreased indicating that hydrogenation of butyronitrile occurred. The initial reaction rate was calculated from the variations in the bands to be $316 \cdot 10^{-6}$ $mmol_{butyronitrile} \cdot m_{cat.}^{-2} \cdot s^{-1}$. After ca. 100 min further changes were not observed and the hydrogenation of butyronitrile was completed. Over the course of the hydrogenation, changes in the region of the C=N stretching vibrations (1679 - 1659 cm^{-1}) were not observed. Thus, it is concluded that N-

butylidene-butylamine was formed only in trace amounts. This observation was confirmed by GC analysis of the final reaction mixture, where di-n-butylamine was not found. Thus, the selectivity to n-butylamine was close to 100 %.

Interesting observations were noted in the mass balance over the course of hydrogenation over LiOH-modified Raney-Co (Figure 4-6).

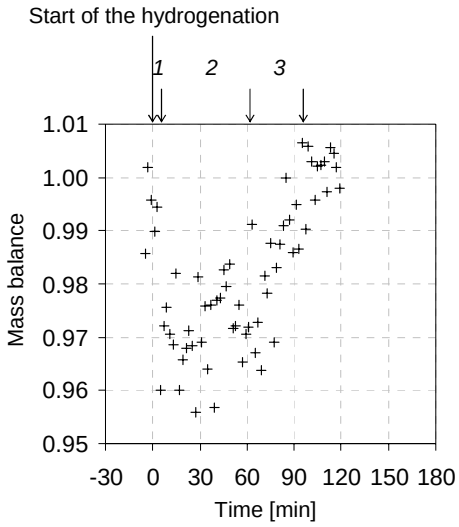

Figure 4-6: Mass balance calculated as $\frac{c_{(\text{butyronitrile})} + c_{(\text{n-butylamine})}}{c_{0\,(\text{butyronitrile})}}$ during the selective hydrogenation of butyronitrile over LiOH-modified Raney-Co.

Three main phases in respect to the reaction time could be distinguished. Right after addition of hydrogen to the system, the mass balance (99.5 ± 0.5 %) quickly decreased as more and more molecules were not spectroscopically recognized as either butyronitrile or n-butylamine. In the second phase, a steady-state was reached with about 3 ± 1 % of molecules unaccounted for. In the third part, the mass balance re-approached 100 %. The mass balance based only on the *in situ* spectroscopically measured concentrations of butyronitrile and n-butylamine indicates the presence of reaction intermediates.

It is speculated that on the catalyst surface these intermediates exist as adsorbed nitrene and/or carbene species [14]. Additionally, butylidenimine could be present on the surface. However, any desorbing butylidenimine would immediately react in the liquid phase to N-butylidene-butylamine.

In the first step, the concentration of the partially hydrogenated species builds up on the catalyst surface. Then, a steady state corresponding to a dynamic equilibrium between the formation of the surface intermediate (by hydrogenation of butyronitrile) and consumption (*via* hydrogenation to n-butylamine) is established. Towards the end of the reaction, the rate of formation of the intermediate slows down as the surface coverage in butyronitrile decreases.

4.3.1.1 Control of the Condensation Reaction

The higher selectivity, which was observed with LiOH doped Raney-Co is speculated to be caused by an increase in the rate of hydrogenation relative to the rate of the condensation reaction. To test this hypothesis n-butylamine was disproportionated at high hydrogen pressure to compare the catalytic activity for the condensation reaction of parent and LiOH-modified Raney-Co.

The concentration profiles for the disproportionation of n-butylamine to di-n-butylamine over (a) parent and (b) LiOH-modified Raney-Co were derived from *in-situ* IR analysis quantified with off-line GC analysis (Figure 4-7).

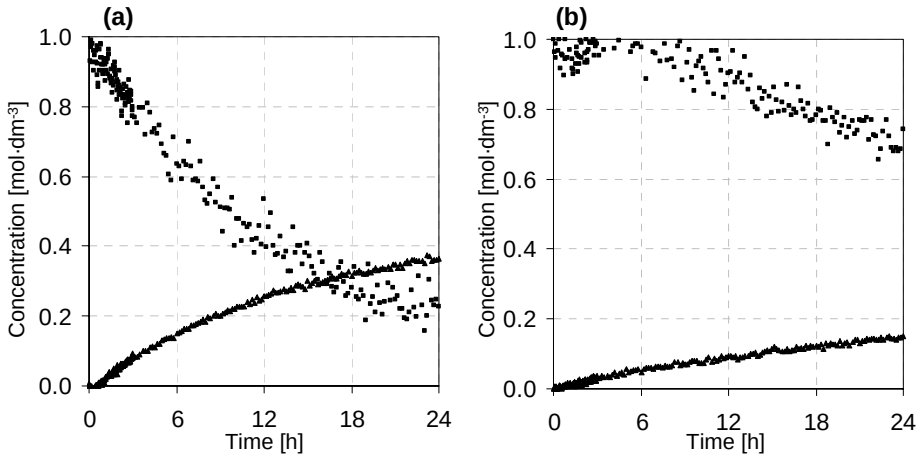

Figure 4-7: Concentration profiles during disproportionation of n-butylamine over (a) parent and (b) LiOH-modified Raney-Co at 421 K, p_{H2} = 41 bar, c_0(n-butylamine) = 1 mol·dm^{-3}. (■) n-butylamine, (▲) di-n-butylamine.

The disproportionation of n-butylamine over Raney-Co led to the formation of di- and tri-n-butylamine and ammonia. After 24 h at 421 K the molar ratio of 1°, 2° and 3° butylamines and ammonia in the reaction mixture was 0.26 : 0.36 : 0.01 : 0.38. The ratio deviated from the equilibrium mole fraction calculated for this temperature (0.02 : 0.47 :

0.02 : 0.50) [15]. Thus, full disproportionation was not accomplished. The rate was approximated with a first order dependence and the reaction rate constant (k_{Co}) was calculated to be $16.8 \cdot 10^{-6}$ s^{-1}. LiOH doping retarded the rate of the disproportionation reaction significantly. After 24 h the molar ratio of n-butylamine to di-n-butylamine and ammonia was 0.70 : 0.15 : 0.15, respectively; tri-n-butylamine was not detected. Similar to the parent Raney-Co the reaction was first order in n-butylamine. The rate constant ($k_{LiOH/Co}$) was $4.2 \cdot 10^{-6}$ s^{-1}. A control experiment in the absence of catalyst showed that the reaction does not occur in the fluid phase.

The disproportionation of n-butylamine is catalyzed by cobalt. Under experimental conditions (liquid phase, presence of hydrogen) the catalyst surface is likely saturated with n-butylamine. However, the hydrogenation/dehydrogenation function of cobalt was necessary for catalyzing the reaction. The strongly decreased rate of the condensation reaction over the LiOH-modified catalyst ($k_{Co(LiOH)}/k_{Co} = 0.25$) could be related to a lower number of catalytically active metal sites for dehydrogenation. The catalytic surface area was 25 % lower than for the parent material. This shows the high sensitivity of the reactivity with respect to a modest decrease in available Co on the surface. Further, the results suggest that LiOH inhibits the condensation reaction on the catalyst surface. There is no uniform kinetic description of the disproportionation of amines in the literature. Some studies have been presented on a zero order and a higher-than-one order disproportionation of ethylamine [16]. Based on isotopic studies of the disproportionation of methylamine Anderson and Clark concluded that the most likely mechanism is a surface bimolecular reaction between adsorbed amine residues [17].

4.3.2 Reactions of N-butylidene-butylamine

N-butylidene-butylamine has been identified as the key intermediate with respect to selectivity in the hydrogenation of butyronitrile to n-butylamine over Raney-Co. One strategy for improving the selectivity of the overall reaction is to convert N-butylidene-butylamine which has formed to n-butylamine. Formally, this can be done by adding ammonia to N-butylidene-butylamine and reductive C – N bond cleavage. This reaction constitutes the reverse of the condensation reaction. However, it should be noted that equilibrium thermodynamics suggests that the reaction will hardly proceed.

4.3.2.1 Cleavage of N-butylidene-butylamine to n-Butylamine

A mixture of N-butylidene-butylamine with excess ammonia ($n(NH_3)/n$(N-butylidene-butylamine) > 15) was equilibrated for 14 h at 333 K over the parent or the LiOH-modified Raney-Co. In line with the expectations, the intensity of C=N stretching band was constant during the equilibration period (*in situ* IR), confirming the absence of significant reactions. At the end of the equilibration period GC analysis was performed. Only a slight decrease (< 5 %) in N-butylidene-butylamine concentration was observed over each catalyst sample demonstrating that it hardly reacted with ammonia under the process conditions employed. Over the parent catalyst small amounts of n-butylamine were detected, while over the LiOH-modified catalyst some butyronitrile was formed. It has to be noted, however, that the GC analysis of the two mixtures showed that some (not identified) high molecular weight products were formed. At elevated temperature N-butylidene-butylamine would undergo aldol condensation [18].

The mixtures were then hydrogenated. The reaction was followed with *in-situ* IR spectroscopy and off-line GC analysis (Figure 4-8).

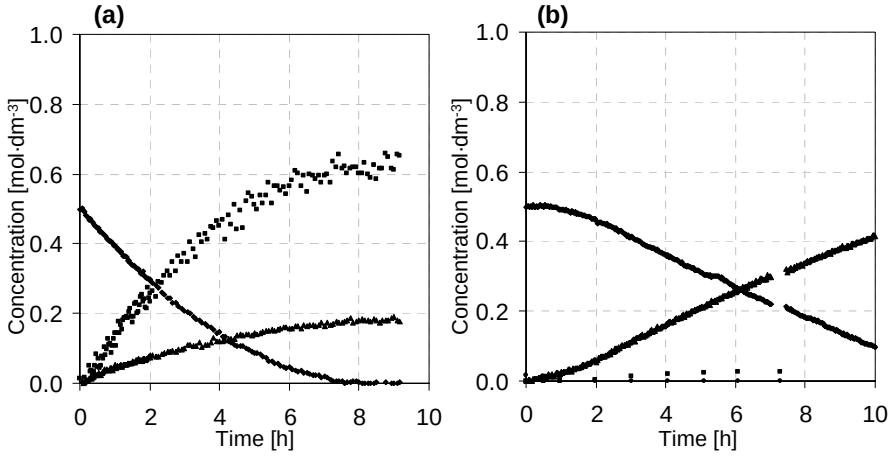

Figure 4-8: Concentration profiles during hydrogenation of a mixture N-butylidene-butylamine (c_0 = 0.05 mol·dm^{-3} in octane) and ammonia over 0.300 g (a) parent Raney-Co ($n_0(NH_3)$ = 0.39 mol) and (b) LiOH-modified Raney-Co ($n_0(NH_3)$ = 0.51 mol) at 333 K, p_{total} = 41 bar. (●) butyronitrile, (■) n-butylamine, (▲) di-n-butylamine, (♦) N-butylidene-butylamine.

Over the parent catalyst the hydrogenation of N-butylidene-butylamine in the presence of NH_3 led to a mixture of n-butylamine and di-n-butylamine. Whereas both amines were primary products, a higher selectivity to the primary amine was observed (64 % at the end of hydrogenation). The initial rate (r) of N-butylidene-butylamine consumption was

$264.6 \cdot 10^{-6}$ $mmol_{N\text{-butylidene-butylamine}} \cdot m_{cat}^{-2} \cdot s^{-1}$. The initial rate of formation of di-n-butylamine (r_1) and n-butylamine (r_2) was $120.0 \cdot 10^{-6}$ and $168.1 \cdot 10^{-6}$ $mmol_{N\text{-butylidene-butylamine}} \cdot m_{cat}^{-2} \cdot s^{-1}$, respectively.

In contrast, over LiOH-doped catalyst di-n-butylamine was the main product (97 % at 85 % conversion). The reaction started after an induction period, which correlated with the presence of butyronitrile in the mixture (formed during the equilibration period). Once all butyronitrile had been hydrogenated to n-butylamine, the hydrogenation of N-butylidene-butylamine proceeded with an apparent zero-order kinetic regime (the rate constant was estimated to be $157.6 \cdot 10^{-6}$ $mmol_{N\text{-butylidene-butylamine}} \cdot m_{cat}^{-2} \cdot s^{-1}$).

The hydrogenation of N-butylidene-butylamine in the presence of ammonia over the parent catalyst actually included two competing transformations. The first one was hydrogenation of N-butylidene-butylamine to di-n-butylamine (rate r_1); the other one was cleavage of the C-N bond in N-butylidene-butylamine to n-butylamine (overall rate r_2). Over parent catalyst, the rate of the latter reaction was so high ($r_2/r_1 = 1.4$) that the selectivity to n-butylamine prevailed. Over LiOH-doped catalyst the selectivity and the kinetics of hydrogenation of (N-butylidene-butylamine + NH_3) mixture changed dramatically. The conversion was slower but highly selective to di-n-butylamine. As a consequence of LiOH inhibition of the latter reaction hardly more n-butylamine was formed but that from the hydrogenation of butyronitrile found at the end of the equilibration period.

The observed differences between parent and LiOH-modified Raney-Co during the ammonolysis of N-butylidene-butylamine could originate from three aspects. N-butylidene-butylamine and ammonia are probably part of coupled equilibrium reactions (Figure 4-9).

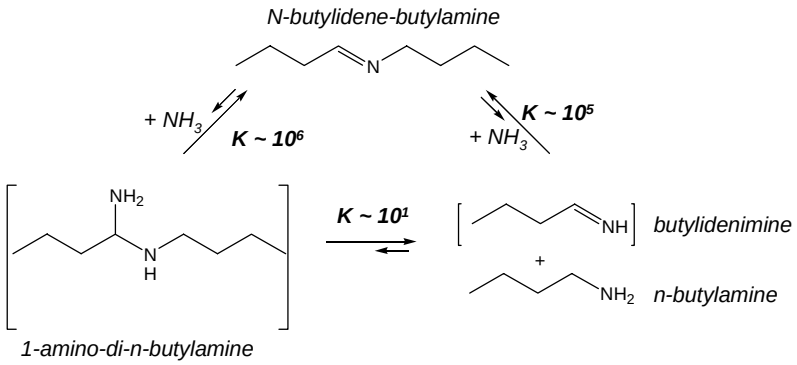

Figure 4-9: The set of equilibria that involve N-butylidene-butylamine and ammonia. The reactions equilibria (T = 333 K) were estimated from the DFT computed thermodynamic properties for each molecule.

The thermodynamically stable compounds are N-butylidene-butylamine, ammonia and n-butylamine, while 1-amino-di-n-butylamine and butylidenimine are the unstable species. Thus, the equilibrium is strongly shifted to N-butylidene-butylamine and NH_3 and only minute amounts of 1-amino-di-n-butylamine or butylidenimine could be formed. Note, that in presence of a strong nucleophile (i.e., OH^-) a hindrance of the nucleophilic addition of ammonia to N-butylidene-butylamine is possible.

Additionally, butylidenimine could be engaged in an equilibrium that forms 1-amino-n-butylamine [19]. On the other hand, butylidenimine undergoes other reactions such as polymerization [20] (Figure 4-10).

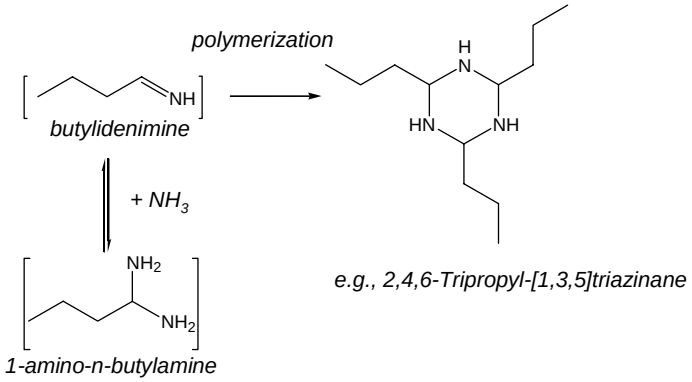

Figure 4-10: Reactions of butylidenimine during the ammonolysis experiment over Raney-Co.

With the parent catalyst, a slow accumulation of n-butylamine during the equilibration period is feasible, because butylidenimine is consumed by the polymerization reaction and, thus, removed from the coupled equilibration reactions presented in Figure 4-9.

The metal catalyst present in the system catalyzes the dehydrogenation of the surface species. The final product is butyronitrile.

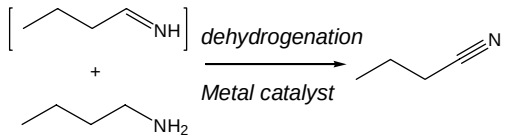

Figure 4-11: Dehydrogenation of surface species.

Only with LiOH-modified Raney-Co dehydrogenation was significant. This is attributed to a markedly weaker adsorption (of hydrogen) compared to the parent catalyst. The weaker adsorption of hydrogen on the LiOH modified catalysts is observed indirectly by the need for higher hydrogen pressures to rapidly start the hydrogenation reaction [21].

Let us discuss now the hydrogenation of intermediates from the mixture of N-butylidene-butylamine and ammonia leading to di-n-butylamine and / or n-butylamine. Di-n-butylamine forms *via* the hydrogenation of the surface-adsorbed N-butylidene-butylamine. The reaction occurs over both catalysts.

The formation of n-butylamine occurs through: (*i*) the hydrogenation of the surface-formed butylidenimine and/or (*ii*) hydrogenolysis of the C-N bond (in 1-amino-di-n-butylamine or 1-amino-n-butylamine) (Figure 4-12).

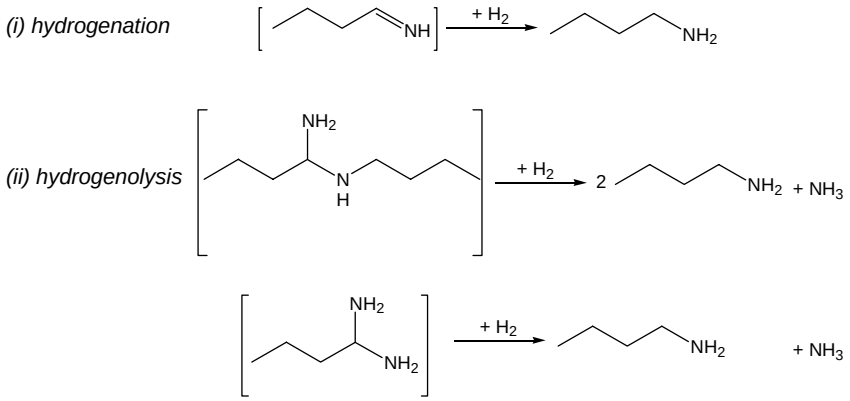

Figure 4-12: Formation of n-butylamine from the intermediate.

Over the parent catalyst the selectivity to n-butylamine is higher than to di-n-butylamine. Thus, the coupled equilibria of n-butylidene-butylamine and ammonia are easily restored as the surface species are consumed (Figure 4-12). Over LiOH-modified Raney-Co hardly any n-butylamine is formed (with the exception of that from the hydrogenation of butyronitrile found at the end of the ammonolysis period). We speculate that the

competing addition of a stronger nucleophile (OH^-) to the surface-adsorbed N-butylidene-butylamine hinders the reaction between ammonia and N-butylidene-butylamine.

4.3.2.2 Hydrogenation and Deuteration of N-butylidene-butylamine

The hydrogenation of the C=N bond in N-butylidene-butylamine is part of the reaction network (Scheme 4-1). In order to asses the rate of this step for the two catalysts the kinetics with the parent and the LiOH-modified catalyst was explored. Concentration profiles for the hydrogenation/deuteration of N-butylidene-butylamine over parent and LiOH-modified Raney-Co are shown in Figure 4-13.

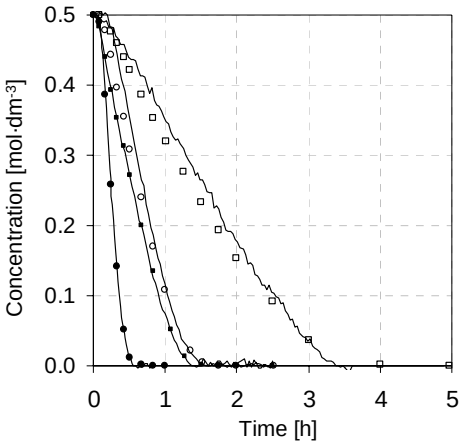

Figure 4-13: Concentration profiles for the hydrogenation of N-butylidene-butylamine over 0.300 g catalyst samples using either hydrogen or deuterium. Points represent GC-data: (•) H_2/parent catalyst, (○) D_2/parent catalyst (■) H_2/LiOH-modifiedRaney-Co (□) D_2/LiOH-modified Raney-Co, solid lines represent IR-data. Reaction conditions for each experiment: T = 373 K, p = 21 bar, c^0(N-butylidene-butylamine) = 0.5 mol·dm^{-3}.

The overall observations were similar for all experiments, regardless of the catalyst and the hydrogen isotope used. Typically the reaction started after a short induction period that lasted about 5 minutes after introduction of H_2 (or D_2) into the reactor. After that, N-butylidene-butylamine was hydrogenated (deuterated) with apparent zero-order dependence with respect to N-butylidene-butylamine until most of it had been consumed (> 90 %).

The reaction rates strongly depended on the catalyst and the hydrogen isotope used. For the parent catalyst the rate of hydrogenation and deuteration was calculated to $3.25 \cdot 10^{-3}$ and $1.13 \cdot 10^{-3}$ $mmol_{N\text{-butylidene-butylamine}} \cdot m_{cat}^{-2} \cdot s^{-1}$, respectively. For the LiOH-modified Raney-Co the rate of hydrogenation and deuteration was calculated to $1.47 \cdot 10^{-3}$ and

$0.60 \cdot 10^{-3}$ $mmol_{N\text{-butylidene-butylamine}} \cdot m_{cat}^{-2} \cdot s^{-1}$, respectively. Thus, with LiOH-modified Raney-Co, hydrogenation of N-butylidene-butylamine was significantly slower than with the parent material. An isotope effect was observed over both catalysts. The deuteration/hydrogenation reaction was highly selective to di-n-butylamine, although the GC chromatograms showed small amounts of high molecular weight by-products.

Each experiment was followed with *in situ* IR spectroscopy and an interesting difference between hydrogen and deuterium was observed (Figure 4-14 a and b, respectively).

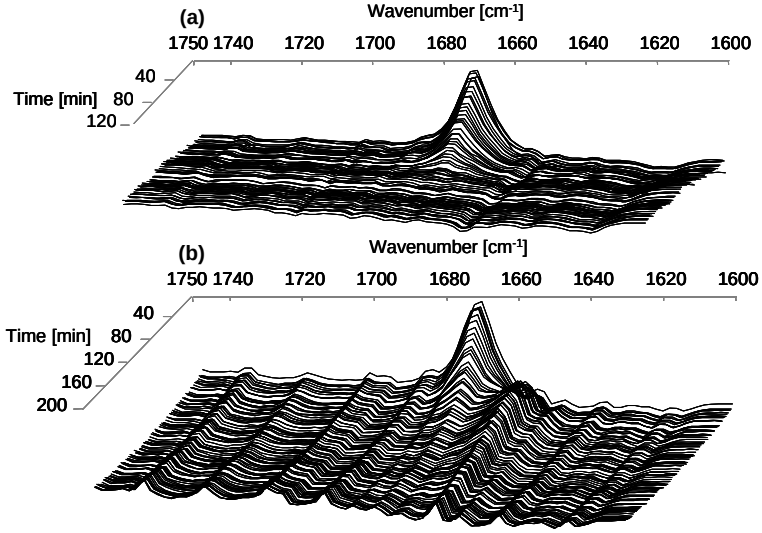

Figure 4-14: Time resolved -IR spectra from (a) hydrogenation and (b) deuteration of N-butylidene-butylamine over 0.300 g LiOH-modified Raney-Co (T = 373 K, p = 21 bar, c_0(N-butylidene-butylamine) = 0.5 $mol \cdot dm^{-3}$).

During the hydrogenation experiments a correlation between the decreasing intensity of the $\nu_{C=N}$ vibration (integration region 1683 - 1658 cm^{-1}) and the concentration determined by gas chromatography was observed. The formation of di-n-butylamine was evidenced by a band at 1133 cm^{-1}. During the first minutes of deuteration experiments a second band was observed at 1659 and 1656 cm^{-1} over parent and LiOH-modified Raney-Co, respectively in addition to the band of N-butylidene-butylamine at 1671 cm^{-1}. The intensity of both peaks decreased as the reaction progressed. The comparison with the data of gas chromatography indicated that N-butylidene-butylamine must account for both bands (i.e., 1683 - 1640 cm^{-1}). The band of deuterated di-n-butylamine was shifted to higher wavenumbers (peak maximum shifted from 1133 to 1214 cm^{-1}).

LiOH-modified Raney-Co has a lower activity for hydrogenation (2.2 times) and deuteration (1.9 times) of the C=N double bonds compared to the parent catalyst. This is in contrast to the improved activity observed in hydrogenation of butyronitrile. We speculate that the significantly weaker adsorption of N-butylidene-butylamine on the LiOH-doped catalyst causes the lower rate of the C=N bond hydrogenation in analogy to other catalysts selectively catalyzing the hydrogenation of C≡C triple bonds [22].

Assuming a Langmuir - Hinshelwood model, the kinetics of the saturation of the C=N bond is accomplished in two steps on the catalyst surface. The isotope effect on the reaction rate (r_H/r_D = 2.9 and 2.5 over parent and LiOH-modified catalyst, respectively) may arise either from the first or the second hydrogen transfer. Because r_H/r_D is largely determined by the difference in zero-point energy associated with the dissociating bond of surface adsorbed hydrogen and deuterium, the light hydrogen isotope reacts faster than deuterium since $E_{0(H)} > E_{0(D)}$ [23] (Equation 4-1; it is assumed that the dissociating or forming bond is so weak that the zero-point energy is negligible for the activated state marked "$\neq$")

$$k_H / k_D = \exp\left[\frac{\left(E^{\neq}_{0(D)} - E^{\neq}_{0(H)}\right) - \left(E_{0(D)} - E_{0(H)}\right)}{RT}\right] \qquad \text{Equation 4-1}$$

The zero-point energy difference between H_2 and D_2 (about 7.53 kJ·mol^{-1}) and a kinetic isotope effect during dissociative chemisorption of H_2 / D_2 on the catalyst surface does not play a role as this step reaches equilibrium (i.e., the Langmuir -Hinshelwood model). However, the thermodynamic isotope effect on the surface concentration of reactants (hydrogen and deuterium) should be considered. It has been reported that D_2 adsorbs stronger on Ni having the larger heat of adsorption of about 4.2 kJ·mol^{-1} than H_2 [24]. Similar effect on cobalt would lead to $\theta_D > \theta_H$ under given experimental conditions. Further, this would increase the saturation rate defined as $r = k \cdot \theta_{H(D)} \cdot \theta_{C=N}$. Modification of the cobalt surface with LiOH changes the catalyst sorption properties. Therefore, r_H/r_D for parent and LiOH-modified catalyst are expected to be different as it has been observed.

During deuteration, an unexpected shift in the stretching vibration of the C=N group to lower wavenumbers was observed ($\Delta\nu$ = 12 - 15 cm^{-1}). However, none of the atoms directly contributing to the $\nu_{C=N}$ stretch vibration was isotopically exchanged. If isotopic scrambling of deuterium and formation of $CH_3CH_2CHDCD=N(CH_2)_3CH_3$ is postulated, then the observed shift to lower wave numbers could be explained [25]. Note that the N-butylidene-butylamine is in equilibrium with its tautomeric form but-1-enyl-butylamine. If the second step is the slower, than the first step of the saturation reaction is in partially reversible and an isotopic scrambling within N-butylidene-butylamine would occur.

Aliphatic secondary amines with primary α-carbons (CH_2-NH-CH_2) have a medium-strong band at 1146 – 1132 cm^{-1} due to the asymmetric C-N-C stretch vibration [26]. After isotope exchange of hydrogen by deuterium at the nitrogen and α-carbon atoms a shift of vibration to higher wave numbers ($\Delta\nu$ = 81 cm^{-1}) is expected.

4.3.2.3 Imine-Enamine Tautomerism of N-butylidene-butylamine

For N-butylidene-butylamine four different isomers are possible: (E-) and (Z-) N-butylidene-butylamine and (E-) and (Z-) but-1-enyl-butyl-amine. The isomerization requires formal transfer of one hydrogen atom within the molecule (Figure 4-15). (E-) and (Z-) N-butylidene-butylamine could be involved in the cleavage route to n-butylamine via ammonolysis/hydrogenolysis of the C=N bond. Thus, it is of special interest to characterize the N-butylidene-butylamine/but-1-enyl-butyl-amine tautomeric mixture to obtain information about the thermodynamic and kinetic aspects of that equilibrium [27, 28, 29].

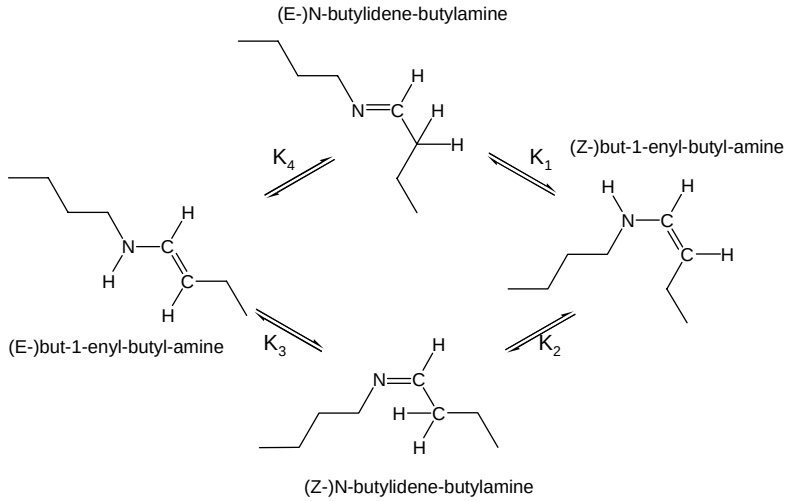

Figure 4-15: Imine-enamine tautomerism of N-butylidene-butylamine.

A comparison of the typical heat of hydrogenation of an isolated C=C double bond (115 - 120 kJ·mol^{-1}) with that reported for the hydrogenation of N-butylidene-butylamine (86 kJ·mol^{-1}) [30] indicates that the imine is thermodynamically more stable than the enamine. Therefore, under equilibrium conditions the imine form will be present in a higher concentration. The DFT calculation of the stability of each isomer showed that that (E-) N-butylidene-butylamine would be the prevailing isomer. Increase in temperature leads to an increase in the concentration of the thermodynamically less stable isomers. However, at the reaction conditions used in this study (~ 373 K) only 0.02 mol % of but-1-enyl-butyl-amine is formed.

A map of the ethylidene to vinylamine tautomerization and the possible structure of the transition state is presented in Figure 4-16. The hydrogen is transferred first to the imine carbon atom which changes hybridization from sp^2 to sp^3. In this way the hopping hydrogen remains bound to the molecule at the transition state and is then transferred to the nitrogen. A large energy barrier (ca. 312 [kJ·mol^{-1}]) was calculated for this reaction.

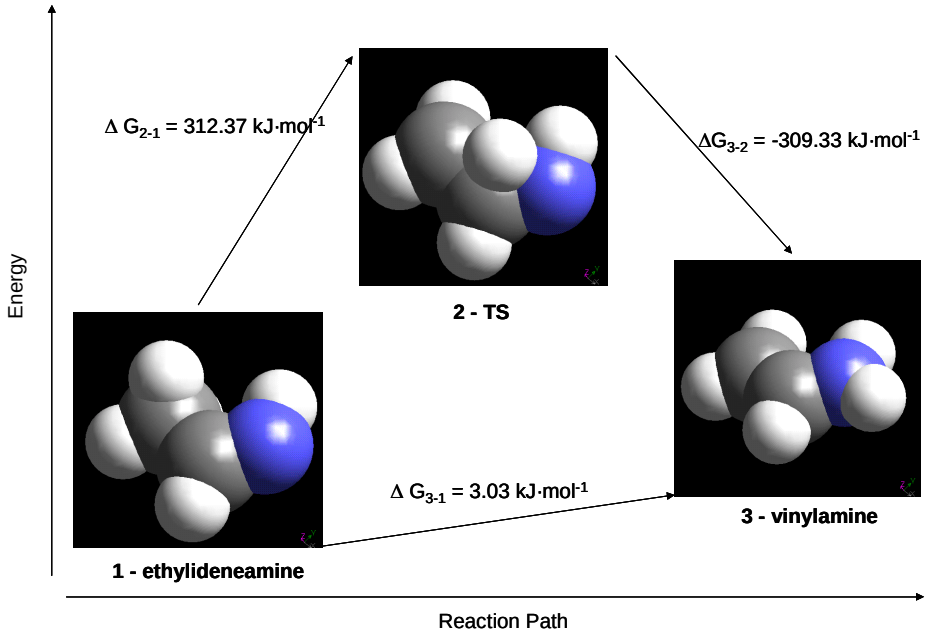

Figure 4-16: A computed map of the ethylidene to vinylamine tautomerization including possible structure of the transition state (DMol3).

The higher thermodynamic stability of the imine relative to the enamine is in agreement with the experimental observations for this and similar reaction systems [31]. High energy of activation of the tautomerization reaction practically prevents formation of the enamine isomers. On the other hand a catalytic enhancement for this reaction will be possible on metal surfaces (i.e., Raney-Co) in particular in a presence of atomic hydrogen on the surface.

4.4 Discussion

During hydrogenation of butyronitrile over Raney-Co the competing reactions are (*i*) hydrogenation of unsaturated CN groups (rate r_H) and (*ii*) nucleophilic condensation (rate r_{NC}). The system is kinetically controlled (i.e., selectivity to n-butylamine ~ 90 %) and does not reach the thermodynamic equilibrium state under which a mixture of 1°, 2° and 3° n-butylamines and ammonia is formed (n-butylamine ~ 1 %). When Raney-Co is modified with LiOH an even higher selectivity to n-butylamine is observed (> 99 %). The selectivity enhancement originates from an increase in the ratio r_H/r_{NC}. In the presence of LiOH adsorbate-surface interactions are decreased. Furthermore, an inhibiting effect of the strong nucleophile OH^--group is proposed.

4.4.1 Formation of N-butylidene-butylamine

Over parent catalyst a side-reaction yields N-butylidene-butylamine. The reaction involves two molecules originating from butyronitrile. The probable mechanism of N-butylidene-butylamine formation is based on a nucleophilic condensation mechanism. A reactive species with unsaturated carbon atom undergoes nucleophilic attack by a nitrogen species to form a new C-N bond. The process is accompanied by the release of NH_3. It is generally assumed that the reactive intermediate is imine i.e., butylidenimine. It should be noted that in *situ* spectroscopy has not provided direct evidence for this step. However, the butylidenimine concentration in the liquid phase may be well below the detection limit of the IR probe used in the study. Further, even if butylidenimine desorbs in very minute amounts, it would undergo rapid condensation in the liquid phase [32]. The reaction between N-butylidene-butylamine and ammonia has been tested as a reverse route to those species. Over the parent catalyst n-butylamine (the nucleophile) is found, whereas short-living butylidenimine is not found. Instead, some high molecular weight products are detected. Note that n-butylamine in reaction with butylidenimine would directly yield N-butylidene-butylamine.

Over LiOH-modified Raney-Co the hydrogenation of butyronitrile is selective to n-butylamine. Because LiOH remains on the catalyst surface during reaction, it is evident that only surface species can be prevented from nucleophilic condensation. This has been demonstrated by the surface-catalyzed disproportionation of n-butylamine to di-n-butylamine. Thus, in the mechanism of butyronitrile hydrogenation a number of surface-adsorbed species should be considered. The presence of carbene species could still lead to the formation of N-butylidene-butylamine as the reactive center on the unsaturated carbon atom is available. However, it is speculated that the strong nucleophile OH^- inhibits nucleophilic attack of other nucleophiles (nitrogen compounds) and thus hinders the formation of the C-N bond.

Over LiOH-modified catalyst ammonolysis of N-butylidene-butylamine unexpectedly yields only butyronitrile. This implies fast dehydrogenation of the products (i.e., butylidenimine and n-butylamine). Probably LiOH-modified Raney-Co exhibits better dehydrogenation and hydrogenation activity than parent catalyst. It has been reported that

over oxides (e.g., MgO) dehydrogenation of primary amines to nitriles easily proceeds [33]. Consequently, the transient surface concentration in species reacting to N-butylidene-butylamine (like butylidenimine) would be decreased and the rate of the bi-molecular surface reactions would be retarded.

4.4.2 Cleavage of N-butylidene-butylamine

Over Raney-Co the amount of N-butylidene-butylamine produced is inversely correlated with the selectivity to n-butylamine for the hydrogenation of butyronitrile. Thus, a decrease in its concentration before full saturation to di-butylamine can be proposed as a selectivity enhancement. The reaction of N-butylidene-butylamine with ammonia in presence of hydrogen indeed yields n-butylamine. However, hydrogenation to di-n-butylamine also occurs. It should be mentioned that it is not realistic to expect full conversion of N-butylidene-butylamine to n-butylamine, because N-butylidene-butylamine also exists in its tautomeric form as but-1-enyl-butyl-amine. The tautomerization occurs *via* intramolecular hydrogen transfer and is likely catalyzed by the metal. But-1-enyl-butyl-amine probably does not react with ammonia and its hydrogenation contributes to the formation of di-n-butylamine.

In contrast, in the presence of LiOH, N-butylidene-butylamine hardly reacts with NH_3 and practically only di-n-butylamine is obtained after hydrogenation. Most likely, the much stronger nucleophile OH^- (i.e., LiOH) forms a surface adsorbed amino-alcohol (or its salt) and protects the C=N group from nucleophilic attack of ammonia. Further hydrogenolysis produces di-n-butylamine. By analogy it could also be possible that LiOH inhibits the nucleophilic condensation among partially hydrogenated intermediates during the hydrogenation of butyronitrile.

4.5 Conclusions

In the hydrogenation of butyronitrile to n-butylamine over Raney-Co N-butylidene-butylamine is the product of a side-reaction on the catalyst surface. Modification of Raney-Co with LiOH (0.4 wt. % Li^+) gives a more active and selective catalyst (> 99 % selectivity). With the modified catalyst hardly any N-butylidene-butylamine is formed. Probably the hydrogenation-dehydrogenation properties of the LiOH-modified catalyst

are enhanced compared to the parent catalyst. This would lead to a drastically lower transient concentration in reactive species on the catalyst surface. Additionally, the nucleophilic condensation among products of partial hydrogenation of butyronitrile in the presence of a much stronger nucleophile (OH^-) is likely inhibited.

Acknowledgments

Dr. Jeno Bodis is gratefully acknowledged for many elucidating discussions.

References

1 M. G. Turcotte, T. A. Johnson in: J. I. Kroschwitz (Ed.), Kirk-Othmer Encyclopedia of Chemical Technology Vol. 2 (4th Ed.), John Wiley & Sons, NY, 1992, p. 369 - 386

2 M. Hudlicky, Reductions in Organic Chemistry - ACS Monograph Vol. 188, American Chemical Society, Washington DC, 1996, p. 239 - 241

3 HSC Chemistry 5.1 - Chemical Reaction and Equilibrium Software with extensive Thermochemical Database, Outokumpu Research Oy.

4 F. Medina, P. Salagre and J.E. Sueiras, J. Mol. Cat. 81 (1993) 363

5 P. N. Rylander, Catalytic Hydrogenation over Platinum Metals, Academic Press, NY and London, 1967, p. 203 – 226

6 A. Chojecki, T. E. Müller and J. A. Lercher, Characterization of Raney-Ni and Raney-Co and Their Use in the Selective Hydrogenation of Butyronitrile *to be submitted*

7 B. Delley, J. Chem. Phys. 92 (1990) 508

8 The BET area was not measured for that sample, however, another batch of LiOH-doped Raney-Co (0.5 wt. % Li^+) showed BET area of 14.78 $m^2 \cdot g_{cat}^{-1}$.

9 R. A. Benkeser and D.C. Snyder, J. Organomet. Chem. 225 (1982) 107

10 N. B.Colthup, L. H. Daly and S.E. Wiberley, Introduction to Infrared and Raman Spectroscopy, Academic Press, NY and London, 1990 (3rd Ed.), p. 344 - 345

11 P. N. Rylander, Hydrogenation Methods, Academic Press, London, 1988 (2nd Ed.), p. 94 – 103

12 A. Fási, J.T. Kiss, B. Török and I. Pálinkó, Appl. Catal., A 200 (2000) 189

13 Y. Huang and W.M.H. Sachtler, Appl. Catal., A 191 (2000) 35

14 B. Coq, D. Tichit and S. Ribet, J. Catal. 189 (2000) 117

15 HSC Chemistry 5.1 - Chemical Reaction and Equilibrium Software with extensive Thermochemical Database, Outokumpu Research Oy.

16 A. Baiker and J. Kijenski, Catal. Rev. – Sci. Eng., 27 (1985) 653 and references therein

17 J.R. Anderson and N.J. Clark, J. Catal. 5 (1966) 250

18 R.W. Layer, Chem. Rev. 63 (1963) 489

19 P. N. Rylander, Hydrogenation Methods, Academic Press, London, 1988 (2nd Ed.), p. 94 – 103

20 M.R. Crampton, S.D. Lord and R. Millar, J. Chem. Soc., Perkin Trans. 2, (1997) 909

21 A. Chojecki, T. E. Müller and J. A. Lercher, Characterization of Raney-Ni and Raney-Co and Their Use in the Selective Hydrogenation of Butyronitrile *to be submitted*

22 M. Gruttadauria, R. Noto, G. Deganello and L.F. Liotta, Tetrahedron Lett., 40(14) (1999) 2857

23 A. Ozaki, Isotopic Studies of Heterogeneous Catalysis, Kodansha Ltd., Tokyo, Academic Press, London, 1977, p. 169 – 203.

24 G. Wedler, F.J. Bröker, G. Fisch and G. Schroll, Z. Phys. Chem. N. F. 76 (1971) 212

25 W. Fresenius, J. F. K. Huber, E. Pungor, W. Simon, Th. S. West, Tabellen zur Strukturaufklärung organischer Verbindungen mit spektroskopischen Methoden, Springer-Verlag, Berlin, 1986.

26 N.B.Colthup, L.H. Daly and S.E. Wiberley, Introduction to Infrared and Raman Spectroscopy, Academic Press, NY and London, 1990 (3rd Ed.), p. 341

27 K. Lammertsma and B.V. Prasad, J. Am. Chem. Soc. 116 (1994) 642

28 P. Perez and A. Toro-Labbe, Theor. Chem. Acc. 105 (2001) 422

29 W. Koch and M.C. Holthausen, A Chemist's Guide to Density Functional Theory (2nd Ed), Wiley-VCH, Weinheim, 2001

30 G. Hafelinger and L. Steinmann, Angew. Chem. Int. Ed. Engl. 16 (1977) 47

31 S.P. Lu and A.H. Lewin, Tetrahedron, 54 (1998) 15097

32 M.R. Crampton, S.D. Lord and R. Millar, J. Chem. Soc., Perkin Trans. 2 (1997) 909

33 H. Abe and A.T. Bell, J. Catal. 142 (1993) 430 and references therein

Chapter 5

In order to characterize the catalytic process during the hydrogenation of butyronitrile on the surface of parent and LiOH-modified Raney-Co Incoherent Inelastic Neutron Scattering (INS) spectroscopy was used in combination with ab initio computational study of molecular vibrations. Because of the large scattering contrast INS can be used as a surface technique to study the adsorption of hydrogen and hydrogenation reactions on the transition metal surfaces.

Sorption of hydrogen onto Raney-Co at low pressure is mainly related to the three-fold sites. Wet deposition of LiOH onto Raney-Co and subsequent temperature treatment at 473 K creates clustered rather than layered lithium hydroxide which vibrational frequencies are well described by the factor group analysis of crystalline LiOH. On Raney-Co butyronitrile and hydrogen promptly react yielding a number of (partially-) hydrogenated derivatives that are characterized by the presence of hydrogen atom(s) on the nitrogen atom. In consequence the condensation reaction leading to condensation products (i.e., N-butylidene-butylamine) is feasible.

5 Inelastic Neutron Scattering Study of Hydrogen and Butyronitrile Adsorbed on Raney-Co Catalysts

5.1 Introduction

Raney catalysts are sponge-like particles formed by selective leaching of aluminum (using e.g., $NaOH_{aq.}$) from binary or multicomponent alloys of Al with catalytically active metals (typically Cu, Ni, Co) and promoters (e.g., Cr, Fe, Mo) [1]. Raney-Co catalysts are used commercially, e.g., in the reduction of nitriles with molecular hydrogen to primary amines [2]. Although the reactions which occur on the metal surface have not been directly followed yet, it is generally assumed that this reaction proceeds step-wise. Imines as well as surface-adsorbed nitrene and carbene species have been postulated as partially hydrogenated intermediates (Figure 5-1) [3, 4, 5]. Intermediates with unsaturated carbon atoms are susceptible to nucleophilic condensation reactions. These side reactions lead to the formation of Schiff bases and enamines that are further hydrogenated to secondary and tertiary amines [6]. As a result, mixtures of primary, secondary and tertiary amines and ammonia are frequently obtained.

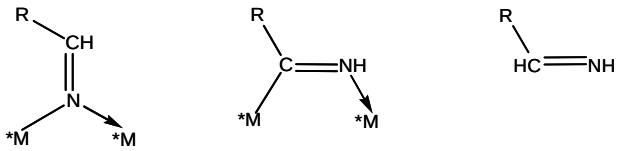

Figure 5-1: Possible intermediates in the catalytic hydrogenation of nitriles over transition metal catalysts.

In the absence of ammonia which is generally used as solvent in the commercial process, the thermodynamically controlled selectivity to primary amines is very low (< 1 mol % in the hydrogenation of butyronitrile [7]). A high selectivity to primary amines requires kinetic control where the hydrogenation of unsaturated C-N groups is much faster than the formation of by-products. It is apparent that the choice of the catalyst strongly influences the relative rate of reaction [8]. Enhancement of the kinetic control of selectivity can be accomplished in the presence of alkali additives [9]. In order to characterize the catalytic process during the hydrogenation of butyronitrile on the surface of parent and LiOH-modified Raney-Co, Inelastic Neutron Scattering (INS) spectroscopy was used in combination with an *ab initio* computational study of molecular vibrations.

INS is particularly sensitive to vibrational modes that involve hydrogen motion in the molecules because of a large incoherent scattering contrast between ^{1}H and all other elements and isotopes (including ^{2}H) [10]. Due to virtual transparency of condensed matter for neutrons (low absorption cross-section), INS becomes a surface characterization technique for studying hydrogen adsorption and hydrogenation reaction on the transition metal surfaces [11, 12, 13].

5.2 Experimental

5.2.1 Sample Preparation

Raney-Co (GRACE Davison Chemical Division of W.R. Grace & Co grade # 2700 lot # 7865) with the chemical composition: Al, 1.85; Co, 97.51; Fe, 0.3; Ni, 0.34 wt. % was used. The catalyst (212 g) was washed with deionized water until the pH of the wash water was ~ 7. The volatiles were removed in low vacuum (< 4 mbar) and the catalyst was dried (at 323 K, 10 h). Doping with LiOH was carried out in an aqueous solution of LiOH (3.254 g in 100 cm^3 deionized water, room temperature, left for 1 h) followed by drying in low vacuum (at 323 K, 10 h). The concentration of Li^+ in Raney-Co(LiOH) was 0.5 wt. % as measured with AAS (UNICAM 939 AA-Spectrometer). Pre-dried Raney-Co catalysts, both the parent and the LiOH-modified samples (m_{cat} = 25 g) were placed inside aluminum containers used for INS experiments under inert atmosphere. Note that N_2 adsorption for 0.5 g samples of the parent and the LiOH-modified Raney-Co activated in high vacuum at 473 K for 1 h had shown a specific BET surface area of 24.5 and 14.8 $m^2 \cdot g_{cat.}^{-1}$, respectively. For INS the catalysts were further activated at UHV ($p \leq 10^{-6}$ mbar) at 473 K for 6 h. For reference measurements, samples of such activated Raney-Co and LiOH-Raney-Co were used. Another Raney-Co sample was equilibrated with H_2 at 0.2 bar. Two other samples of parent and LiOH-doped Raney-Co were in contact with butyronitrile (13.02 and 9.41 mmol of butyronitrile, respectively) and were subsequently equilibrated with 0.2 bar H_2.

5.2.2 Measurement

Experiments were carried out at 10 K. The beryllium-filter detector spectrometer IN1BeF at ILL in Grenobxle with a Cu (220) monochromator plane was used. The instrument

resolution was varying from 25 cm^{-1}, at low energy transfers, to 50 cm^{-1} at large energy transfers. Note that the spectra were recorded in meV, and are presented in wavenumber units (1 meV = 8.065 cm^{-1}) after subtracting the Be-filter energy shift of 40 cm^{-1}. Apart from the Raney-Co samples, reference spectra of solid butyronitrile (Aldrich) and an empty aluminum container were recorded.

5.2.3 Data Treatment

Vibrational modes of hydrogen adsorbed on different cobalt clusters were computed in Dmol^3 version 4.2.1 from the Cerius^2 program suite (2001), Accelrys Inc. [14]. Cobalt clusters (4 – 5 atoms) were cut out from the bulk crystal of hcp Co. Each calculation included minimization of a hydrogen atom over 1 to 4 cobalt atoms with fixed coordinates, followed by computation of the vibrational frequencies of the system at the optimized geometry. The generalized gradient approximation (gga) DFT method with Perdew-Wang 1991 (p91) Hamiltonian and double numeric basis functions including polarization functions (dnp) in expansion of molecular orbitals were used in the runs. In order to meet the SCF convergence criteria electronic state was set on 'thermal' which allows electrons to be smeared out among all orbitals within in the vicinity of the Fermi level. Note, that the crystal structure of cobalt is hexagonal close-packed with dominant crystal morphology of (100), (101) and (002) planes (40.79, 39.65 and 19.65 % of the facet area, respectively) [15]. For butyronitrile, n-butylamine and butylideneimine a*b initio* quantum mechanical calculations with the B3LYP hybrid functional (a 6-31G** basis set) and Hartree-Fock approximation followed by a MØller-Plesset correlation energy correction truncated at second-order (MP2) were done with GAUSSIAN 98 [16]. The a-CLIMAX software was used to calculate the INS spectra from the theoretical frequency and amplitude results [17].

5.3 Results and Discussion

The INS spectra of the activated parent Raney-Co and after adsorption of hydrogen on the parent catalyst are shown in Figure 5-2 a. The INS spectrum of the activated LiOH modified Raney-Co is presented in Figure 5-2 b.

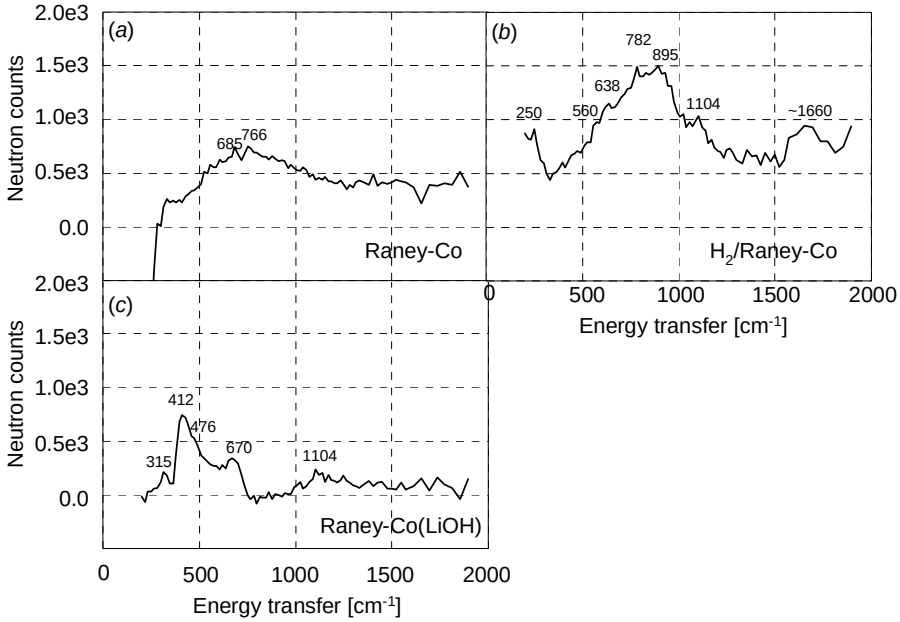

Figure 5-2: (a) The INS spectrum of activated Raney-Co after subtraction of INS spectrum of Al-container (b) the INS spectrum activated Raney-Co equilibrated with H_2 (0.2 bar) after subtraction of INS spectrum of activated Raney-Co; (c) the INS spectrum of activated LiOH-modified Raney-Co after subtraction of INS spectrum of activated Raney-Co.

The spectrum of Raney-Co showed a broad background in the range 450 - 1200 cm^{-1} with two maxima at 685 and 766 cm^{-1}. Above 1200 cm^{-1} the spectrum was flat. The difference spectrum of Raney-Co equilibrated with hydrogen was characterized by a much more intense background compared to the parent sample. A number of small peaks sitting on the background were exposed (i.e., 250, 560, 638, 782, 895 and 1104 cm^{-1}). Another peak was detected in the high energy transfer region (~ 1660 cm^{-1}). The spectrum of Raney-Co(LiOH) showed a small peak at 315 cm^{-1}, a strong peak at 412 with a shoulder at 476 and a peak at 670 cm^{-1}.

In the INS spectrum of the activated Raney-Co a contribution of the quantized lattice vibrations of the Co hcp crystal are expected below 300 cm^{-1} with maxima at approximately 250, 200, and 133 cm^{-1} [18] (the Co fcc phonon frequencies are also below 300 cm^{-1} [19]). On the other hand, the activation procedure might not have been

sufficient to remove all the residual hydrogen and water, compare reference [1]. Note that the multiply-bound, strongly adsorbed hydrogen appears in the spectrum below 1200 cm^{-1} [20, 21]. Water adsorbed on Co-surface is dissociated to atomic hydrogen and atomic oxygen [22]. Thus, with the catalyst surface of high heterogeneity a wide range of adsorption sites for residual hydrogen could be observed.

After adsorption of hydrogen on Raney-Co, multiply-bound hydrogen is mainly observed. An assignment of different adsorption sites to hydrogen on Raney-Co after DFT-calculated vibration modes of hydrogen on different cobalt facets (Figure 5-3) is presented in Table 5-1. For comparison, an assignment of hydrogen adsorbed on Raney-Ni is included [23].

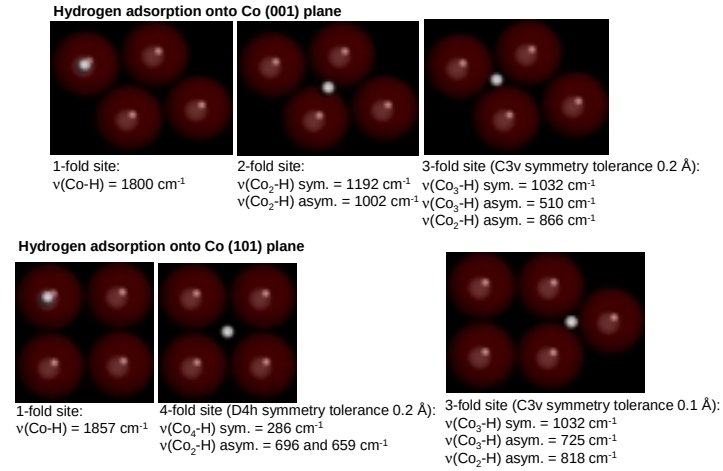

Figure 5-3: Hydrogen adsorption onto Co(001) and Co (101) planes computed with DMol[3].

Table 5-1: Assignment of hydrogen adsorption mode onRaney-Co and Raney-Ni.

Raney-Co [cm^{-1}]	Proposed Interpretation	Raney-Ni [cm^{-1}]	Description after [23]
~ 250	Hydrogen on 4-fold sites with D4h symmetry (i.e., 101 plane); Co_4-H symmetric stretching vibrations.		
~ 573	Hydrogen on 3-fold sites with C3v symmetry (i.e., 001 plane); Co_3-H antisymmetric stretching vibrations.	~ 600	The symmetric stretching of μ4-H species adsorbed on (100) facets
~ 637	Hydrogen on 3-fold sites with C3v symmetry (i.e., 101 plane); Co_3-H antisymmetric stretching vibrations. Probably some contribution from 4-fold sites (‘hollow sites’) with D4h symmetry: Co_2-H antisymmetric stretching vibrations.		
~ 782	Hydrogen on 3-fold sites with C3v	~ 800	The antisymmetric stretching of μ3-H

	symmetry (i.e., 101 plane); Co_2-H asymmetric stretching vibrations.		species adsorbed on (110) facets
~ 894	Hydrogen on 3-fold sites with C3v symmetry (i.e., 001 plane); Co_2-H antisymmetric stretching vibrations.	~ 940	The antisymmetric stretching of μ3-H species adsorbed on (111) facets
~ 1100	Hydrogen on 3-fold sites with C3v symmetry (i.e., 001 and 101 planes); Co_3-H symmetric stretching vibrations.	~ 1100 ~ 1130	The symmetric stretching of μ3-H species adsorbed on (110) facets The symmetric stretching of μ3-H species adsorbed on (111) facets
~ 1660	Probably hydrogen on some 1-fold sites. However, the DFT calculations of single bound hydrogen on 101 and 001 planes yield a peak at 1800 – 1860 cm^1.	~ 1800	The stretching vibrations of μ1-H species (on-top hydrogen); the bending mode is expected between 800 and 1130 cm^{-1}, and is thus hidden by the more intense features due to multiply bound hydrogen

It is particularly noteworthy to mention that sorption of hydrogen onto Raney-Co at low pressure is mainly related to the three-fold sites (corresponding to maxima at 782, 895 and 1100 cm^{-1}). Relatively small contribution of 'on-top' hydrogen has been observed, however, this binding mode can be prevailing at a high hydrogen pressure.

The wet deposition of LiOH onto Raney-Co surface and the subsequent activation procedure at 473 K may lead to a number of lithium compounds. Most likely, a surface reaction of lithium hydroxide monohydrate ($LiOH \cdot H_2O$) with bayerite (aluminum hydroxide found on the surface of Raney catalysts) produce lithium dialuminate ($Li_2Al_2(OH)_7 \cdot 2H_2O$) [24]. Removal of structural water from $Li_2Al_2(OH)_7 \cdot 2H_2O$ occurs below 473 K [25], whereas the crystal water of $LiOH \cdot H_2O(s)$ is removed already at ~ 380 K [26]. Thus, dehydrated lithium hydroxide (mostly) and small amount of lithium aluminates are expected. The former having hydrogen in the structure should significantly contribute to the INS differential spectrum of LiOH deposited on Raney-Co. The crystal structure of lithium hydroxide belongs to the tetragonal symmetry group D_{4h}^7 ≡ P4/nmm and each Bravais cell contains two formula units of LiOH [27, 28]. The internal and external fundamental vibrations are classified into five symmetry species of the D_{4h}^7 group (i.e., a_{1g}, e_g, b_{1g}, a_{2u}, e_u) [29]. The IR and Raman vibrational active modes have been studied in detail [30, 31, 32, 33], and a high-temperature study of polycrystalline LiOH by INS has been presented by Safford and LoSacco [34].

The observed bands in the INS differential spectrum of LiOH deposited on Raney-Co mainly result from vibrations that involve motions of the OH^- group. Consequently, it is

proposed that the INS band at 315 cm^{-1} represents translational lattice vibrations (i.e., T'(OH^-)) of the a_{1g} species (329 and 332 cm^{-1} in Raman and INS spectra of polycrystalline LiOH, respectively). The very strong INS vibration at 412 cm^{-1} can be assigned to the rocking lattice mode of OH^- (R'(OH^-)) of the e_u symmetry species (419 cm^{-1} in IR spectrum). The adjacent, less intense INS vibration (the shoulder at 476 cm^{-1}) reveals probably T'(OH^-) of the a_{2u} species. The literature data on this vibration are conflicting. The IR data by Yoshida and Hase refer to a vibration at 595 cm^{-1} as the a_{2u} species' coupled vibration of T'(OH^-) and T'(Li^+) [35, 36]. On the other hand, Buchanan *et. al.* have reported a vibration at 495 cm^{-1} as the IR active vibration of the a_{2u} symmetry species [37]. Also Safford and LoSacco have presented the INS spectrum of LiOH with an intense peak at 468 cm^{-1}. The vibration at 670 cm^{-1} in the INS spectrum might be assigned to the pure rotational vibration of OH^- groups of the e_g species. The R'(OH^-) with a contribution from the mechanical coupling with T'(Li^+) is recorded at 620 cm^{-1} in the Raman spectrum and corresponds to the INS peak at 625 cm^{-1} of LiOH. Note that the acoustic lattice vibrations of LiOH and the internal stretching modes of OH^- are expected to appear outside the energy scale of the INS spectrum considered (i.e., below 200 and above 3000 cm^{-1}, respectively).

In Figure 5-4, the differential INS spectra of co-adsorbed butyronitrile and hydrogen on parent (*a*) and LiOH-modified Raney-Co (*c*) are shown after subtraction of the reference background. The INS spectrum of a solid sample of butyronitrile (*b*) is also included.

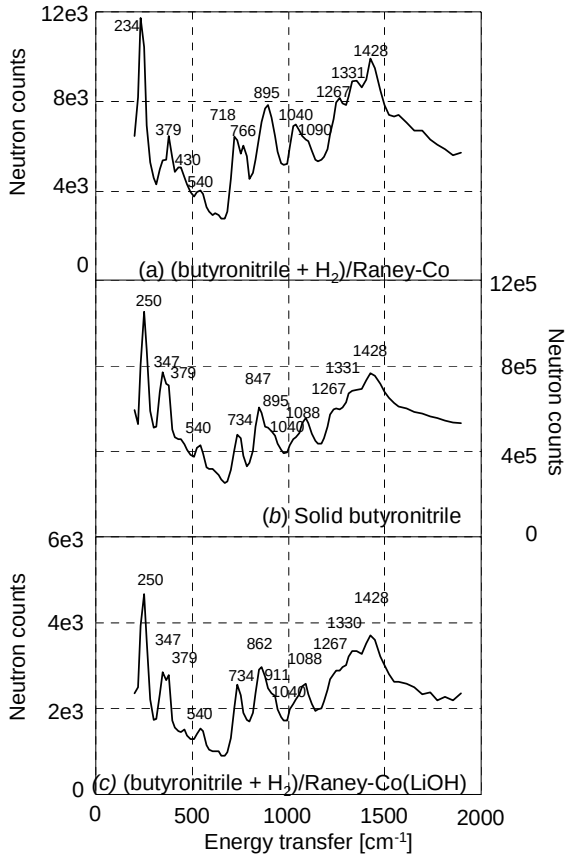

Figure 5-4: The INS spectra of co-adsorbed butyronitrile and hydrogen on parent (*a*) and LiOH-modified Raney-Co (*c*) after subtraction of the reference background. The INS spectrum of a solid sample of butyronitrile (*b*) is included for comparison.

The intensity of the INS spectrum of solid butyronitrile was higher by two orders of magnitude than those of the other two spectra. This is related to the higher amounts of the scatterer present in the former sample. The visual comparison of the spectra disclosed that different INS spectra of co-adsorbed hydrogen and butyronitrile were obtained when either parent or LiOH-modified Raney-Co was used as adsorbent. The latter fairly well matched the INS spectrum of butyronitrile as the peak shapes and the peak positions were reproduced. The only exception was noted for the peak at 862 cm^1 (with the shoulder at 911 cm^{-1}) that position was slightly shifted compared to the peak at 847 cm^{-1} (with the shoulder at 895 cm^{-1}) in the INS spectrum of solid butyronitrile. In contrast, the INS spectrum of butyronitrile and hydrogen co-adsorbed on the parent catalyst featured a number of peaks that were absent or got modified when set against the INS spectrum of butyronitrile. Note a doublet at 347 and 379 cm^{-1} in the INS spectrum of butyronitrile that in the INS spectrum of co-adsorbed butyronitrile and hydrogen on parent catalyst was

replaced by one peak (at 389 cm^{-1}) accompanied by a new peak at 430 cm^{-1} of a low intensity. Another peak at 734 cm^{-1} found in the INS spectrum of butyronitrile was absent in the INS spectrum of co-adsorbed butyronitrile and hydrogen on the parent catalyst. Instead, a double peak at 718 and 766 cm^{-1} was found. Further, an asymmetric peak at 847 cm^{-1} with a shoulder at 895 cm^{-1}, observed in the spectrum of butyronitrile, was replaced by a fairly symmetric peak at 895 cm^{-1} when butyronitrile was co-adsorbed with hydrogen on cobalt surface. However, all three spectra were fairly similar above 1200 cm^{-1} (i.e., the peaks at ~1428, ~1331 and ~1267 cm^{-1}). Probably, the hydrocarbon fragment of butyronitrile does not interact significantly with the surface of the cobalt catalysts.

A detailed description of vibrational modes of the butyronitrile molecule based on DFT calculations and a proposed assignment of observed peaks in the INS spectrum is presented in Table 5-2. The IR vibrations are included for comparison.

Table 5-2: Detailed description of vibrational modes of the butyronitrile molecule based on DFT calculations and a proposed assignment of observed peaks in the INS and ATR-IR spectra of butyronitrile.

vibration	Description of the vibrations of the butyronitrile molecule $C^{(\gamma)}H_3\text{-}C^{(\beta)}H_2\text{-}C^{(\alpha)}H_2\text{-}C\equiv N$	DFT [cm^{-1}]	INS [cm^{-1}]	IR [cm^{-1}]
ν_3	Torsion of C(γ)H3 , τ(C(γ)H3)	g98: 252 DMol^3: 226	250	
ν_4	In-plane deformation of the carbon chain at C(γ)-C(β)-C(α) and C(α)-C≡N (in-phase)	g98: 350 DMol^3: 339	347	
ν_5	Out-of-plane deformation of the carbon chain at C(α)-C≡N	g98: 367 DMol^3: 389	379	
ν_6	In-plane deformation of the carbon chain at C(α)-C≡N	g98: 521 DMol^3: 515	540	
ν_7	Rock vibration of the methylene groups C(β)H2 and C(α)H2 (out-of-phase) and rock vibration of the C(γ)H3	g98: 761 DMol^3: 717	734	741 768
ν_8	Rocking C(α)H2, twisting of C(β)H2 and rocking of the C(γ)H3	g98: 899 DMol^3: 846	847	841
ν_9	Stretching ν(C(γ)-C(β)) and ν(C(β)-C(α)) and ν(C(α)-CN) (in-phase)	g98: 906 DMol^3: 864	895	874
ν_{10}	Stretching ν(C(γ)-C(β)) and ν(C(α)-CN) (out-of-phase)	g98: 984 DMol^3: 959		917 944
ν_{11}	Stretching ν(C(γ)-C(β)) and ν(C(β)-C(α)) (out-of-phase)	g98: 1096 DMol^3: 1023	1040	1050
ν_{12}	Stretching ν(C(γ)-C(β)) and ν(C(α)-CN) (in-phase)	g98: 1151 DMol^3: 1082		1090
ν_{13}	Deformation of the chain C(γ)-C(β)-C(α)-C≡N	g98: 1162		1098

		DMol^3: 1093		
ν_{14}	Twisting, C(α)H2 and C(β)H2 (out-of-phase)	g98: 1300 DMol^3: 1223		1235
ν_{15}	Wagging, ρ(C(β)H2) and ρ(C(α)H2) (in-phase)	g98: 1338 DMol^3: 1277	1267	1262
ν_{16}	Twisting of C(β)H2 and C(α)H2 (in-phase)	g98: 1367 DMol^3: 1305		1281
ν_{17}	Wagging, ρ(C(β)H2) and ρ(C(α)H2) (out-of-phase)	g98: 1434 DMol^3: 1353	1331	1339 1343
ν_{18}	Bending, δ(C(γ)H3) "the umbrella bend"	g98: 1469 DMol^3: 1372		1387
ν_{19}	Bending, δ(C(α)H2) "the scissoring bend" (conjugation with the nitrile group)	g98: 1527 DMol^3: 1415	1428	1427
ν_{20}	Bending, δ(C(β)H2) "the scissoring bend" and deformation of C(γ)H3 (in-phase)	g98: 1551 DMol^3: 1445		
ν_{21}	Deformation C(γ)H3	g98: 1559 DMol^3: 1458		
ν_{22}	The scissoring bend of C(β)H2 and deformation of C(γ)H3 (out-of-phase)	g98: 1566 DMol^3: 1460		1464

It had been expected that hydrogen and butyronitrile, activated on the cobalt surface, might react to a number of partially hydrogenated species (full hydrogenation yields n-butylamine). Surprisingly, the hydrogenation reaction is apparently retarded on the cobalt surface modified with LiOH since the INS spectrum of butyronitrile is virtually reproduced for this sample. In this respect a prolonged induction period had been observed in the catalytic hydrogenation of butyronitrile with Raney-Co(LiOH) [38]. While few butyronitrile molecules could react with the co-adsorbed hydrogen, the hydrogen pressure was believed to reach equilibrium at 0.2 bar (the free volume of the experimental cell would confine up to 0.3 mmol of H_2). Consequently, the molar ratio H_2 to butyronitrile might be insufficient to observe hydrogenation process in the INS spectrum. The only indication of the reaction proceeding is a shift of the peak at 847 to 863 cm^{-1} (the shoulder is shifted from 895 to 911 cm^{-1}).

The INS spectrum of co-adsorbed hydrogen and butyronitrile on the parent Raney-Co depicts a cobalt surface covered with partially hydrogenated butyronitrile. In addition, the presence of co-adsorbed atomic hydrogen on the three-fold sites is disclosed by the large peak at ~ 895 cm^{-1} (compare with the H_2 adsorption onto parent Raney-Co, Figure 5-2 b). In order to characterize observed surface species the INS spectrum of co-adsorbed butyronitrile and hydrogen on the parent catalyst (*b*), is compared with computed spectra

of the products of full and partial hydrogenation of butyronitrile, i.e., n-butylamine (*a*) and butylidenimine (*b*) (Figure 5-5).

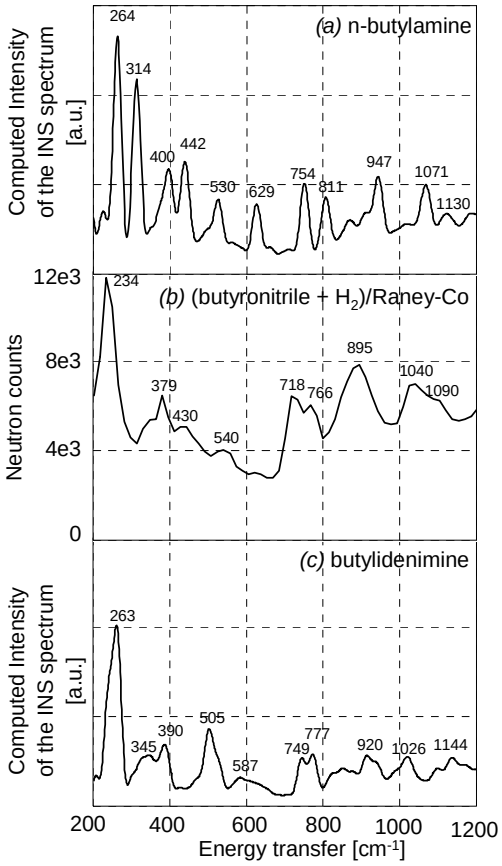

Figure 5-5: The comparison of the differential INS spectrum of co-adsorbed butyronitrile and hydrogen on parent catalysts with the computed spectra of butylamine and butylidenimine (GAUSSIAN 98, followed by a Fourier smoothing procedure).

In general, the computed spectrum of butylidenimine better reproduced the experimental spectrum. Remarkably, the presence of two overlapping peaks in the experimental spectrum at 718 and 766 cm^{-1} was also computed in the INS spectrum of butylidenimine (at 749 and 777 cm^{-1}). However, similar but slightly more separated peaks occurred also in the computed spectrum of butylamine (at 754 and 811 cm^{-1}). The considered doublet indicates a motion of one (two) hydrogen atom(s) attached to the nitrogen atom (i.e., wagging and twisting vibrations).

The step-wise hydrogenation of the nitrile group on the metal surface may proceed *via* a number of surface-adsorbed species (Figure 5-6). The selectivity to primary amine is high as long as the probability of condensation of the electrophilic carbon center with nitrogen

nucleophiles with formation of a new C – N bond remains low. In this respect a low surface coverage in reactive species and a protection of the reactive carbon center are important factors. Note that if hydrogenation preferentially runs *via* nitrene species (Figure 5-6, route a) then after the second addition of a hydrogen atom, the carbon center becomes saturated and the condensation is not feasible anymore. Furthermore, nitrene species binding strongly to the metal center would be non-reactive for the condensation reaction. The partially hydrogenated derivatives of the butyronitrile molecule can be characterized as carbene species that have an electrophilic reaction center on the unsaturated carbon atom and a nucleophilic reaction center on the (partially) hydrogenated nitrogen atom. The condensation reaction leading to N-butylidene-butylamine among carbene species is possible (Figure 5-6, route b).

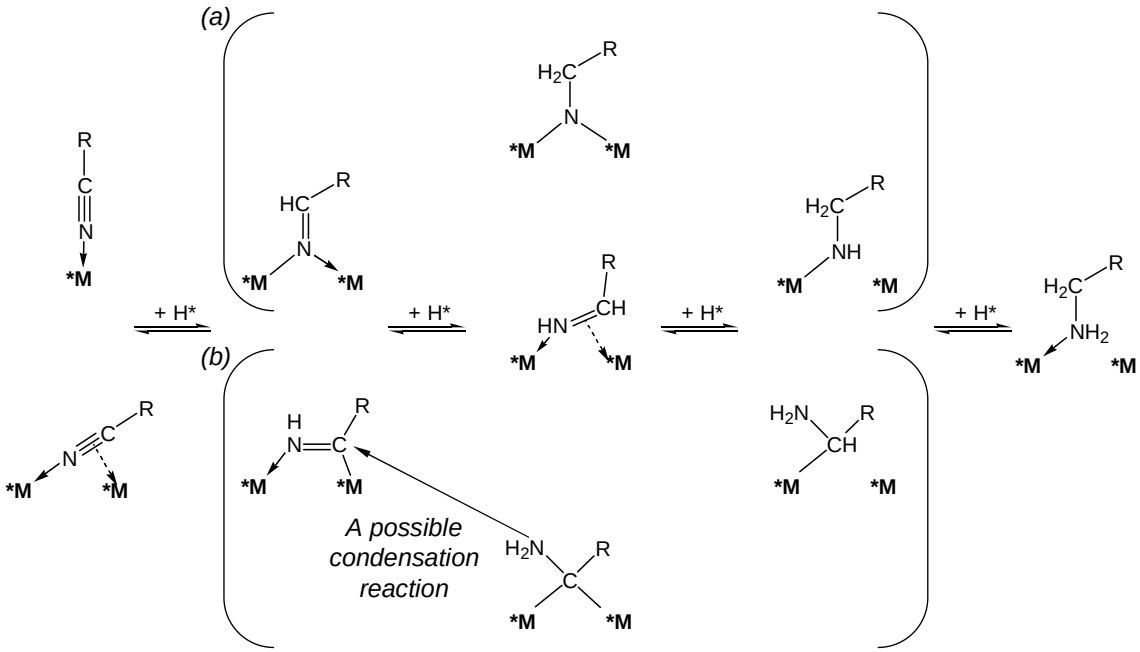

Figure 5-6: Possible intermediates during the hydrogenation of the C≡N group.

The protection of the carbon center could be provided by a competing surface nucleophile, e.g. by the LiOH modification of the Raney-Co. On the other hand, if the alkali-doped cobalt surface adsorbs nitrogen species stronger *via* the nitrogen atom then the nitrile preferential adsorption mode is vertically to the surface. Consequently the reactivity of the carbon atom for hydrogenation is enhanced, and the nitrene route of the hydrogenation is dominant.

5.4 Conclusions

Sorption of hydrogen onto Raney-Co at low pressure is mainly related to the three-fold sites. Wet deposition of LiOH onto Raney-Co and subsequent temperature treatment at 473 K creates clusters of LiOH rather than a thin film on the cobalt surface. The factor group analysis can be used to describe vibrational frequencies of LiOH crystallites on the cobalt surface. On Raney-Co, butyronitrile and hydrogen react promptly to partially-hydrogenated derivatives that are characterized by the presence of hydrogen atom(s) on the nitrogen atom. The condensation reaction leading to N-butylidene-butylamine is feasible. Treatment of Raney-Co with LiOH leads to modified sorption properties of the catalyst surface. It is speculated that strong binding *via* the nitrogen atom may stimulate swift hydrogenation of the carbon atom in the nitrile group. This preserves it from secondary condensation reactions. However, further experimental evidence is necessary to proof the presence of nitrene species populating the surface of Raney-Co(LiOH) during the reaction.

Acknowledgment

Dr. Herve Jobic (Institut de Recherches sur la Catalyse, France), PD. Andreas Jentys, PhD, and Prof. Dr. Winfried Petry (Lehrstuhl für Experimentalphysik IV, TUM) are gratefully thanked for the introduction to INS spectroscopy, help with ab initio calculations, and the discussion of the results. Institut Laue-Langevin is thanked for access to the IN1-BeF spectrometer and, in particular, Alexander Ivanov for assistance during the INS experiments. A sample of Active Raney-Co grade # 2700 lot # 7865 was kindly donated by Unichema Chemie GmbH, Emmerich, Germany.

References

1 M.S. Wainwright in: G. Ertl, H. Knözinger, J. Weitkamp (Eds.), Preparation of Solid Catalysts, Wiley-VCH, Weinheim, 1999, p. 28 – 43

2 M. G. Turcotte, T. A. Johnson in: J. I. Kroschwitz (Ed.), Kirk-Othmer Encyclopedia of Chemical Technology Vol. 2 (4th Ed.), John Wiley & Sons, NY, 1992, p.369 - 386

3 P. R. Rylander, Hydrogenation Methods, Academic Press, London, 1988 (2nd Ed.), p. 94 - 103

4 B. Coq, D. Tichit and S. Ribet, J. Catal. 189 (2000) 117

5 F.J.G. Alonso, M.G. Sanz, V. Riera, Organometallics 11 (1992) 801

6 Y. Huang, W.M.H. Sachtler, Appl. Catal. A 182(2) (1999) 365

7 Calculation performed in HSC Chemistry for Windows 5.1, Outokumpu Research Oy, P.O. Box 60, FIN – 28101 Pori, Finland, Fax: +358 – 2 – 626 – 5310; Phone: +358 – 2 – 626 – 6111

8 F. Medina, P. Salagre and J.E. Sueiras, J. Mol. Cat. 81 (1993) 363

9 H. Greenfield, Ind. Eng. Chem. Prod. Rev. Dev. 6 (1967) 142

10 B. S. Hudson, J. Phys. Chem. A 105 (2001) 3949

11 D. Graham, J. Howard and T. C. Waddington, J. Chem. Soc., Faraday Trans. 1, 79 (1983) 1281

12 H. Jobic and A. Renouprez, J. Chem. Soc., Faraday Trans. 1, 80 (1984) 1991

13 J.M. Nicol, Spectrochim. Acta 48A(3) (1992) 313

14 B. Delley, J. Chem. Phys. 92 (1990) 508

15 J. D. Donnay and G. Harker, Am. Mineral. 22 (1937) 446; particles morphology was computed in Cerius^2 program suite (2001, Accelrys Inc.) using Crystal Builder and Surface Builder modules.

16 M.J. Frisch, G.W. Trucks, H.B. Schlegel, G.E. Scuseria, M.A. Robb, J.R. Cheeseman, V.G. Zakrzewski, J.A. Montgomery, R.E. Stratmann, J.C. Burant, S. Dapprich, J.M. Millam, A.D. Daniels, K.N. Kudin, M.C. Strain, O. Farkas, J. Tomasi, V. Barone, M. Cossi, R. Cammi, B. Mennucci, C. Pomeli, C. Adamo, S. Clifford, J. Ochterski, G.A. Petersson, P.Y. Ayala, Q. Cui, K. Morakuma, D.K. Malick, A.D. Rabuck, K. Raghavachari, J.B. Foresman, J. Cioslowski, J.V. Ortiz, B.B. Stefanov, G. Lui, A. Liashenko, P. Piskorz, I. Komaromi, R. Gomperts, R.L. Martin, D.J. Fox, T. Keith, M.A. Al-Laham, C.Y. Peng, Nanayakkara, C. Gonzalez, M. Challacombe, P.M.W. Gill, B.G. Johnson, W. Chen, M.W. Wong, J.L. Andreas, M. Head-Gordon, E.S. Repolgle, J.A. Pople, GAUSSIAN 98 (Revision A.9), Gaussian, Pittsburg, PA, 1998.

17 aCLIMAX v. 4.0, the new software for analyzing and interpreting INS spectra; J.A. Ramirez-Cuesta, to be published

18 N. Wakabayashi, R. H. Schrem and H. G. Smith, Phys. Rev. B 25 (1982) 5122

19 B. Strauss, F. Frey, W. Petry, J. Trampenau, K. Nicolaus, S. M. Shapiro, J. Bossy, Phys. Rev. B 54 (1996) 6035

20 M. Sayers and C. J. Wright, J. Chem. Soc., Faraday Trans. 1, 80 (1984) 1217

21 H. Jobic and A. Renouprez, J. Chem. Soc., Faraday Trans. 1, 80 (1984) 1991

22 F. Grellner, B. Klingenberg, D. Borgmann and G. Wedler, Surf. Sci. 312 (1994) 143

23 F. Hochard, H. Jobic, J. Massardier and A. Renouprez, J. Mol. Catal. A 95 (1995) 165

24 J. P. Thiel, C. K. Chiang, and K. R. Poeppelmeier, Chem. Mater. 5 (1993) 297

25 M. Nayak, T. R. N. Kutty, V. Jayaraman and G. Periaswamy, J. Mater. Chem. 7 (1997) 2131

26 J.M. Kiat, G. Boemare, B. Rieu and D. Aymes, Solid State Commun. 108 (1998) 24

27 T. Ernst, Z. Phys. Chem. B20 (1933) 65

28 H. Dachs, Z. Krystallogr. 112 (1959) 60

29 K. A. Wickersheim, J. Chem. Phys. 31 (1959) 863

30 Y. Hase and I. V. Pagotto-Yoshida, Chem. Phys. Lett. 65 (1979) 46

31 F. Harbach and F. Fisher, J. Phys. Chem. Solids, 36 (1975) 601

32 I. V. P. Yoshida and Y. Hase, Spectrosc. Lett. 12 (1979) 409

33 R. A. Buchanan, H. H. Caspers and H. R. Marlin, 40 (1964) 1125

34 G. J. Safford and F. J. LoSacco, J. Chem. Phys. 44 (1966) 345

35 I. V. P. Yoshida and Y. Hase, Spectrosc. Lett. 12 (1979) 409

36 Y. Hase and I. V. P. Yoshida, J. Mol. Struct., 56 (1979) 297

37 R. A. Buchanan, H. H. Caspers and H. R. Marlin, J. Phys. Chem. 40 (1964) 1125

38 'Characterization of Raney-Ni and Raney-Co Catalysts and Their Use in the Selective Hydrogenation of Butyronitrile' A. Chojecki, T.E. Müller, J.A. Lercher *to be submitted*

Chapter 6

Summary of the research.

6 Summary

6.1 Summary of the Research

The research work presented in this thesis has started as a project in collaboration with Air Products and Chemicals, Inc. The aim was to explore the role of LiOH as promoter for Raney-catalysts [1, 2] in the hydrogenation of nitriles to primary amines (Figure 6-1).

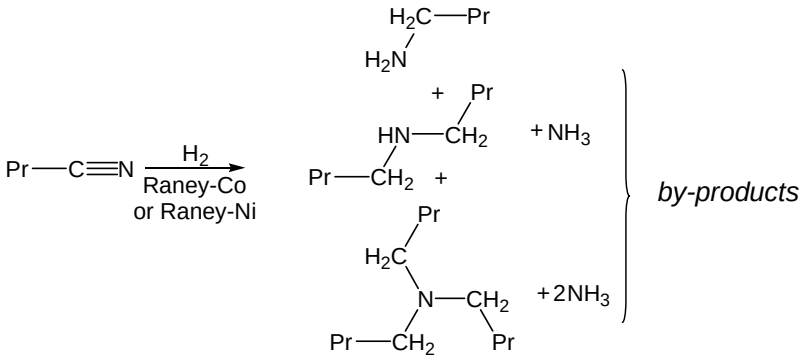

Figure 6-1: The hydrogenation of butyronitrile can yield a mixture of primary, secondary and tertiary n-butylamines and ammonia.

Active catalysts for this reaction (Raney-Co, Ni-Cr promoted Raney-Co, LiOH-modified Raney-Co and Raney-Ni) were characterized with a variety of techniques: AAS, XRD, BET, H_2-chemisorption, XPS, TPD and ammonia-TPD, calorimetric measurements of the heat of adsorption of butyronitrile, and adsorption of n-butylamine and butyronitrile from the liquid phase.

Further, catalytic tests in a three-phase high pressure reactor were performed to determine the activity and selectivity of each catalyst in the hydrogenation of butyronitrile to n-butylamine (Chapter 3).

The apparently straightforward reaction turned out to be part of a complex reaction network. Therefore, the catalytic performance of Raney-Co and LiOH-modified Raney-Co was followed in-situ by ATR-IR spectroscopy. Model reactions representing parts of the network included (i) the hydrogenation of butyronitrile, (ii) the disproportionation of n-butylamine (iii) the hydrogenation of N-butylidene-butylamine in the presence of ammonia and (iv) the hydrogenation /deuteration of N-butylidene-butylamine. The thermodynamics of the N-butylidene-butylamine - but-1-enyl-butyl-amine

tautomerisation reaction and a possible structure of the transition state structure were studied using *ab initio* methods (Chapter 4).

Incoherent Inelastic Neutron Scattering (INS) spectroscopy was used in combination with *ab initio* computational study of molecular vibrations to (i) study the hydrogen species adsorbed on the surface of Raney-Co (ii) characterize the LiOH-modification of Raney-Co and (iii) identify possible reaction intermediates during co-adsorption of hydrogen and butyronitrile on the surface of parent and LiOH-modified Raney-Co (Chaper 5).

6.2 Conclusions

The metal surface active for hydrogenation is only a fraction of the total surface area of the Raney-catalysts studied. Although the amount of alumina on the surface of Raney-Ni, Raney-Co(NiCr) and Raney-Co follows the trend of the bulk composition Al seems to be enriched at the surface. The nature of the oxide deposit and its morphology are influenced by the LiOH additive. Firstly, LiOH quenches the sites which are associated with the alumina Lewis acidity (Al_2O_3) and lithium dialuminate $Li_2Al_2(OH)_7{\cdot}2H_2O$ is probably formed. Secondly, clustering of the oxide deposit takes place as the fraction of the clean metal surface area increases relative to the total surface. On cobalt the adsorption mode of butyronitrile on the surface probably is probably characterized by σ-binding through the nitrogen atom with the C≡N bond vector largely normal to the surface plane (low heat of adsorption). In contrast on nickel an aslant mode where the C≡N π-system also interacts with the surface dominates (high heat of adsorption). Modification of Raney-Co with LiOH gives a catalyst with an intermediate heat of adsorption, although, it is speculated that this modification leads to an increase in the strength of the nitrogen binding to the cobalt surface. In line, the rate of the hydrogenation of butyronitrile is higher over nickel than over cobalt; also LiOH-modification of Raney-Co leads to an enhanced catalytic activity (Figure 6-2).

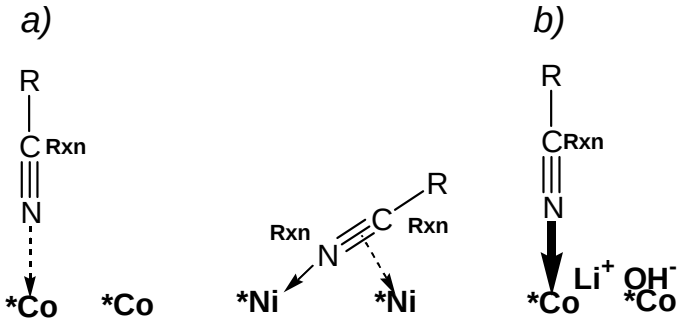

Figure 6-2: a) Different ways in which nitriles can be bound to cobalt and nickel. *Co and *Ni denote surface-exposed cobalt and nickel atoms, respectively. Rnx indicates reaction centers in the activated nitrile molecule. b) Increased strength of adsorption *via* nitrogen binding to the cobalt surface on Raney-Co(LiOH).

During the hydrogenation of butyronitrile to n-butylamine over Raney-Ni and Raney-Co the formation of a side-product, N-butylidene-butylamine, was observed. The side-product stems from a bi-molecular condensation reaction. In contrast over LiOH-modified Raney-Co the hydrogenation of butyronitrile is nearly 100 % selective to n-butylamine. Because LiOH remains on the catalyst surface during the reaction, it is evident that only surface species can be prevented from reacting to the side-products. A direct control over the rate of surface condensation reactions can be realized by changing the conditions in such a way that the surface coverage in the reacting molecules is as small as possible. These species will exist in a low steady-state surface concentration if a high ratio of active hydrogen to butyronitrile is maintained. The concentration of the reactive species on the surface decreases after LiOH doping; in parallel the selectivity increases. In particular, LiOH modification of Raney-Co leads to an enhanced selectivity by (i) reducing the catalyst sorption capacity for butyronitrile and amines, (ii) increasing the probability of a step-wise hydrogenation *via* nitrene species and (iii) poisoning of Al^{3+} Lewis acid sites that catalyze the condensation reaction.

Over Raney-Co the amount of N-butylidene-butylamine produced is inversely correlated with the selectivity to n-butylamine for the hydrogenation of butyronitrile. The most likely mechanism of N-butylidene-butylamine formation is based on nucleophilic condensation among partially hydrogenated derivatives of butyronitrile. In particular, the presence of carbene species on the catalyst surface might be responsible for the formation of N-butylidene-butylamine as a reactive center on the unsaturated carbon atom is available.

). It should be noted that in *situ* spectroscopy has not provided evidence that any butylidenimine, which was frequently postulated as reaction intermediate, was formed or desorbed into the liquid phase.

The reaction between N-butylidene-butylamine and ammonia has been explored as the reverse of the condensation reaction observed during the hydrogenation of butyronitrile. However, the reaction hardly proceeded. Over the parent catalyst ammonolysis of N-butylidene-butylamine produced traces of n-butylamine and some high molecular weight products. Note that n-butylamine in reaction with butylidenimine would directly yield N-butylidene-butylamine. Over LiOH-modified catalyst ammonolysis of N-butylidene-butylamine unexpectedly yielded only butyronitrile. This implies fast dehydrogenation of reactants or products (i.e., butylidenimine and n-butylamine). Probably the LiOH-modified Raney-Co exhibits better dehydrogenation and hydrogenation activity than the parent catalyst.

The reaction of N-butylidene-butylamine with ammonia in the presence of hydrogen will lead to n-butylamine. Over parent catalyst the reaction yields n-butylamine, however, di-n-butylamine is also obtained. In contrast, in the presence of LiOH on the catalyst surface, N-butylidene-butylamine hardly reacts with NH_3 and practically only di-n-butylamine is formed after hydrogenation. Most likely, the much stronger nucleophile OH^- forms a surface adsorbed amino-alcohol (or its salt) and protects the C=N group from nucleophilic attack of ammonia. By analogy it could also be possible that LiOH inhibits the nucleophilic condensation among partially hydrogenated intermediates.

INS spectroscopy indicated that sorption of hydrogen onto Raney-Co at low pressure is mainly related to the three-fold sites. Wet deposition of LiOH onto Raney-Co and subsequent temperature treatment at 473 K creates clustered rather than layered lithium hydroxide. On Raney-Co butyronitrile and hydrogen promptly react yielding a number of (partially-) hydrogenated derivatives that are characterized by the presence of at least one hydrogen atom on the nitrogen atom. In consequence the condensation reaction leading to condensation products (i.e., N-butylidene-butylamine) is feasible. Modification of Raney-Co with LiOH significantly changes the sorption properties of the catalyst surface. It is speculated that strong binding *via* the nitrogen atom may in the first place stimulate

hydrogenation of the carbon atom in the nitrile group. This preserves it from a nucleophilic attack and subsequent condensation reactions. However, further experimental evidence of the nitrene species populating the surface of Raney-Co(LiOH) during the reaction is necessary.

References

1 T. A. Johnson, US Patent No. 5 869 653 (1999), to Air Products and Chemicals, Inc.

2 T. A. Johnson and D. P. Freyberger in: M. E. Ford (Ed.), Catalysis of Organic Reactions - Chemical Industries Series Vol. 82, Marcel Dekker, 2000, p. 201 – 227